AEDC-TR-71-241

cy 2

REFLECTANCES OF CO_2 AND H_2O CRYODEPOSITS AT SOLAR WAVELENGTHS

B. A. Seiber, A. M. Smith, and B. E. Wood

ARO, Inc.

November 1971

Approved for public release; distribution unlimited.

VON KÁRMÁN GAS DYNAMICS FACILITY
ARNOLD ENGINEERING DEVELOPMENT CENTER
AIR FORCE SYSTEMS COMMAND
ARNOLD AIR FORCE STATION, TENNESSEE

NOTICES

REFLECTANCES OF CO_2 AND H_2O CRYODEPOSITS AT SOLAR WAVELENGTHS

B. A. Seiber, A. M. Smith, and B. E. Wood
ARO, Inc.

FOREWORD

The research reported herein was sponsored by Headquarters, Arnold Engineering Development Center (AEDC), Air Force Systems Command (AFSC), Arnold Air Force Station, Tennessee, under Program Element 64719F.

The results of the research were obtained by ARO, Inc. (a subsidiary of Sverdrup & Parcel and Associates, Inc.), contract operator of AEDC, AFSC, under Contract F40600-72-C-0003. The work was performed under ARO Project Nos. SW5007 and VW5122 during the period from January 1970 through June 1971. The manuscript was submitted for publication on September 14, 1971.

This technical report has been reviewed and is approved.

Michael G. Buja
Captain, USAF
Research and Development Division
Directorate of Technology

R. O. Dietz
Acting Director
Directorate of Technology

ABSTRACT

A careful study of the reflectances of carbon dioxide and water cryodeposits was made in a vacuum integrating sphere in the solar wavelength range (0.30 to 2.55 μ). These deposits were formed on liquid-nitrogen-cooled black epoxy paint and polished stainless steel substrates. The reflectances of these deposits were studied while varying the deposit thickness, view angle, and wavelength. The reflectance dependence on thickness was also predicted theoretically and the values obtained were in excellent agreement with the experimentally determined values. Most of the water deposits studied were of amorphous structure, but upon warming, the deposits crystallized resulting in a significant change in the reflectance. No structural changes were observed when the carbon dioxide frosts were warmed. From the results of this study, conclusions are drawn with regard to the application of these findings to several current problems.

CONTENTS

APPENDIX

I. ILLUSTRATIONS

SECTION I
INTRODUCTION

With the present increased use of cryogenic cooling, it has become common to encounter the condensation of gases on cooled surfaces forming cryodeposits. These cryodeposits can even form on cryogenically cooled surfaces under vacuum. Their presence can have substantial optical effects on testing in vacuum solar simulation chambers, the usefulness of cooled optics such as mirrors and lenses, thermal balance testing, and in general most cases where cryogenic cooling is used in association with optical or thermal measurements.

The solar reflectances of cryodeposits are also of interest in the study of planetary frosts, particularly the polar caps of Mars.

Carbon dioxide and water are the most common cryodeposits which form on liquid-nitrogen-cooled surfaces. Measurements of the reflectance of these two cryodeposits have previously been inadequate for several reasons. In several studies, deposits were formed and their reflectances were measured at atmospheric pressure. In other studies, the measurements were valid for only a specific source or else had a large uncertainty. Most previous reflectances were obtained by calorimetric measurements and therefore valid only for a specific radiation source, or else they were spectral measurements over a limited wavelength range which inadequately represents the solar spectrum. Further, most previous spectral measurements have been relative to a reflectance standard such as magnesium oxide. This increases the uncertainty of the measurements because of the difficulty of knowing the absolute reflectance of the standard and of problems with the stability of the standard with time.

In this study, the absolute reflectances of carbon dioxide and water cryodeposits were measured throughout the solar wavelength region. These spectral measurements were made in situ after the deposits formed on a liquid-nitrogen-cooled surface under vacuum. A specially designed integrating sphere 12 in. in diameter was calibrated and used to make the measurements. Reflectances were obtained at wavelengths from 0.30 to 2.55 μ which includes 95.4 percent of the solar energy. The cryodeposit reflectances were measured as a function of wavelength, λ, deposit thickness, τ, view angle, θ, and substrate.

SECTION II
TECHNIQUE OF DETERMINING REFLECTANCE

Absolute, spectral reflectance measurements of cryodeposits were obtained for both water and carbon dioxide cryodeposits. The reflectance which was measured is the hemispherical-angular reflectance defined (Refs. 1 and 2) by

$$\rho_{ha}(\psi, \lambda) = \frac{I_r(\psi, \lambda)}{e_{i,h}(\lambda)/\pi} = \frac{I_r(\psi, \lambda)}{I_i(\lambda)} \tag{1}$$

where $I_r(\psi, \lambda)$ is the reflected intensity for a small collection solid angle $\Delta\omega_r$ (0.02 steradians) which is inclined at the angle, ψ, and $e_{i,h}(\lambda)$ is the hemispherically incident radiant energy. Associated with $e_{i,h}(\lambda)$ is the diffuse incident intensity $I_i(\lambda)$. In all cases, λ indicates the particular monochromatic wavelength of the measurement. In this study, the same solid angle was used for measuring both $I_r(\psi, \lambda)$ and $I_i(\lambda)$ so that the absolute hemispherical reflectance can be found from the right hand side of Eq. (1). In the case where the hemispherically incident energy is diffusely distributed as it was in this study and when the surface is isotropic, it is shown (Ref. 2) that the hemispherical-angular reflectance, $\rho_{ha}(\psi, \lambda)$, is equal to the angular-hemispherical reflectance, $\rho_{ah}(\theta, \lambda)$, with $\psi = \theta$. The angular-hemispherical reflectance corresponds to a sample which is illuminated by a beam with solid angle, $\Delta\omega_i$, at an angle of incidence θ, with the reflected radiant energy collected over the entire hemispherical space. Note, when $\rho_{ha}(\psi, \lambda)$ is equal to $\rho_{ah}(\theta, \lambda)$, the solid angles are equal, $\Delta\omega_r = \Delta\omega_i$, and the angle of viewing for ρ_{ha} is the same as the angle of incidence for ρ_{ah}. Thus, the hemispherical-angular reflectance at a view angle of ψ as measured in this study corresponds to the angular-hemispherical reflectance with an incidence angle of θ which is often seen in the literature.

In order to determine the absolute hemispherical-angular reflectance of a sample at a given wavelength using Eq. (1), it was necessary to measure $I_r(\psi, \lambda)$ and $I_i(\lambda)$. These measurements were obtained (also see Ref. 1) by viewing the sample at a given wavelength and obtaining a detector output $D_r(\lambda)$, which was proportional to $I_r(\psi, \lambda)$, $D_r = C\, I_r(\psi, \lambda)$. A portion of the sphere wall which was not directly irradiated by the source was then viewed under the same conditions of $\Delta\omega_r$ and λ obtaining a detector output, D_i, which was proportional to $I_i(\lambda)$, $D_i = C\, I_i(\lambda)$. The proportionality constant, C, depends only on the viewing optics and detection system and is the same in both cases. Further, since the

sphere wall was perfectly diffuse, it was uniformly irradiated by multiple reflections. The intensity of the radiation reflected from the sphere wall is then equal to the intensity which is incident on the test surface. By ratioing the two detector outputs, the absolute reflectance was determined since

$$\frac{D_r}{D_i} = \frac{C\, I_r(\psi, \lambda)}{C\, I_r(\lambda)} = \rho_{ha} \tag{2}$$

It should be stressed that the reflectances obtained with this technique are absolute. The reflectance is measured directly and is not referenced to a standard reflector. By using these principles, the absolute, hemispherical-angular reflectances of samples were obtained.

SECTION III
APPARATUS

The solar integrating sphere (see Figs. 1 and 2, Appendix) used in this study consisted of two stainless steel hemispheres 12 in. in diameter and a centrally located test surface. As was noted above, it was important that the interior of the sphere was a diffuse reflector. This was accomplished by smoking the interior of the sphere with a thick (greater than 3 mm) coat of magnesium oxide (MgO) in the case of the measurements involving carbon dioxide (CO_2) cryodeposits on a black substrate. Magnesium oxide is a good diffuse reflector but it has the disadvantages of slowly changing reflectance with time and of poor mechanical stability. This made it necessary to resmoke the sphere immediately prior to each experimental run. In later experiments involving CO_2 cryodeposits on a polished stainless steel substrate and water (H_2O) cryodeposits on a black painted substrate, a barium sulfate paint was used. This paint was diffuse (Ref. 3) in the solar wavelength region, and it had a reflectance and mechanical stability which was much better than smoked MgO. No problems were encountered using this paint in vacuum.

The entire apparatus was similar to that described in Refs. 1 and 4. The cryosurface on which the deposits formed was a hollow stainless steel cylindrical block 6.35 cm in diameter by 1.14 cm wide (Fig. 3). This cryosurface was mounted vertically in the center of the sphere and was cooled internally by continuously flowing liquid nitrogen through it. The cryosurface had a total surface area of 121.2 cm^2. The test surface was one of the vertical circular faces of the cryosurface and was either the bare stainless steel which had been polished or was the same

face coated with a black epoxy paint. A copper-constantan thermocouple was silver soldered onto the test surface allowing the test surface temperature to be continuously monitored. The liquid-nitrogen supply lines to the cryosurface were vacuum jacketed which prevented cryopumping anywhere except on the outside of the cryosurface. This vacuum jacket also supported the cryosurface in the center of the sphere and allowed the circular test surface to rotate under vacuum about its vertical centerline. By rotating the test surface, the view angle, which was measured from the test surface normal, could be changed allowing reflectance measurements to be made from zero to 60 deg.

The inside of the assembled integrating sphere could be evacuated using an ion pump, a 4-in. oil diffusion pump with a liquid-nitrogen cold trap, and a mechanical pump. Chamber pressures inside the integrating sphere were measured using an ion gage or an alpha particle gage which was corrected for the gas present; i. e., air, H_2O, or CO_2.

Light from a 1000-watt tungsten-halogen bulb was chopped at 13 Hz and then focused through a quartz window onto a portion of the back wall inside the integrating sphere. The light was then reflected diffusely throughout the sphere by the wall coating and was hemispherically incident on the test surface with a diffuse distribution. The radiation passed through a quartz window on the viewport and was collected by an off-axis paraboloidal mirror after it was reflected either from a portion of the wall which was not directly irradiated or from the test surface. Then, an off-axis paraboloidal mirror focused the radiation on the entrance slit of a Perkin Elmer model 99 monochromator. Both the monochromator and the paraboloidal mirror were mounted on a table top which could be rotated about the vertical centerline of the viewport allowing the collection of the radiation from either the test surface or the sphere wall. The procedure was similar to that used in Ref. 4 for a smaller infrared integrating sphere.

The monochromator had a quartz prism and was used in the single-pass mode. After the radiation passed through the monochromator where the wavelength of interest was selected, it was detected by a photomultiplier tube at the shorter wavelengths and by a lead sulfide cell at the longer wavelengths. The signal from the detector was then amplified and recorded on a strip chart recorder. This system allowed the hemispherical-angular reflectances of a sample to be measured spectrally throughout the solar wavelength region from 0.30 to 2.54 μ. The system had the demonstrated capability of making measurements to a wavelength of 0.25 μ using a different photomultiplier tube. All of the cryodeposit reflectances were measured in situ after deposit formation.

SECTION IV
PROCEDURE

During this study, cryodeposits were formed in vacuum by condensing either CO_2 gas or water vapor at a constant rate on the liquid-nitrogen-cooled substrates. The CO_2 gas which was used had less than 0.01-percent impurities and was introduced into the chamber at a constant mass addition rate, $\dot{m}$, using a calibrated constant leak.

For the H_2O cryodeposit measurements, distilled water in a reservoir was outgassed by vigorously boiling the water while pumping out the space above it with a vacuum pump. After outgassing, the water was vaporized under vacuum in the reservoir and then conducted into the integrating sphere at a known constant mass flow rate. For all studies, a baffle was over the gas inlet to eliminate any direct path for the gas to the cryoplate and to help ensure a uniform deposition over the cryosurface.

The thickness, τ, of both CO_2 and H_2O cryodeposits was found from $\tau = \dot{\tau}t$ by knowing the thickness deposition rate, $\dot{\tau}$, of the deposit on the test surface and the deposition time, t. This was possible since the gas condensed on the cryosurface at a constant rate. The primary method of determining the thickness deposition rate for both CO_2 and H_2O cryodeposits was by recording the monochromatic thin film interference patterns as the deposit formed on the test surface. This method is described in detail in Ref. 5. Since the period between interference maxima was constant in all runs, it was further assured that the thickness deposition rate was constant. The thickness deposition rate determined in this way was independently checked by determining the constant mass addition rate, $\dot{m}$, knowing the deposit density, ρ, and assuming that the deposit formed uniformly thick over the entire cryosurface area, A. Thus

$$\dot{\tau}(\rho) = \frac{\dot{m}}{\rho A}$$

This $\dot{\tau}(\rho)$ agreed with the thickness deposition rate obtained using thin film interference to within 3 percent, which was the accuracy of $\dot{m}$.

The values of deposit density and refractive indices given in Ref. 5 were used for $\dot{\tau}$ determinations since the cryodeposits were formed under similar conditions of temperature, pressure, and deposition rate. Thickness measurements were further verified by using a calibrated mechanical probe to check the depth of the thickest deposits.

Before forming the cryodeposits on the test surface, the integrating sphere was evacuated to 5 x 10^{-7} torr, and the spectral reflectance of the bare test surface was measured throughout the wavelength range for view angles from zero to 60 deg. The cryosurface was then cooled by flowing liquid nitrogen through it with a final test surface temperature of 92°K.

Next the sphere was valved off from the pumping system, and a cryodeposit of thickness τ was formed. During the deposit formation and measurements, the temperature of the test surface was never greater than 97°K except when the water cryodeposits were intentionally warmed. The sphere pressure was from 10^{-4} to 10^{-2} torr during deposition depending on the rate of gas introduction. This chamber pressure was essentially constant with only a very slight increase with increasing deposit thickness.

When each deposit thickness had been formed, the reflectance of the cryodeposit-substrate complex was measured over the entire wavelength range from 0.3 to 2.5 μ. The reflectance was also measured for view angles from zero to 60 deg at wavelengths of 0.40, 0.50, 1.00, 1.50, and 1.95 μ. The thickness of the deposit was then increased, and the reflectance of the complex was again obtained. This process was continued at various thickness increments until the reflectance at the largest deposit thickness had been measured.

SECTION V
RESULTS

5.1 ABSOLUTE CALIBRATION

Because the reflectances in this study are absolute and are not referenced to a standard, it is essential to know the magnitude of any systematic errors in the measurements. In order to determine the systematic errors, an extensive investigation was carried out which involved measuring the reflectance of a wide variety of materials. Reflectances were measured for materials which had both high and low reflectances and which were specular and diffuse. These reflectances were then compared with values obtained using other instruments and with values reported in the literature. Figure 4 shows the results for several different materials. In Fig. 4a, the reflectances measured by the 12-in. integrating sphere used in this study are compared with values obtained using a modified reflectometer. The modified reflectometer was calibrated by using an ASTM absolute calibration (Ref. 6) and was

accurate to a reflectance of 0.015. Figure 4b shows a comparison of values measured on the same sample of white epoxy paint using the present 12-in. integrating sphere, the calibrated reflectometer, and an infrared integrating sphere (Ref. 4). Excellent agreement is seen between all the systems. In addition, reflectances were measured with the present system for freshly smoked magnesium oxide and for evaporated aluminum. These measured reflectance values were in good agreement with values given in the literature. From a full consideration of all these factors, the reflectances measured with the present 12-in. integrating sphere system are accurate to within ±0.015 regardless of what type of reflector the sample is.

5.2 CO_2 ON A BLACK EPOXY SUBSTRATE

The fraction of the incident intensity which is reflected from a complex of a CO_2 cryodeposit on a black epoxy painted substrate is shown in Fig. 5 for wavelengths between 0.35 and 2.54 μ. Note that a reflectance of 1.00 means the reflected intensity equals the incident intensity. The cryodeposits were formed on a liquid-nitrogen-cooled surface at a deposition rate, $\dot{\tau}$ = 0.127 μ/sec, and a deposition pressure of 8×10^{-3} torr. These reflectance values are the average of four separate experimental runs with the reflectance value of each run within 0.02 of the average value shown. For these measurements, the view angle is zero deg at all thicknesses.

At 0-mm thickness, the reflectance is that of the black epoxy painted substrate with no cryodeposit on it. This substrate has a reflectance which is substantially constant at 0.05 over the entire solar wavelength range. With the addition of a 0.109-mm-thick CO_2 cryodeposit, the reflectance monotonically increases as the wavelength decreases below 0.80 μ. Notice that, for all wavelengths greater than 0.60 μ, the reflectance of the cryodeposit-substrate complex is less than the reflectance of the bare substrate at all wavelengths. It is not until the deposit is greater than 0.87 mm thick that the reflectance of the complex is greater than the highly absorbing substrate for all solar wavelengths. The reason for this reflectance decrease will be discussed later. As the cryodeposit thickness increases, the reflectance of the complex increases at all wavelengths. However, the reflectance always continues to increase as the wavelength is decreased for each deposit thickness. A reflectance dependence on wavelength such as this could be due to an increase in absorption with longer wavelength or to a decrease in scattering which would correspond to an increase in transmission by the cryodeposit. With later consideration of the reflectance of a CO_2 deposit on a polished stainless steel substrate, it will be seen that the wavelength

dependence is due to a decrease in scattering at longer wavelengths and hence an increase in the transmission of the deposit. With increasing transmission more of the incident intensity is absorbed by the black substrate which thus lowers the reflectance with wavelength. This effect is also noticed in Ref. 1.

It is not until the cryodeposit is 3.49 mm thick, that a CO_2 absorption band can be identified in the reflectance spectra. At this thickness, an absorption band is seen at a wavelength of 2.0 μ. The appearance of this absorption band is due to the increased path of the light through the deposit with scattering and increased deposit thickness. This in turn increases the amount of absorption in relation to the amount of light reflected. Over all, it is apparent that moderate cryodeposit thicknesses can greatly change the substrate reflectance throughout the entire solar wavelength range.

A study was also conducted on the reflection of thin CO_2 deposits on the black painted substrate using a deposition rate of (3 to 9) x 10^{-2} μ/sec and a deposition pressure of 2 x 10^{-4} torr. The fractional reflectance of these thin deposits is shown in Fig. 6 for deposits 3, 10, and 67 μ thick. These thicknesses were determined by measuring the optical thin film interference as the deposits formed. For a deposit 3 μ thick, the reflectance is less than the base substrate at all wavelengths. For wavelengths greater than 1.5 μ, the reflectance of the complex is almost 30 percent below the substrate reflectance, 0.025 compared with 0.035. At 10-μ thickness, the reflectance at any wavelength is still not above that of the black substrate. It is not until the cryodeposit is 67 μ thick that the spectral reflectance becomes similar to those shown in Fig. 5.

To determine the effect of deposition rate and pressure, the reflectances of cryodeposits were compared for the 3.9 x 10^{-2} μ/sec deposition rate (2 x 10^{-4} torr) and the 1.27 x 10^{-1} μ/sec rate (8 x 10^{-3} torr). No difference in reflectance could be seen at any wavelength for a deposit 0.109 mm thick. However, the maximum reflectance was 0.10, and thus a 10-percent change in reflectance (0.01) due to deposition rate or pressure was the maximum change which could be detected. A smaller change might have occurred. In another study, the reflectance of a 0.87-mm-thick CO_2 cryodeposit on a black substrate was measured in situ, and then the pressure in the integrating sphere was increased to 200 torr using dry nitrogen. After an hour, the reflectance was again measured, and no change was found at any wavelength or any view angle up through 60 deg. A 3-percent change in reflectance could definitely have been detected. This indicates that there was no change in the deposit due to pressure increases after it was formed.

The dependence of reflectance on deposit thickness is shown in Fig. 7 for wavelengths of 0.40, 0.50, 1.00, 1.50, and 1.95 μ. The view angle is again zero deg. For a wavelength of 0.4 or 0.5 μ, the reflectance increases rapidly with increasing thickness up to a thickness of 1.0 mm. Above this, the reflectance increases more gradually until it levels off to a maximum at 3.5 mm thick. This maximum indicates that neither the substrate nor increased thickness would affect the cryodeposit reflectance when the deposit is greater than 4.0 mm thick. At the longer wavelengths, the reflectance is strongly thickness dependent with the λ = 1.95 μ curve showing no indication of reaching a maximum reflectance which is independent of deposit thickness. In fact, the λ = 1.95 μ curve seems to become more dependent on thickness at the larger deposit thicknesses studied.

Figure 8 shows the dependence of reflectance on view angle from zero to 60 deg for the same wavelengths used in the thickness study, λ = 0.40, 0.50, 1.00, 1.50, and 1.95 μ. These curves give an indication of the differences for the CO_2 cryodeposit. At the shorter wavelengths, there is a moderate reflectance dependence on view angle with an increase of about 0.08 at 60 deg over the zero-deg reflectance regardless of the initial zero-deg reflectance. The view angle dependence seems to increase with thickness up to 0.218 mm and then to slowly decrease for larger thicknesses. However, for the longer wavelengths, λ = 1.00, 1.50, and 1.95 μ, the reflectance change between the zero- and 60-deg view angle increases with deposit thickness from about 0.03 at the smaller thickness to 0.14 for the larger thicknesses. View angle effects with increasing angle of incidence are due to the increased front surface reflectance of the deposit with increased angle and to the increased path length in the deposit.

5.3 CO_2 ON A STAINLESS STEEL SUBSTRATE

In order to determine the effect of a specular, highly reflecting substrate on the reflectance of a cryodeposit complex, CO_2 cryodeposits were formed on a polished stainless steel test surface. This test surface is the same as used before, with the black paint removed and the surface polished. The fraction of the incident intensity which is reflected at a view angle of 20 deg is given in Fig. 9 for various deposit thicknesses. The reflectance values shown here were checked by measuring the reflectance of another deposit and comparing the results for the two deposits at cryodeposit thicknesses of 0.090 and 0.360 mm. The reflectances of these two separately formed deposits agreed to within better than 0.01 (better than 2 percent of the value) for all wavelengths.

During formation of these CO_2 cryodeposits, the thickness deposition rate was 0.105 μ/sec on the test surface and the pressure ranged from 1.5×10^{-2} torr for the thin deposits and the initial 2 hr of deposition for thicker deposits to 6×10^{-2} torr at the end of the final deposition (after about 4 hr). Figure 9a shows the reflectance with wavelength of the polished stainless steel substrate without any cryodeposit on it. The reflectance increases monotonically from 0.46 at $\lambda = 0.36\ \mu$ to 0.72 at $\lambda = 2.48\ \mu$. Figure 9b shows the reflectance with a 5.2-μ (0.0052-mm) thick CO_2 deposit on it. It is immediately seen that there is a sharp decrease in the reflectance of the complex when compared with the reflectance of the bare stainless steel over all wavelengths. At $\lambda = 0.36\ \mu$, the reflectance has decreased 25 percent from 0.46 to 0.34. A decrease of about 0.12 is noticed over all wavelengths. In addition, interesting structure is seen at wavelengths greater than 1.5 μ. This structure is due to thin film interference where the maxima represent constructive interference between rays reflected from the top of the deposits and those reflected from the substrate, and the minima represent destructive interference. In a sense, the large substrate reflectance is modulated by light reflected from the front surface of the cryodeposit. This interference pattern (modulation) is caused by a change in the optical path length as the wavelength and refractive index change. Interference patterns were not seen with a change in wavelength for thin CO_2 films on a black substrate. This was because the reflectance from the black substrate with a CO_2 deposit on it was less than 0.001 which produces too small a modulation to be detected.

When the CO_2 cryodeposit was increased to 48.7 μ (0.0487 mm) thick, the reflectance of the cryodeposit-stainless steel complex (Fig. 9c) decreased about 0.05 below the 5.5-μ thickness for all wavelengths. Moreover, the interference patterns are no longer visible. As the deposit thickness increases to 0.180 mm (Fig. 9e), the reflectance at wavelengths greater than 0.6 μ decreases. At the same time, the reflectance in the visible begins to increase. With increasing thickness beyond 0.180 mm, the reflectance increase extends to longer wavelengths until the reflectance has increased for all the solar wavelengths at 2.88 mm (Fig. 9i). Throughout the measurements, the increase is most rapid at the shorter wavelengths because of the wavelength dependence on scattering. The CO_2 absorption band at $\lambda = 2.0\ \mu$ first appears at a thickness of 0.180 mm (Fig. 9e), and it becomes more prominent as the deposit thickness increases.

When the reflectances in Fig. 9 are compared with those in Fig. 5 for CO_2 cryodeposits on black, it is observed that the longer wavelength reflectances are much higher for the stainless steel substrate. Therefore, the deposit must be fairly transparent (low deposit scattering and

absorption) as stated before. At the longer wavelengths, the substrate has a considerable effect on the reflectance.

The reflectance as a function of thickness is presented in Fig. 10 at wavelengths of 0.40, 0.50, 1.00, 1.50, and 1.95 μ. The spectral reflectance of this same CO_2 cryodeposit on stainless steel was presented earlier in Fig. 9. At λ = 0.40 and 0.50 μ (Figs. 10a and b), the reflectance sharply decreases to a minimum when the deposit is about 50 μ thick and then increases rapidly until it levels off at a maximum for the largest thickness studied. At the largest thickness, the reflectance on the stainless steel substrate agrees with that on the black substrate within ±0.01 for these two wavelengths. This indicates that the substrate no longer has an effect at this thickness. For all the wavelengths presented in Fig. 10, the reflectance decreases to about 40 percent of the value for bare stainless steel. The sharp initial decrease is due to a decrease in the relative refractive index of the substrate when a deposit condenses on it, while any further decrease is due to a critical angle effect, as noted before, or to absorption at λ = 1.95 μ. For wavelengths of 1.00 μ and greater, no maximum in the reflectance is reached, and the values of the reflectance are much greater than those for CO_2 cryodeposits formed on a black substrate. This further indicates that the deposit becomes more transparent at the longer wavelengths.

The reflectance dependence on view angle for a 2.88-mm-thick CO_2 deposit on stainless steel is exhibited in Fig. 11. There was only a slight variation with view angle for any wavelength. However, the longer wavelengths do have a stronger view angle dependence. These trends are similar to those seen for a CO_2 cryodeposit on a black substrate (Fig. 8).

5.4 H_2O CRYODEPOSITS ON A BLACK EPOXY PAINTED SUBSTRATE

Since water is the most commonly encountered cryodeposit on a liquid-nitrogen-cooled surface, a study was made of the reflectance of water cryodeposits formed on a black epoxy painted substrate. Water cryodeposits were formed at a thickness deposition rate ($\dot{\tau}$ = 6.97 x 10^{-2} μ/sec) and a deposition pressure of about 5 x 10^{-3} torr for deposit thicknesses from 2 to 42 μ. For thicknesses from 0.104 to 3.25 mm, the deposition pressure was 7.0 x 10^{-3} torr. The substrate temperature was never greater than 97.5°K during the experiments. Many investigators (Refs. 7 and 8) have shown that amorphous ice is formed when water vapor is cryodeposited at temperatures below 110°K at low pressures. It is therefore concluded that the present deposits were composed of amorphous ice.

Figures 12a through i show the spectral reflectance of a water cryodeposit formed on the black substrate for deposit thicknesses ranging from 2 μ up to 3.25 mm. The view angle was zero deg. For the 2.1-μ-thick deposit, the reflectance is decreased by 50 percent from the bare surface reflectance for all wavelengths. For example at λ = 1.00 μ, the bare substrate has a reflectance of 0.04 which decreased to 0.02 when 2.1 μ of H_2O cryodeposit was added. It is not until the deposit is 0.104 mm thick that the reflectance becomes greater than that of the bare substrate, but then only for the shortest wavelengths. For larger thicknesses, the reflectance increases steadily with thickness for wavelengths less than 1.50 μ. The cutoff, at λ = 1.50 μ, of the thickness dependence is abrupt, and the reflectance for longer wavelengths remains essentially unchanged from that at the 2.1-μ thickness, even when the thickness was increased to 3.25 mm.

The reflectance trend for wavelengths less than 1.50 μ is similar to that seen for CO_2 cryodeposits with the reflectance increasing as the wavelength decreases. This is due to the wavelength dependence of the scattering in the deposit. Visually, the deposits thicker than 0.8 mm appeared slightly white, while the thinner deposits could not be seen.

After completing the reflectance measurements on this water deposit, the liquid-nitrogen flow which cooled the cryosurface was turned off, and the test surface was allowed to warm up. While the surface warmed, both the test surface temperature and the reflectance at a wavelength at 1.00 μ were recorded with time. The results are shown in Fig. 13 with the temperature and reflectance shown for corresponding times. Initially, the surface warmed at a rate of 2°K/min. The reflectance was constant until the temperature was about 148°K when there was a sharp irreversible increase in reflectance and also temperature. This is due to the transformation of the cryodeposit from an amorphous to a cubic structure (Ref. 8). With further warming, the temperature increased linearly, and the reflectance increased until it reached a maximum of 0.82 when the temperature was about 190°K. The temperature was increased to 210°K with no further change in reflectance. This gradual change in reflectance at temperatures above 150°K is caused by the cryodeposit changing structure to hexagonal ice. Note that there is a sharp temperature peak beginning at about 125°K with no accompanying change in reflectance. This peak was observed for all thick H_2O deposits studied and occurs while the cryodeposit is still amorphous. It might be due to an exothermic glass transformation.

After warming the deposit to 210°K, the cryosurface was again cooled with liquid nitrogen, and the spectral reflectance was measured. The results are shown in Fig. 14. When compared with the same deposit

before it has been warmed (amorphous ice) in Fig. 12i, it is seen that there has been a very substantial increase in reflectance at all wavelengths. The reflectance for all wavelengths shorter than 0.95 μ is about 0.87. Absorption bands are seen at wavelengths of 1.04, 1.55, and 2.03 μ.

The increase in reflectance is due to an increase in scattering caused either by a drastic increase in the voids present or else by an increase in crystal size. It is unlikely that there was a large increase in the voids in the cryodeposit as no thickness change was observed. Hence, it is probable that the crystal size increased substantially when the water cryodeposit changed structure from amorphous to hexagonal ice. This is as would be expected.

Sharp increases in reflectance with the change to hexagonal ice have been observed even with very small deposit thicknesses. Figure 15 shows the spectral reflectance of a 53.6-μ-thick water deposit before it was warmed (amorphous ice) and after being warmed to 207°K (hexagonal ice). The reflectance of the amorphous ice was less than the black substrate at all wavelengths greater than 0.40 μ. However, when the structure changed to hexagonal the reflectance increased at all wavelengths. At a wavelength of 0.40 μ, the reflectance increased from 0.04 to 0.52, a factor of more than ten. Further absorption bands become visible at 1.55 and 2.03 μ. These changes reflect the large increase in deposit scattering.

The change in the reflectance with thickness of an H_2O cryodeposit on a black substrate is shown in Fig. 16 for the same deposits as shown in Fig. 12. These reflectances are for a viewing angle of zero deg and wavelengths of 0.325, 0.400, 0.500, 1.00, 1.50, and 1.95 μ. For the three shortest wavelengths (Figs. 16a, b, and c), the reflectance decreases sharply when 2 μ of H_2O cryodeposit were added and then increases with increasing thickness. At the largest thickness, 3.25 mm, the reflectance appears to have reached a maximum for amorphous ice at these wavelengths. However, for a wavelength of 1.0 μ (Fig. 16d), the reflectance appears to be very thickness dependent even at the largest thickness. At wavelengths of 1.50 and 1.95 μ (Figs. 16e and f), the reflectance is independent of thickness after an initial deposit is formed. Overall it is observed that the reflectance increases more rapidly with thickness as the wavelength decreases. When the deposit was warmed forming hexagonal ice, the reflectance increased substantially at all wavelengths as indicated by the arrow in each figure. At a wavelength of 1.00 μ, the reflectance doubled from 0.40 to 0.81 after the deposit warmed, while at 1.50 μ, it went from 0.02 to 0.20, a factor of 10, and at 1.95 μ, it went from 0.02 to 0.13, a factor of 6.

In Fig. 17, the effect of view angle on the reflectance is presented for view angles from zero to 60 deg. The results are presented for various thicknesses at the specified wavelengths of 0.40, 0.50, 1.00, 1.50, and 1.95 μ. These deposits were formed at a flow rate of 0.099 μsec and a pressure of 6.7 x 10^{-3} torr. There are no major variations with view angle, and the curves follow the general shapes expected for smooth dielectric surfaces. In Fig. 17, there is no change in the view angle dependence with wavelength, and there is no significant change with thickness. These same trends were observed on all H_2O cryodeposits. The reflectance of a water cryodeposit is less dependent on view angle than is a carbon dioxide deposit.

The reflectance of water cryodeposits formed under similar conditions of temperature, pressure, and deposition rate seemed to vary somewhat. Figure 18 shows the reflectance of three water cryodeposits formed on a black substrate under similar conditions. The wavelength is 0.5 μ, and the view angle is zero deg. At the small thicknesses, the reflectances are nearly identical. However, at the larger thicknesses, the reflectances are somewhat different, but they were within ±0.05 of the average. These differences might be due to differences in particle size in the deposit. After warming the deposits to form hexagonal ice, the reflectances are within ±0.02 of the average value, showing fairly good agreement.

SECTION VI
THEORETICAL RESULTS

A theoretical study was conducted to determine the reflectance of an absorbing and multiple scattering media. This study is described in Refs. 1 and 9. The results were used to determine the reflectance of cryodeposits at different deposit thicknesses. These reflectances were then compared with the experimental reflectances found in this study which gave a comparison of the theory and experiment. The theory assumed that the front surface of the deposit and the substrate both obeyed Fresnel's reflection equations. Internally, the deposit was assumed to be an absorbing and isotropic scattering medium. By using two experimental spectral reflectances found at different deposit thicknesses and the theoretical equations, the absorption, k, and isotropic scattering, σ, coefficients of the deposit were calculated at the specified wavelength. By using these calculated values of absorption and scattering coefficients, the cryodeposit reflectance was then calculated for other deposit thicknesses.

Figure 19 shows the comparison between the theoretical and experimental spectral reflectances for a CO_2 cryodeposit on a black paint substrate. In the figures, the tabulated n is the refractive index of the deposit, σ is the isotropic scattering coefficient, k is the absorption coefficient of the deposit, $\bar{n}$ is the complex refraction index of the substrate, ψ is the view angle, and λ is the wavelength of light. The comparisons are made for wavelengths of 0.50, 0.61, 0.70, 0.793, 0.90, and 1.00 μ. In Fig. 19, both the theoretical and experimental reflectances are also tabulated with thickness. The arrows indicate the two experimental values used to calculate the monochromatic absorption and scattering coefficients of the cryodeposits. These coefficients were used to calculate the theoretical curves. The maximum difference between theory and experiment is 0.03, but almost all the values agree to within less than 0.01 which is within the reproducibility of the measured reflectance values.

Figure 20 shows a similar comparison between the theoretical and experimental reflectances of a water cryodeposit on a black substrate. These comparisons are at wavelengths of 0.50, 0.55, 0.60, 0.65, and 0.70 μ. The maximum difference between theory and experiment is 0.04, but almost all of the values again agree to within 0.01. The comparisons in Figs. 19 and 20 show the excellent agreement between theory and experiment for cryodeposits.

SECTION VII
DISCUSSION

The reflectances of both carbon dioxide and water cryodeposit-substrate complexes have been presented in Figs. 5 through 20. The presence of these cryodeposits can have an appreciable effect on the solar radiative properties of materials. The amount of effect depends on view angle, deposit thickness, and wavelength or wavelength range of interest.

In Fig. 21, the reflectances of both CO_2 and H_2O are shown together in order to directly compare their effect on the black substrate. The reflectances were measured at a wavelength of 0.50 μ and a view angle of zero deg. First, notice that when the cryodeposit is very thin, 3 μ, it lowers the reflectance of the black substrate from 0.04 to 0.03 for CO_2 and to 0.02 for H_2O. As the thickness increases, the reflectance increses rapidly. However, the reflectance increases more rapidly for the H_2O cryodeposit. At a thickness of 0.4 mm, the H_2O reflectance drops below that of CO_2, and it remains below, finally

reaching a maximum 0.14 lower than CO_2 at the largest thickness. When the H_2O deposit is warmed, it changes structure and is 0.12 more reflecting than CO_2. The reflectance behavior in Fig. 21 can be explained by using the theory discussed previously. Figure 22 shows a theoretical comparison of the reflection by CO_2 and H_2O cryodeposits on a black substrate taken from Figs. 19 and 20. The wavelength is again 0.5 μ, and the view angle is 20 deg. Note the overall similarity between the theory shown in Fig. 22 and the experimental results shown in Fig. 21. With the formation of the cryodeposit, the reflectance drops because of the decrease in the relative refractive index of the substrate. Although there is the additional reflection from the top of the cryodeposit, this is not enough to compensate for the lower reflection from the substrate. The reflection from the top of the deposit is the major part of the reflected light at a thickness of 3 μ since the substrate contributes less than 0.002 for either a water or carbon dioxide deposit. Carbon dioxide drops to a minimum reflectance of about 0.03, while water drops to 0.02 because of its smaller refractive index. At the smaller thicknesses, there is very little scattering to increase the reflectance. As the thickness increases beyond 3 μ, the reflectance of both deposits increases rapidly as scattering increases. However, the reflectance of the water increases faster and is soon larger than that for the CO_2 deposit (Figs. 21 and 22). This is because the critical angle of internal reflection is larger for water which allows more of the scattered light to escape from the deposit. Finally, as the deposit thickness increases still further to the largest thicknesses, the CO_2 deposit becomes more reflecting since it has more scattering and less absorption than the water deposit and multiple scattering reduces the critical angle effect. The dominant effect is the higher scattering in the CO_2 caused by its higher refractive index and larger particle size. It is reasonable to say CO_2 deposits have a larger particle size since they are crystalline and the water is amorphous. Moreover, when the water deposit is warmed and transforms to hexagonal ice, its reflectance is larger than that of CO_2. Thus, scattering with increased particle size is the primary cause of the difference in reflectance between CO_2 and water deposits at the largest thicknesses.

The results presented here have a direct bearing on solar radiation problems beyond giving spectral reflectance values and an explanation of what causes them. By using the spectral reflectance values found in this study, the total reflected intensity for all solar wavelengths was calculated for various sources of incident light. The results are shown in Fig. 23 for a CO_2 cryodeposit on a black substrate with a Johnson Curve source, with a xenon arc lamp inside a solar simulation chamber (12V chamber), and with a 1000-watt tungsten-halogen lamp which is sometimes used for solar simulation. As seen

in Fig. 23, there is a substantial difference between the amount of energy reflected using the sun (Johnson Curve) as a source and using a solar simulator consisting of a xenon arc or a 1000-watt lamp. The difference is present at all deposit thicknesses. At the largest thickness, the xenon reflectance is 0.05 below the solar reflectance and the 1000-watt lamp reflectance is 0.23 below it. The results shown here not only illustrate the effect of the presence of a cryodeposit on total reflectance, but also the appreciable effect that spectral mismatch between a solar simulator and the sun can have on solar simulation testing of any material. The total reflectance with a zero-deg view angle of a CO_2 cryodeposit on the black substrate is shown in Fig. 24 for a 6000°K blackbody which is very similar to the sun. Here the thickness is plotted on a logarithmic scale in order to emphasize the smaller thickness. Notice that the total reflectance of the cryodeposit complex is less than that of the bare substrate for deposit thicknesses up to 60 μ.

The presence of CO_2 and H_2O cryodeposits will also have a direct effect on testing in a solar simulation chamber. When thin cryodeposits (less than 50 microns) form on any surface in a solar simulation chamber, they reduce the reflectance of the surface at all solar wavelengths. This effect is strongest for a water cryodeposit. Although the absolute change is relatively small, from 0.04 to 0.02, this represents decreasing the total reflected energy by 50 percent. It is, therefore, possible to make the cooled (77°K or less) black walls of a solar simulation chamber even blacker by coating them with a thin cryodeposit. If the water cryodeposit is used to decrease the reflectance of a material, it is important not to allow the deposit to warm above 110°K since it would transform to a highly scattering, and thus highly reflecting, deposit. Larger cryodeposit thickness (greater than 0.2 mm) increases the reflectance of a black surface substantially, regardless of whether the deposit is water or CO_2. At a thickness of 3.4 mm, the total solar reflectance has increased from 0.04 to 0.63 for a CO_2 deposit and to 0.51 for a water deposit. For a hexagonal ice deposit, the total reflectance is about 0.78 at a 3.4-mm thickness.

The results in this study and Refs. 4 and 8 show that CO_2 or H_2O cryodeposits less than 0.2 mm substantially decrease the reflectance of polished stainless steel at all solar wavelengths. For deposits greater than 0.4 mm thick, the reflectance at wavelengths less than 0.7 μ is increased, while in the infrared region it is decreased. The results for polished stainless steel indicate that cryodeposits on cooled lenses or mirrors would greatly reduce the image quality and transmission by deposit scattering even for very small thicknesses. For thicknesses less than about 5 μ, thin film interference must also be considered in the deposit reflection and transmission. All these effects

can be very important in tests which employ cooled optics when deposit thicknesses greater than 10 microns would probably render then unusable at solar wavelengths.

The results presented here are also of interest with respect to the physical properties of cryodeposits. Previously, phase changes in water cryodeposits from amorphous to cubic to hexagonal were studied and monitored by calorimetric techniques and X-ray or electron diffraction. Figures 12, 13, and 14 show that measuring the reflectance gives a sensitive indication of the phase of the deposit and the occurrence of phase changes (particle size changes). This is particularly true at a wavelength of 1.0 μ. No phase changes were observed in this study of CO_2 cryodeposits. However, it is expected that CO_2 deposits formed on 20°K surfaces would be amorphous and that phase changes could be monitored as the deposit warms by monitoring the deposit reflectance. The results for spectral and total reflectance presented here also have a direct application to the study of planetary frosts. The CO_2 and H_2O cryodeposits were formed under similar conditions of temperature and pressure as the polar caps of Mars. Thus the results are directly applicable to both spectral and solar reflectance of the Martian polar caps. The water cryodeposit reflectance results might also be applied to studies of the reflectances of comets depending on their composition.

SECTION VIII
SUMMARY

In situ spectral reflectance measurements were made of both carbon dioxide and water cryodeposits formed on liquid-nitrogen-cooled surfaces under vacuum. The reflectances were measured for the solar wavelength range from 0.30 to 2.55 μ with view angles from zero to 60 deg using a 12-in.-diam integrating sphere. Measurements of the reflectance of both CO_2 and H_2O cryodeposits on a black epoxy painted test surface were made for deposit thickness from 0.002 to 3.5 mm. On the black surface, the cryodeposits decreased the reflectance for small deposit thicknesses. This was particularly true for water deposits which reduced the reflectance at all solar wavelengths for deposits up to 50 μ thick.

For the larger deposit thicknesses, a CO_2 deposit increased the black surface reflectance substantially at all wavelengths. For a thickness of 3.5 mm, the reflectance increased from 0.04 to 0.230 at a wavelength of 2.50 μ, and from 0.047 to 0.800 at a wavelength of 0.35 μ. The total reflectance of a CO_2 deposit on a black substrate has also been

presented. For an amorphous water cryodeposit 3.25 mm thick, the reflectance of the black surface increased for all wavelengths less than 1.6 μ but decreased for longer wavelengths. The amount of reflectance change increased with decreasing wavelength. For a hexagonal ice deposit 3.25 mm thick, the reflectance is increased at all wavelengths and the change is very wavelength dependent. Absorption bands were seen in the water deposit at 1.04, 1.55, and 2.03 μ.

For a CO_2 deposit formed on a polished stainless steel substrate, the reflectance is decreased at small thicknesses. At the largest thicknesses, the reflectance below a wavelength of 1.00 μ is increased, while at longer wavelengths, it is decreased. A CO_2 absorption band was seen at 2.0 μ for carbon dioxide deposits formed on both a stainless steel and a black substrate.

The formation of either carbon dioxide or water cryodeposits can have a substantial effect on solar simulation testing. These effects are changes in the substrate reflection and changes in resolution and transmission caused by increased scattering for deposits formed on materials and optical components. The changes are dependent on deposit thickness, view angle, substrate, and crystal form in the case of water cryodeposits. The results presented here are also applicable to studies of the physical properties of cryodeposits.

REFERENCES

1. Wood, B. E., Smith, A. M., Seiber, B. A., and Roux, J. A. "Infrared Reflectance of CO_2 Cryodeposits." AEDC-TR-70-108 (AD708509), July 1970.

2. Sparrow, E. M. and Cess, R. D. Radiation Heat Transfer, Brooks/Cole Publishing Company, Belmont, California, 1966.

3. Grum, F. and Luckey, G. W. "Optical Sphere Paint and a Working Standard of Reflectance." Applied Optics 7, No. 11, November 1968, pp. 2289-2294.

4. McCullough, B. A., Wood, B. E., Smith, A. M. and Birkebak, R. C. "A Vacuum Integrating Sphere for In Situ Reflectance Measurements at 77°K from 0.5 to 10 μ." Progress in Astronautics and Aeronautics, Vol. 20, Academic Press, Inc., New York, 1967, p. 137.

5. Müller, P. R., Frost, W., and Smith, A. M. "Measurements of Refractive Index, Density, and Reflected Light Distributions for Carbon Dioxide and Water Cryodeposits." AEDC-TR-69-179 (AD692714), September 1969.

6. "Standard Method for Absolute Calibration of Reflectance Standards." 1967 Book of ASTM Standards, E 306-66, Vol. 30, American Society for Testing and Materials, Philadelphia, 1967.

7. Eisenberg, D. and Kauzmann, W. The Structure and Properties of Water. Oxford, London, 1969.

8. Wood, B. E., Smith, A. M., Seiber, B. A., and Roux, J. A. "Spectral Absolute Infrared Reflectance Measurements of Water Frosts Formed on LN_2 Cooled Surfaces in Vacuum." AEDC-TR-70-215 (AD715915), December 1970.

9. Roux, J. A. "Radiative Heat Transfer of Coatings on a Cryogenic Surface." Ph. D. Dissertation, 1970, University of Tennessee.

APPENDIX
ILLUSTRATIONS

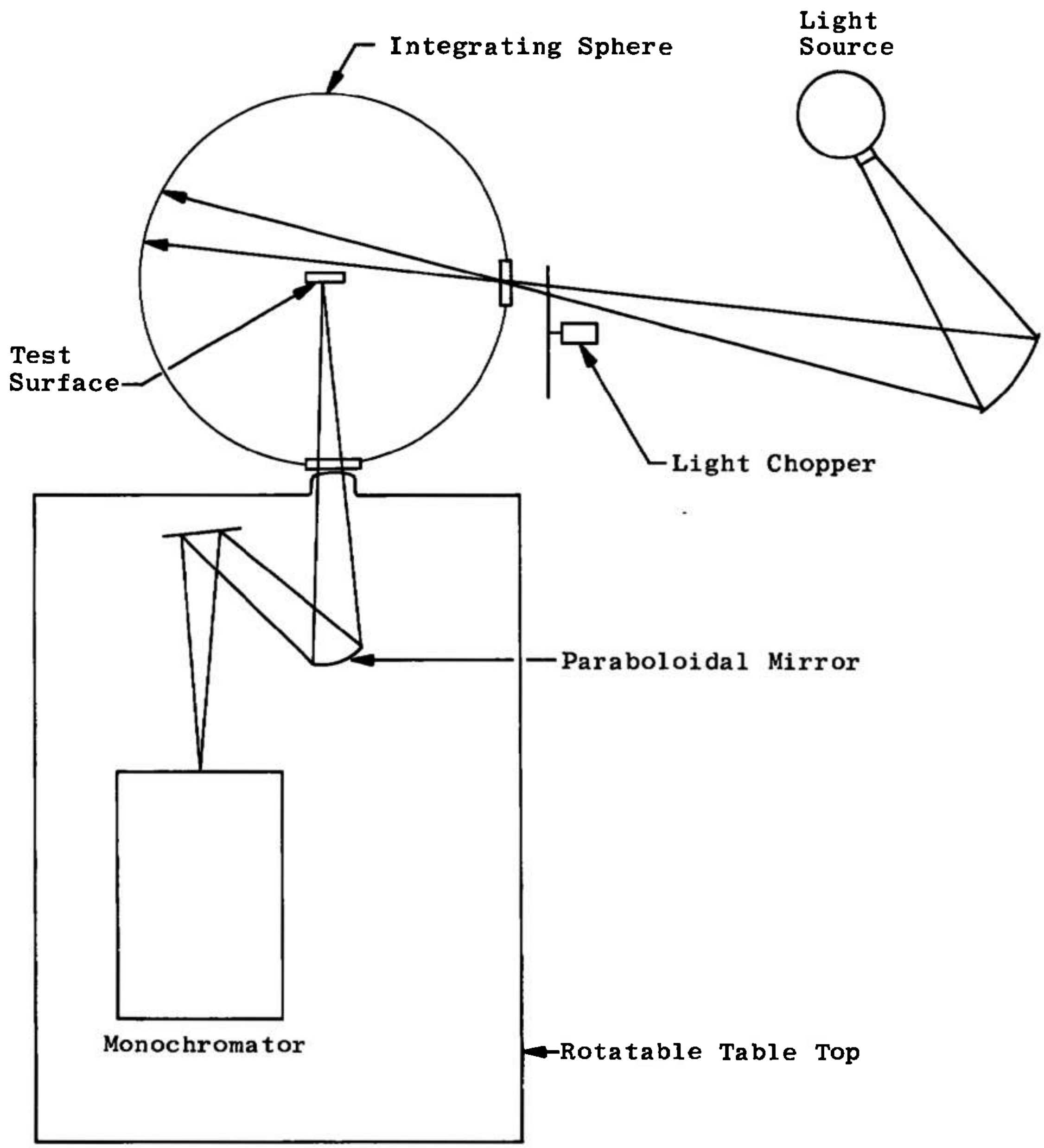

Fig. 1 Schematic of 12-in. Integrating Sphere System

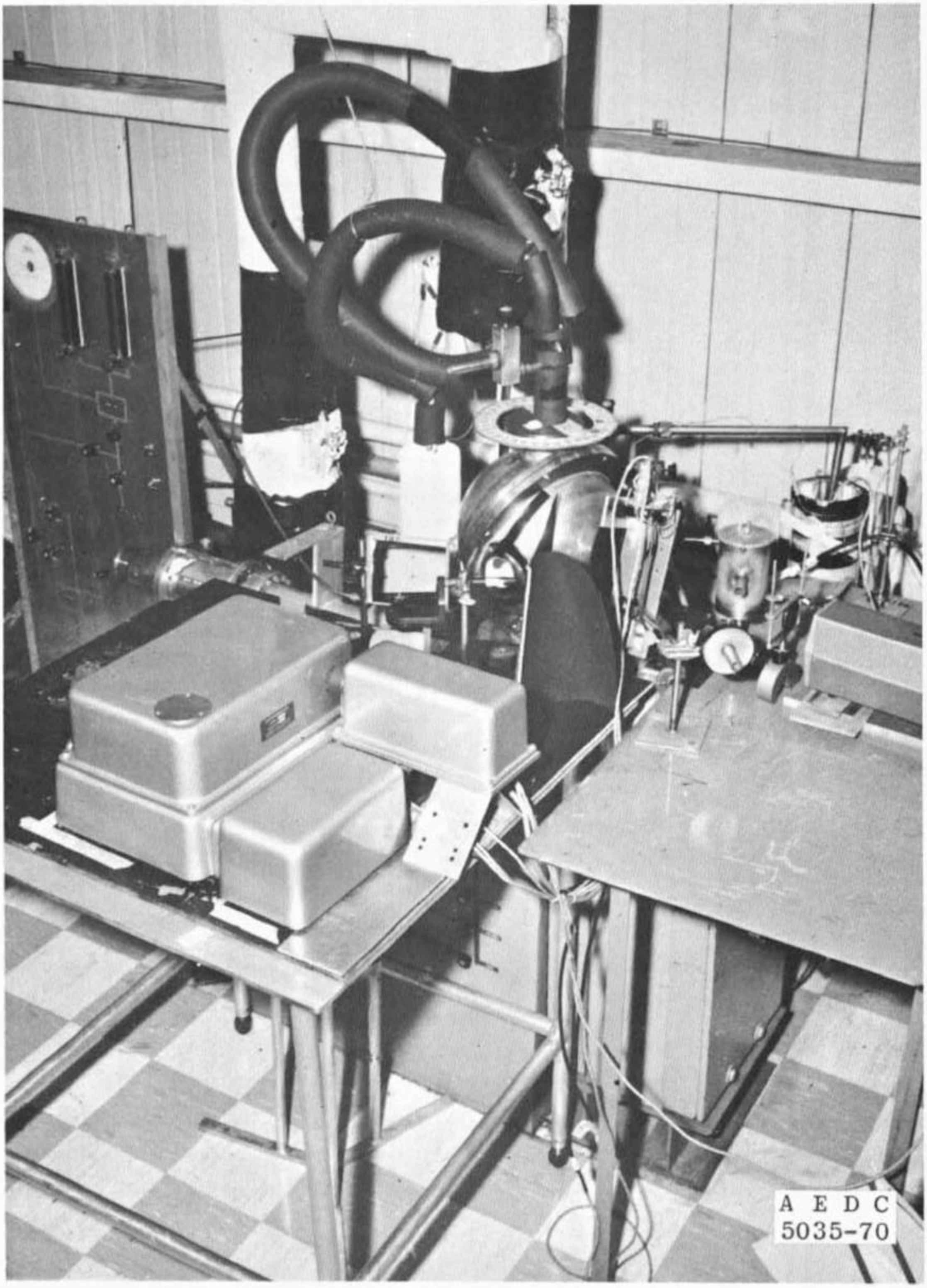

Fig. 2 12-in. Integrating Sphere and Optical System

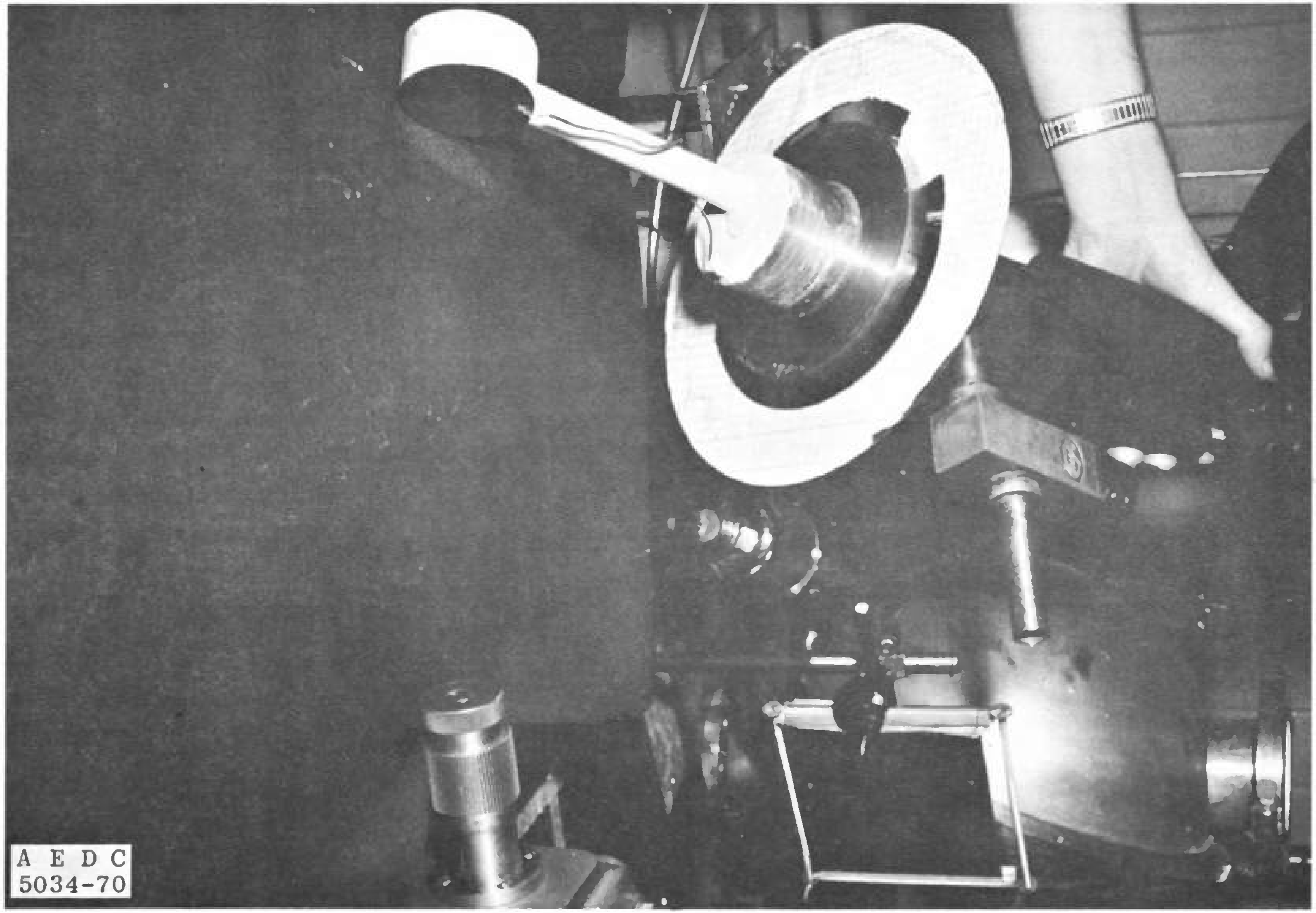

Fig. 3 Cryosurface Assembly

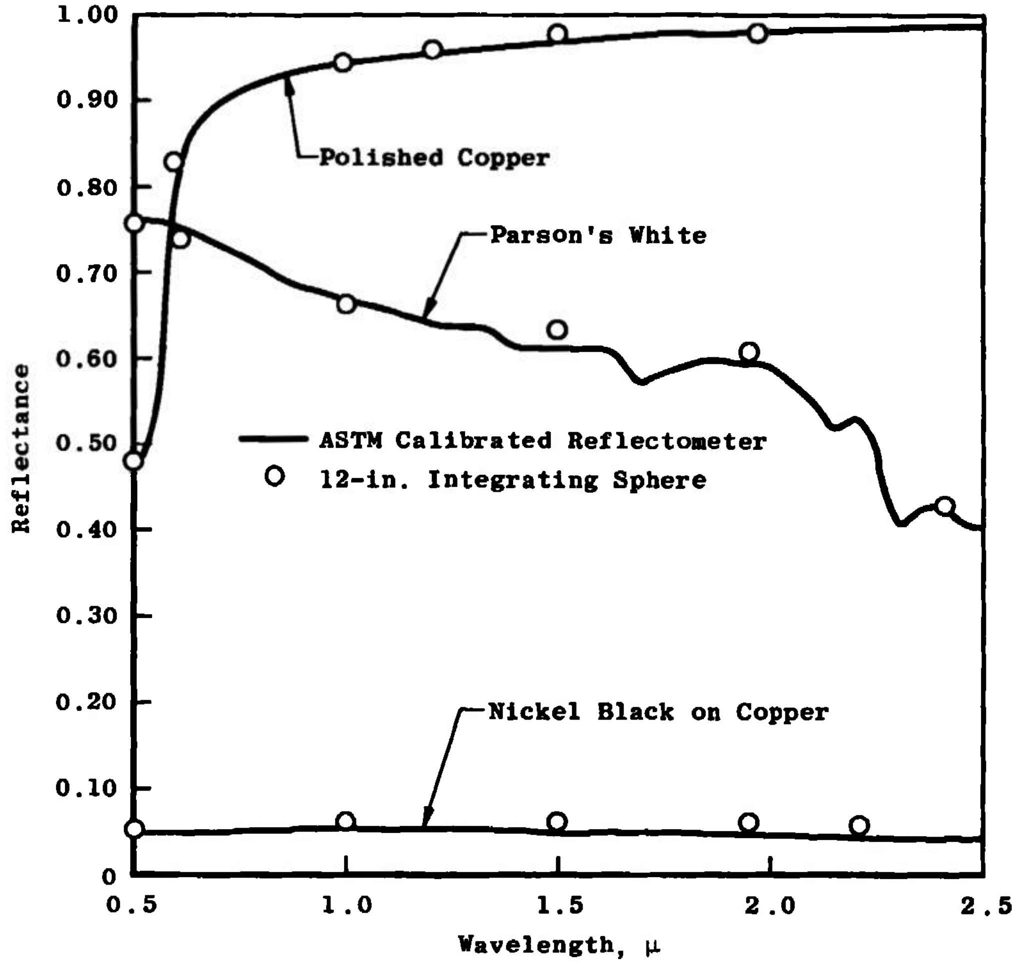

a. Determined Using Two Different Reflectometers
Fig. 4 Comparison of Reflectance Values

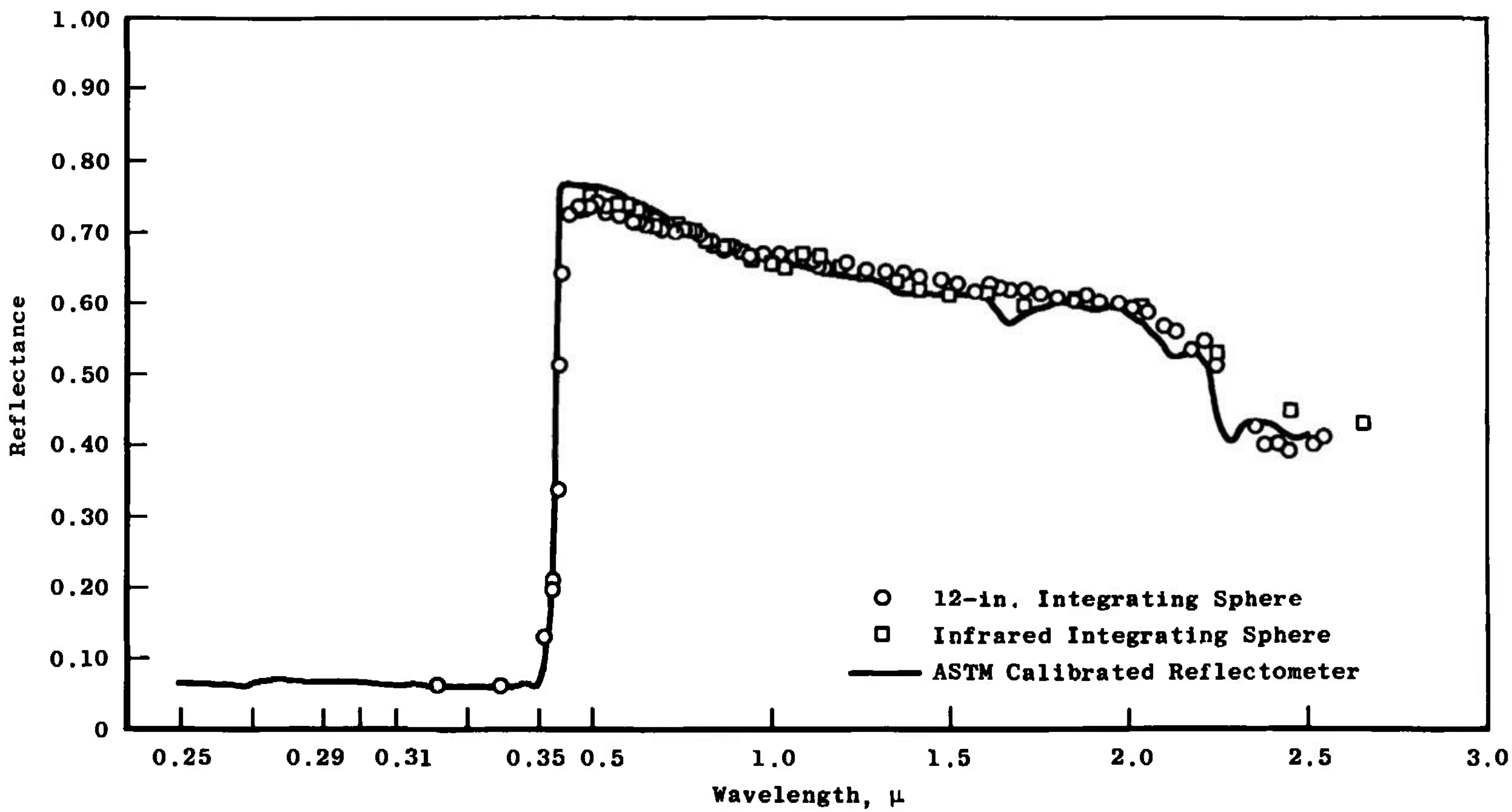

b. Reflectance of a White Epoxy Paint Measured by a Calibrated Reflectometer, an Infrared Integrating Sphere, and the 12-in. Integrating Sphere

Fig. 4 Concluded

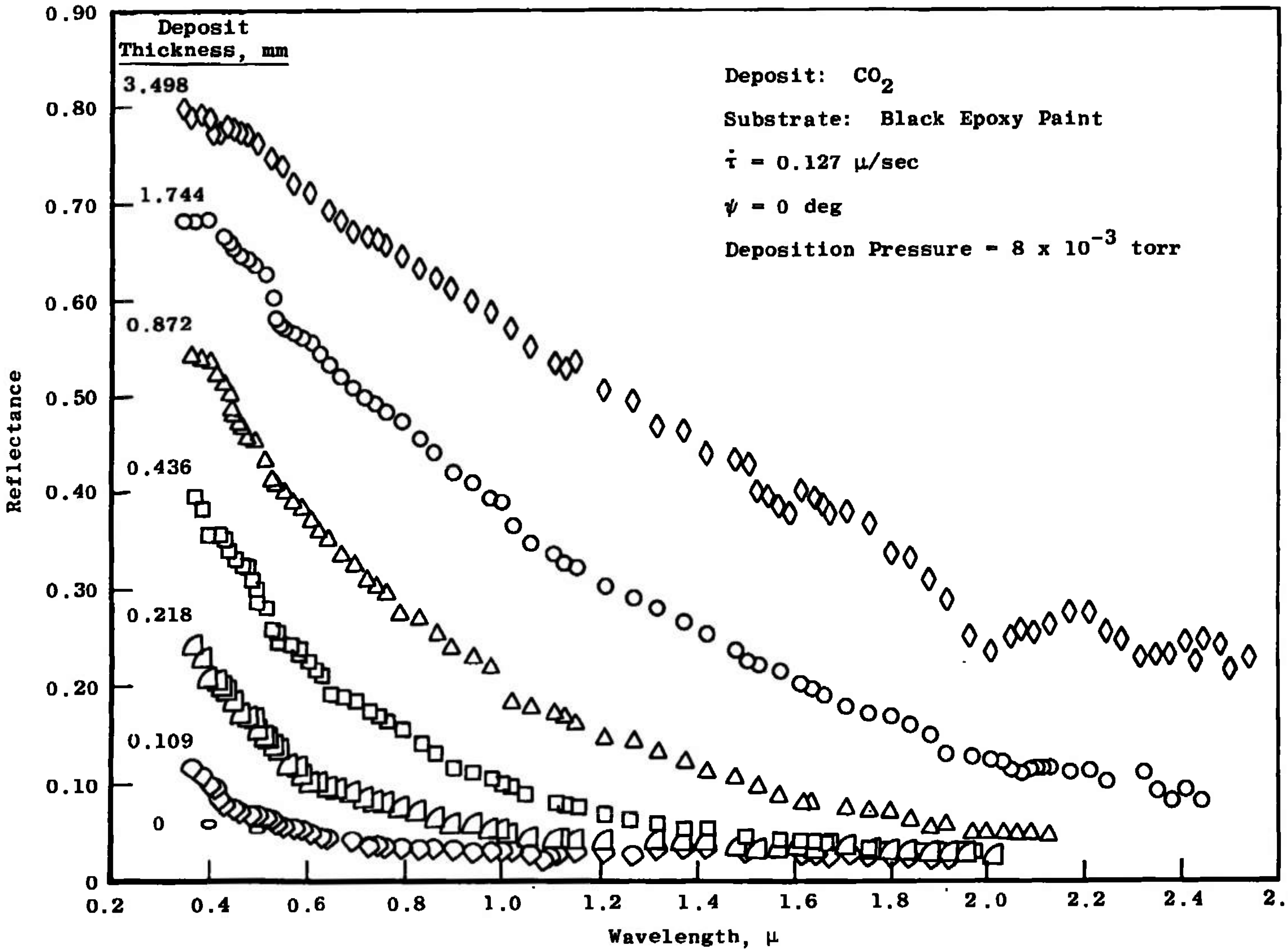

Fig. 5 Reflectance of CO_2 Deposits Formed on Black Epoxy Paint

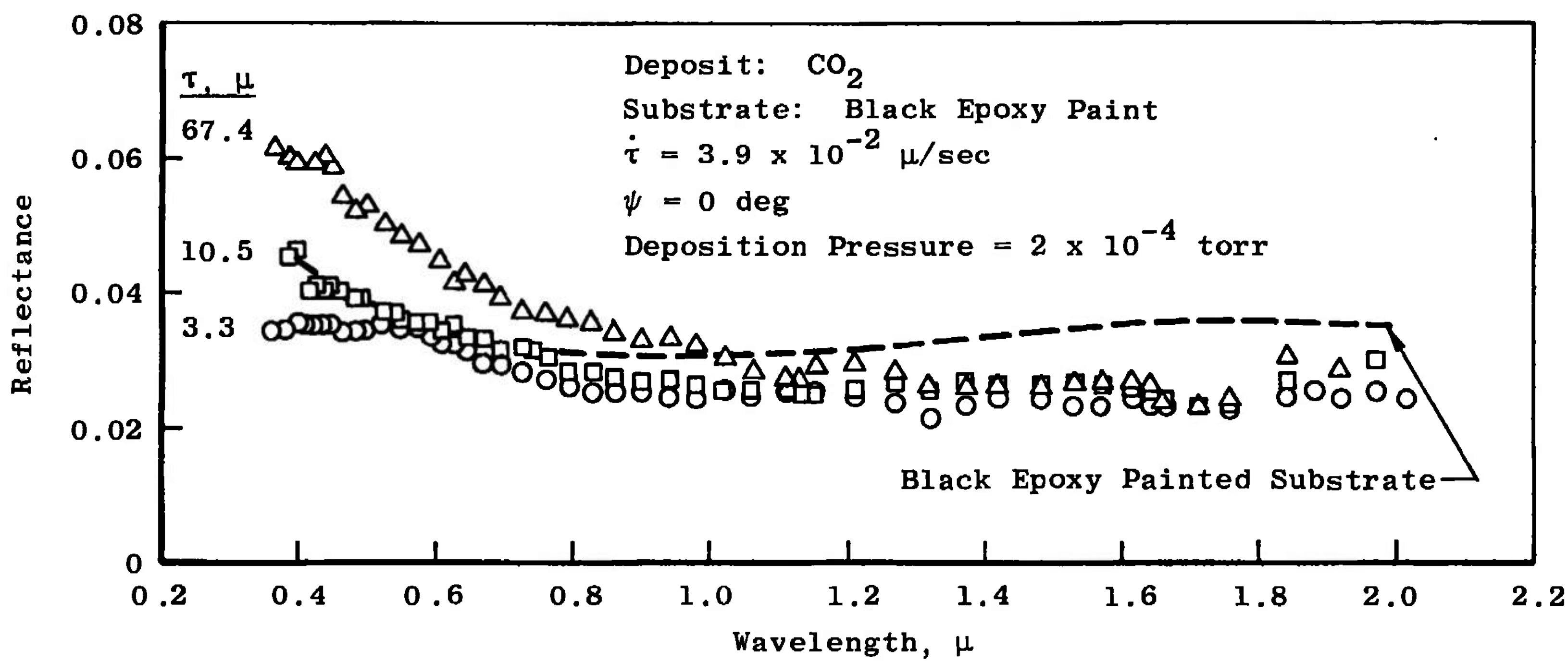

Fig. 6 Reflectance of Thin CO_2 Films on Black Epoxy Paint

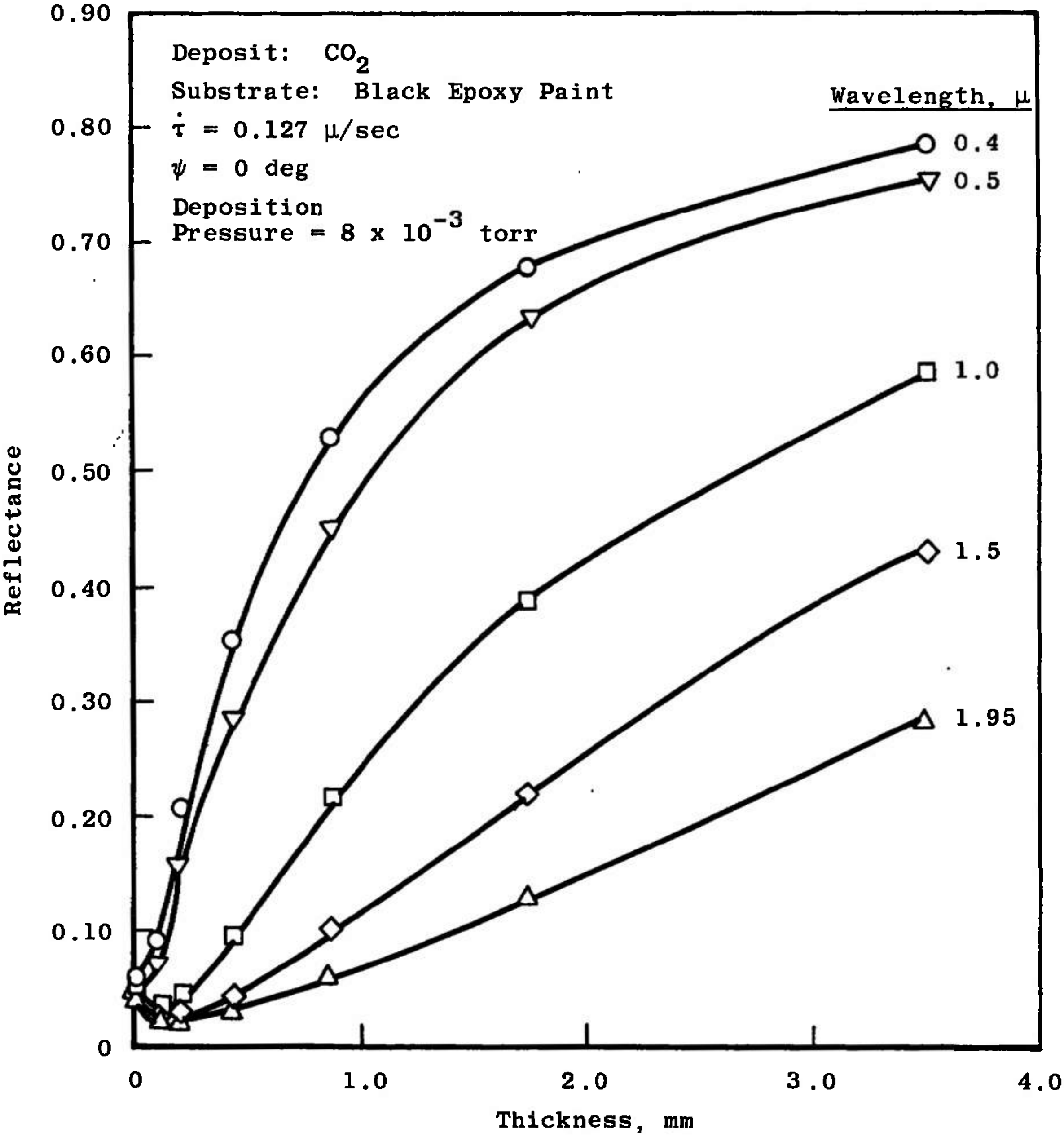

Fig. 7 Reflectance Dependence on Thickness of CO_2 Deposited on Black Epoxy Paint

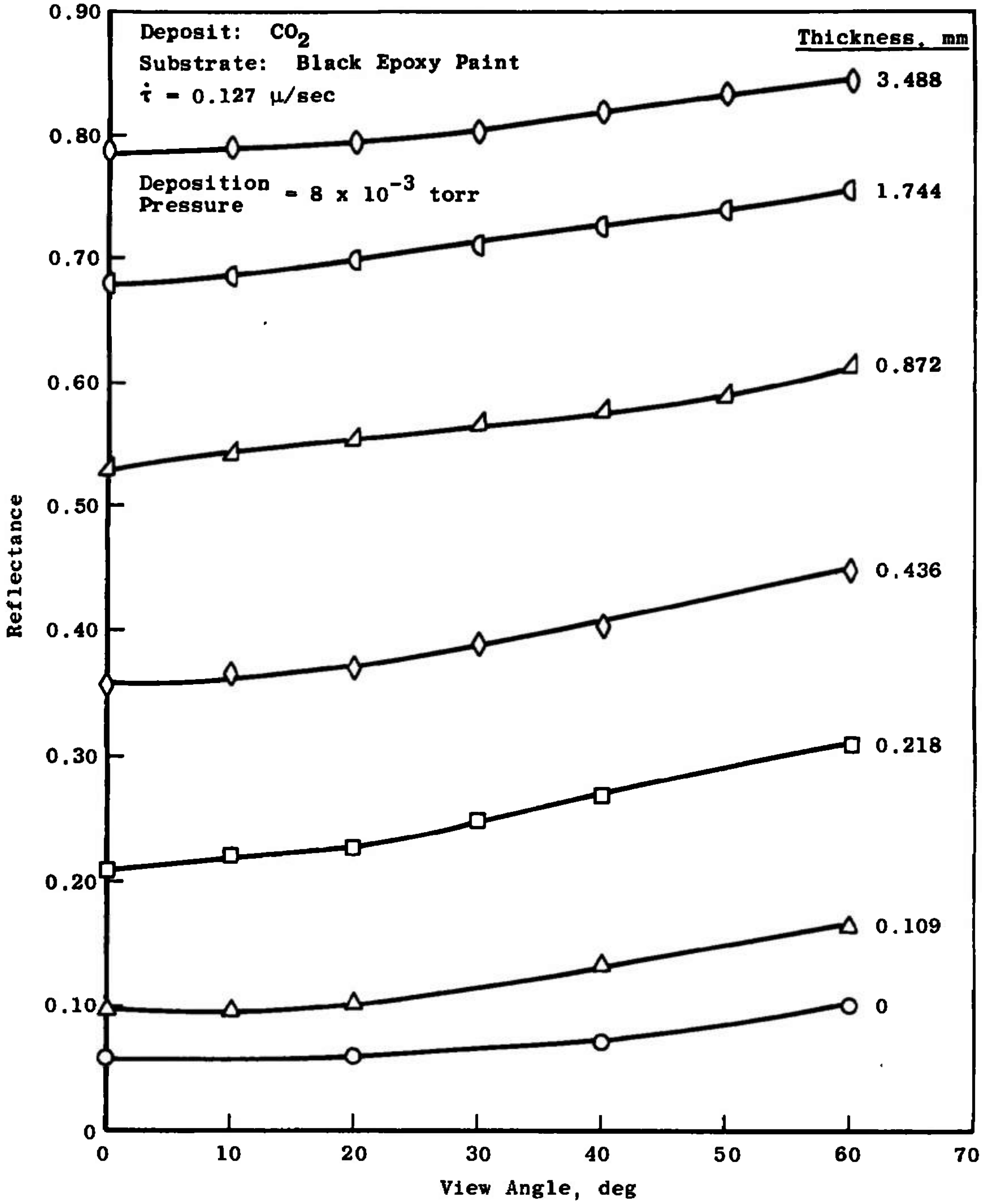

a. $\lambda = 0.4\ \mu$

Fig. 8 Reflectance Dependence on View Angle for CO_2 Deposits on Black Epoxy Paint

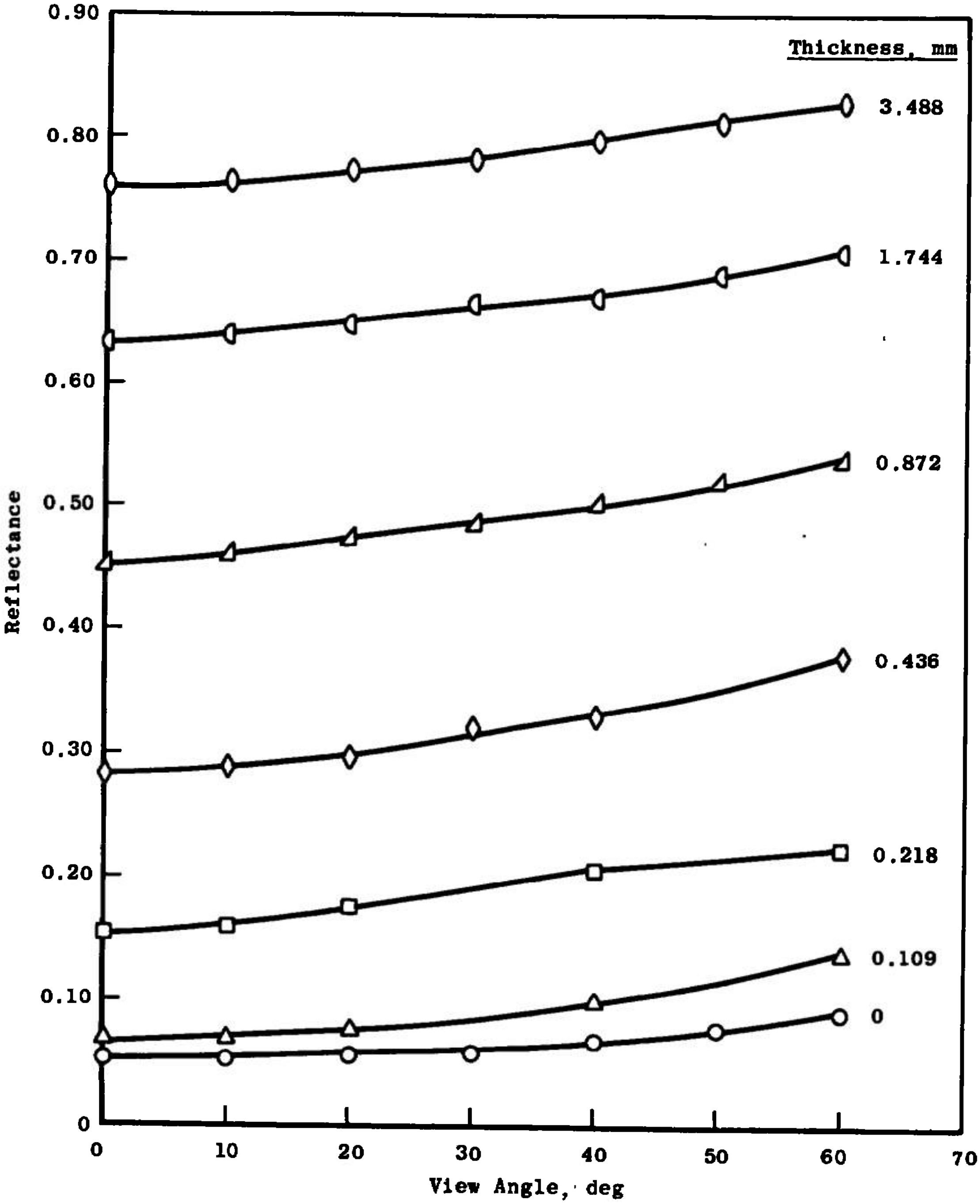

b. $\lambda = 0.5\ \mu$
Fig. 8 Continued

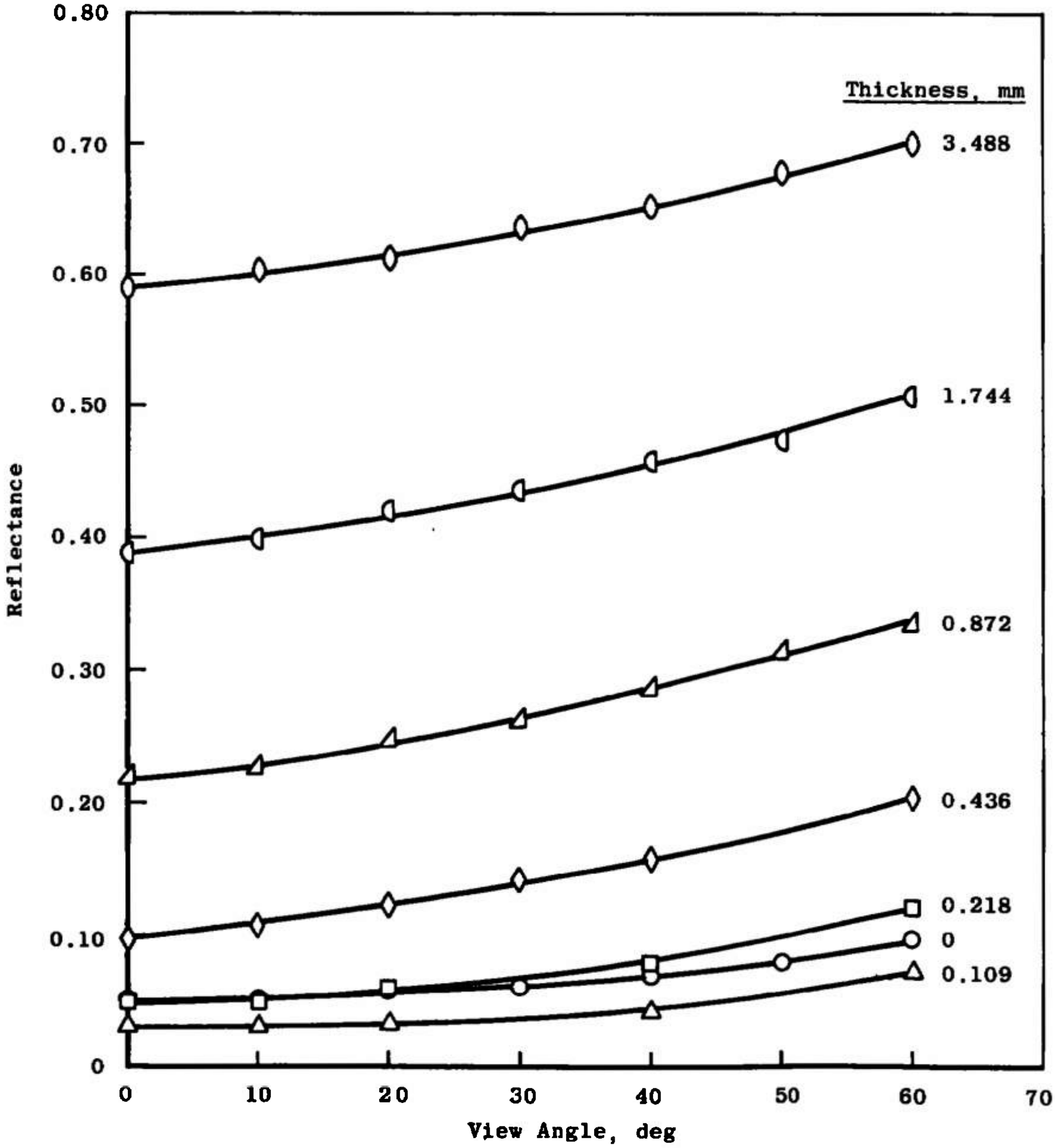

c. $\lambda = 1.0\ \mu$
Fig. 8 Continued

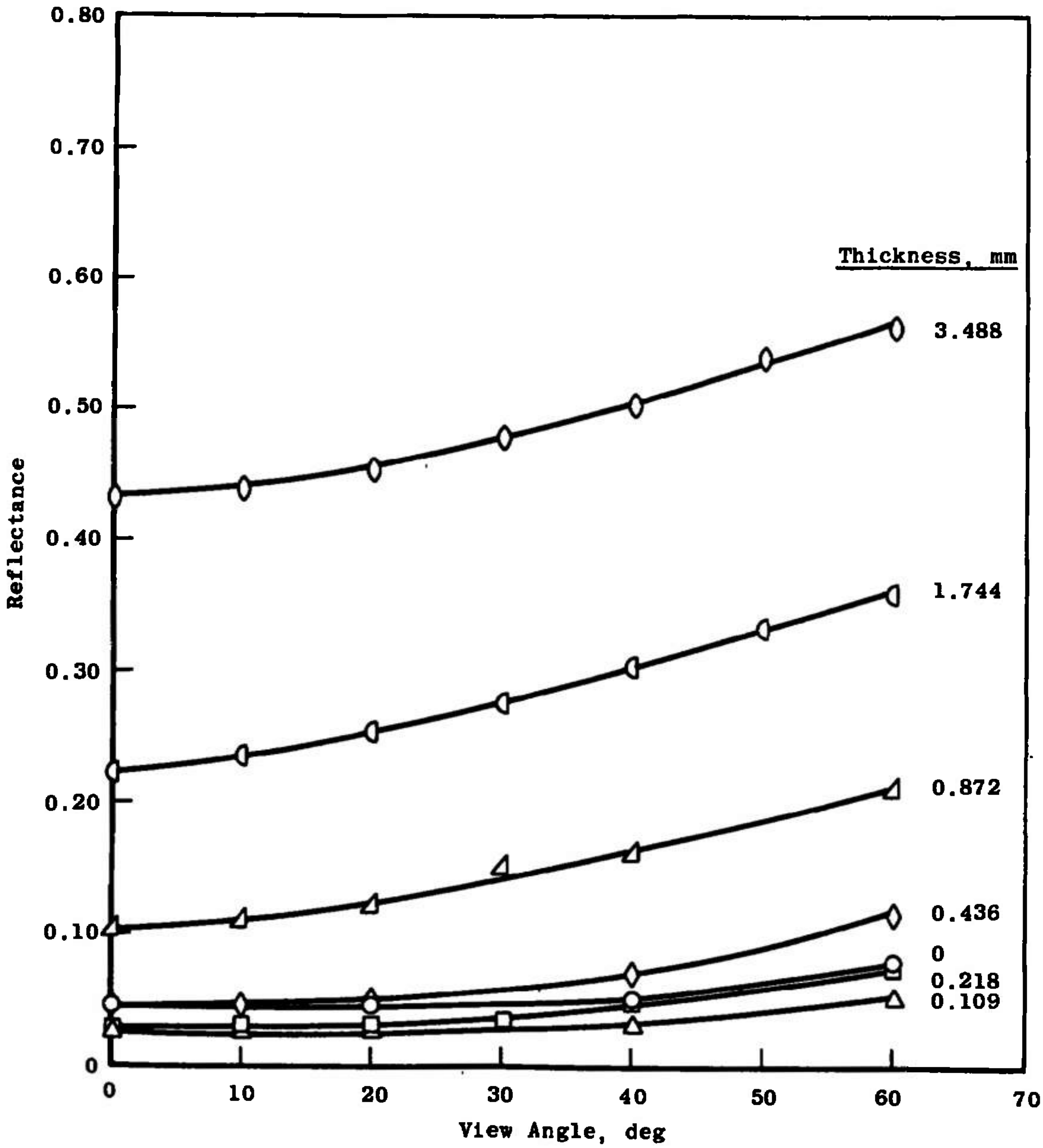

d. $\lambda = 1.5\ \mu$
Fig. 8 Continued

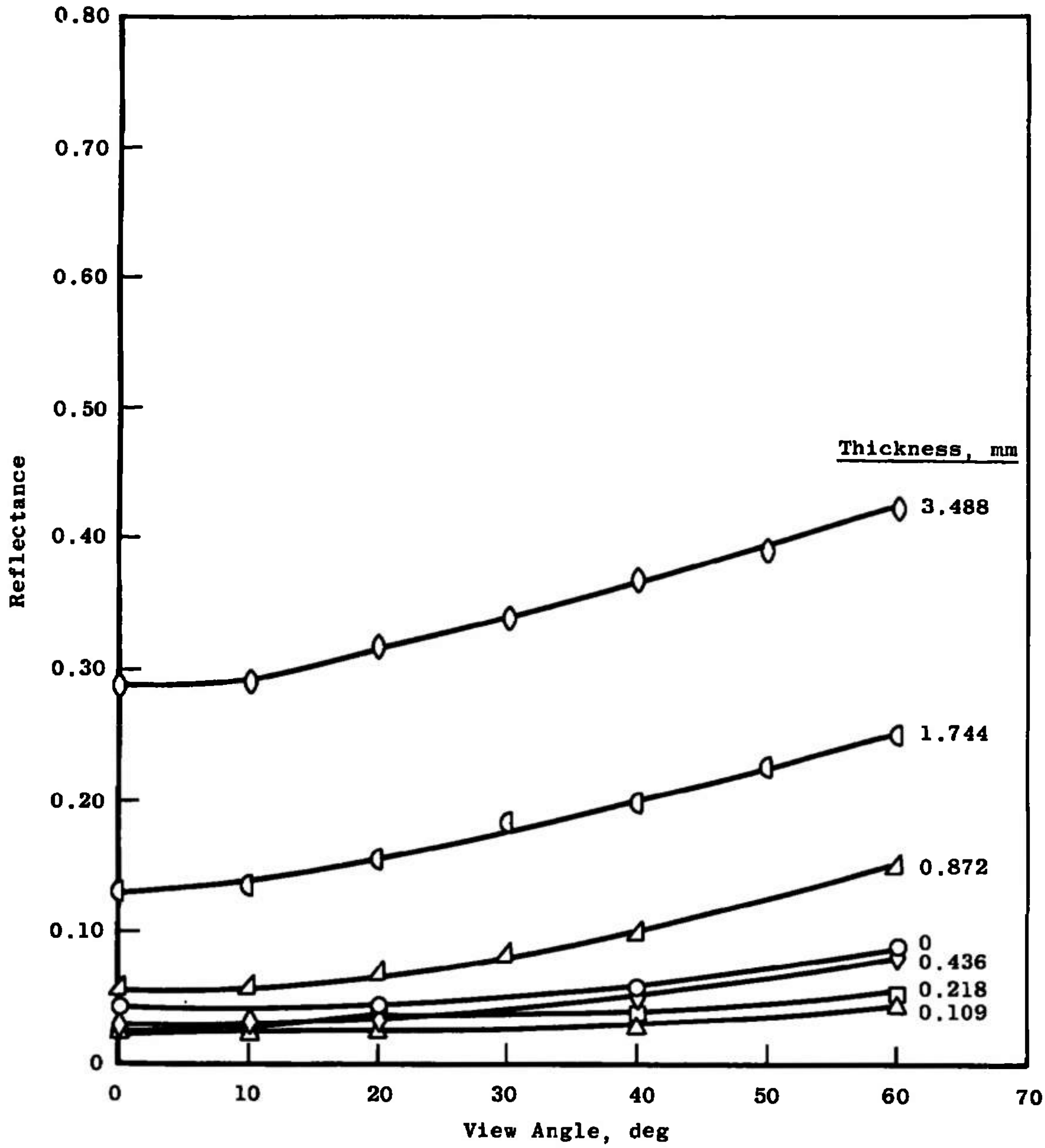

e. $\lambda = 1.95\ \mu$
Fig. 8 Concluded

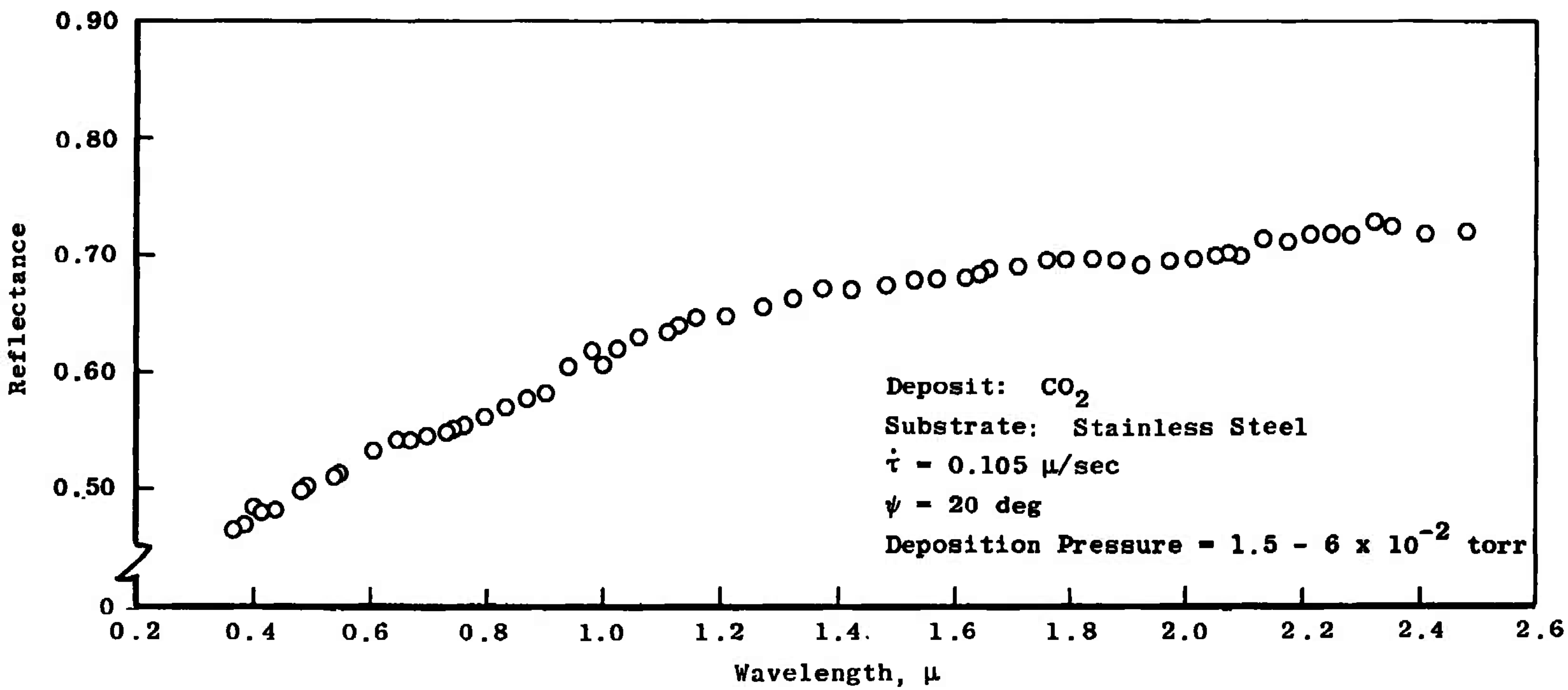

a. τ = 0.0 mm

Fig. 9 Spectral Reflectance of CO_2 Deposits Formed on Polished Stainless Steel

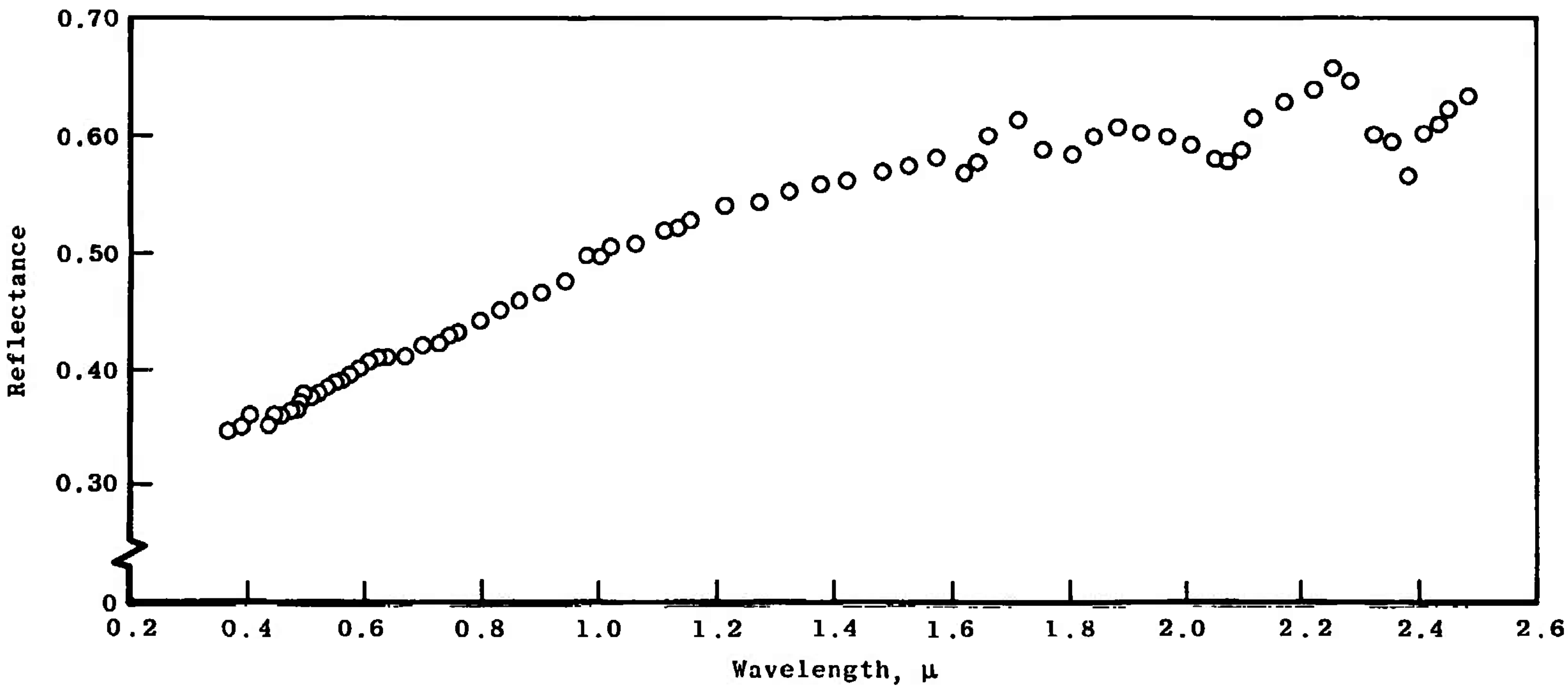

b. $\tau = 5.5\ \mu$
Fig. 9 Continued

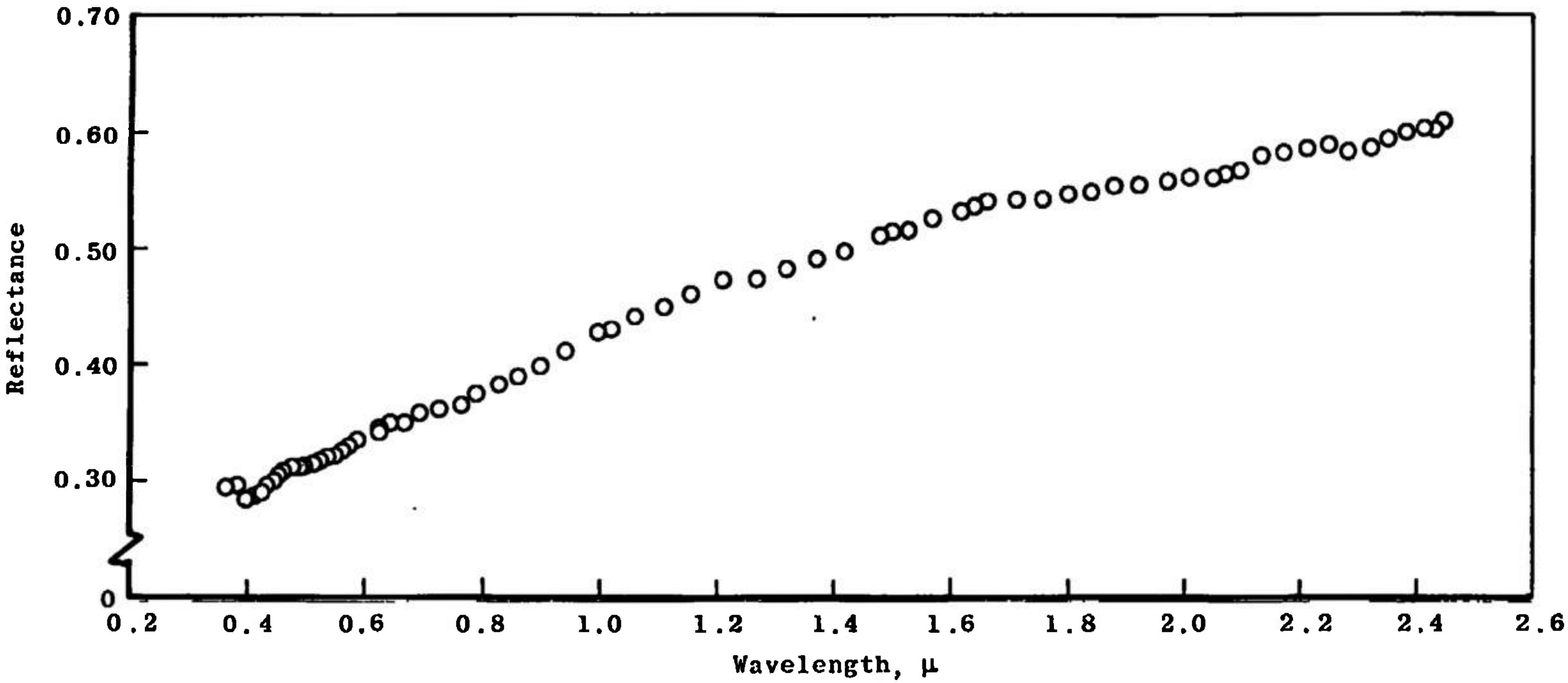

c. $\tau = 48.7\ \mu$

Fig. 9 Continued

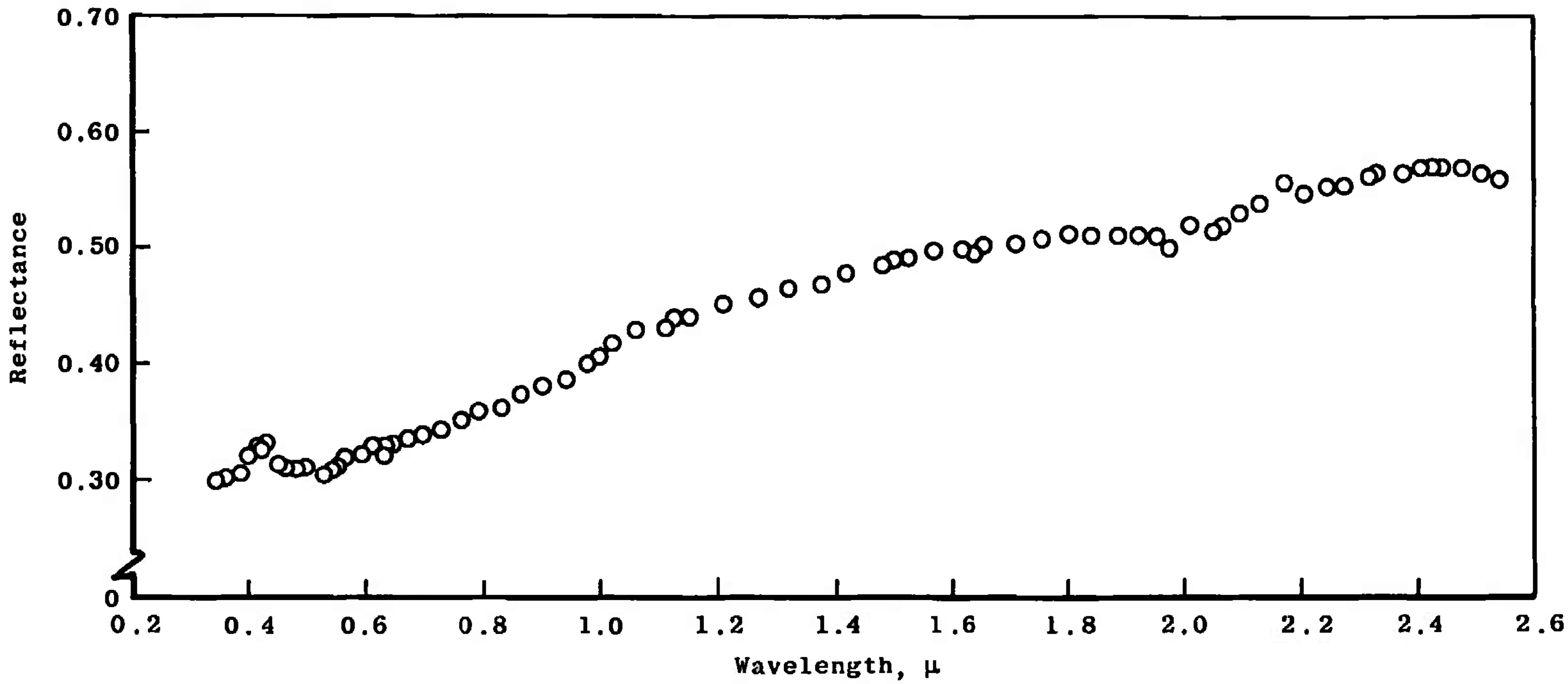

d. τ = 0.09 mm
Fig. 9 Continued

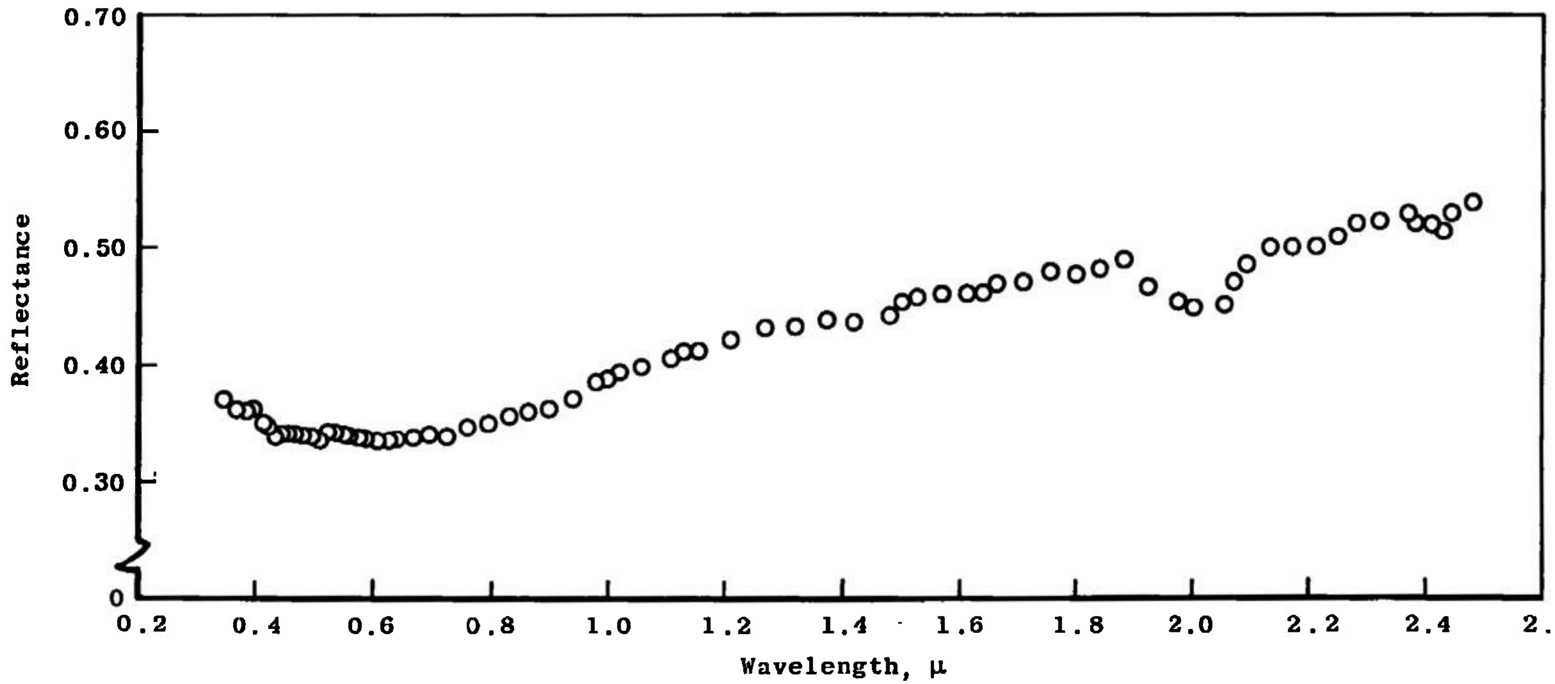

e. τ = 0.18 mm
Fig. 9 Continued

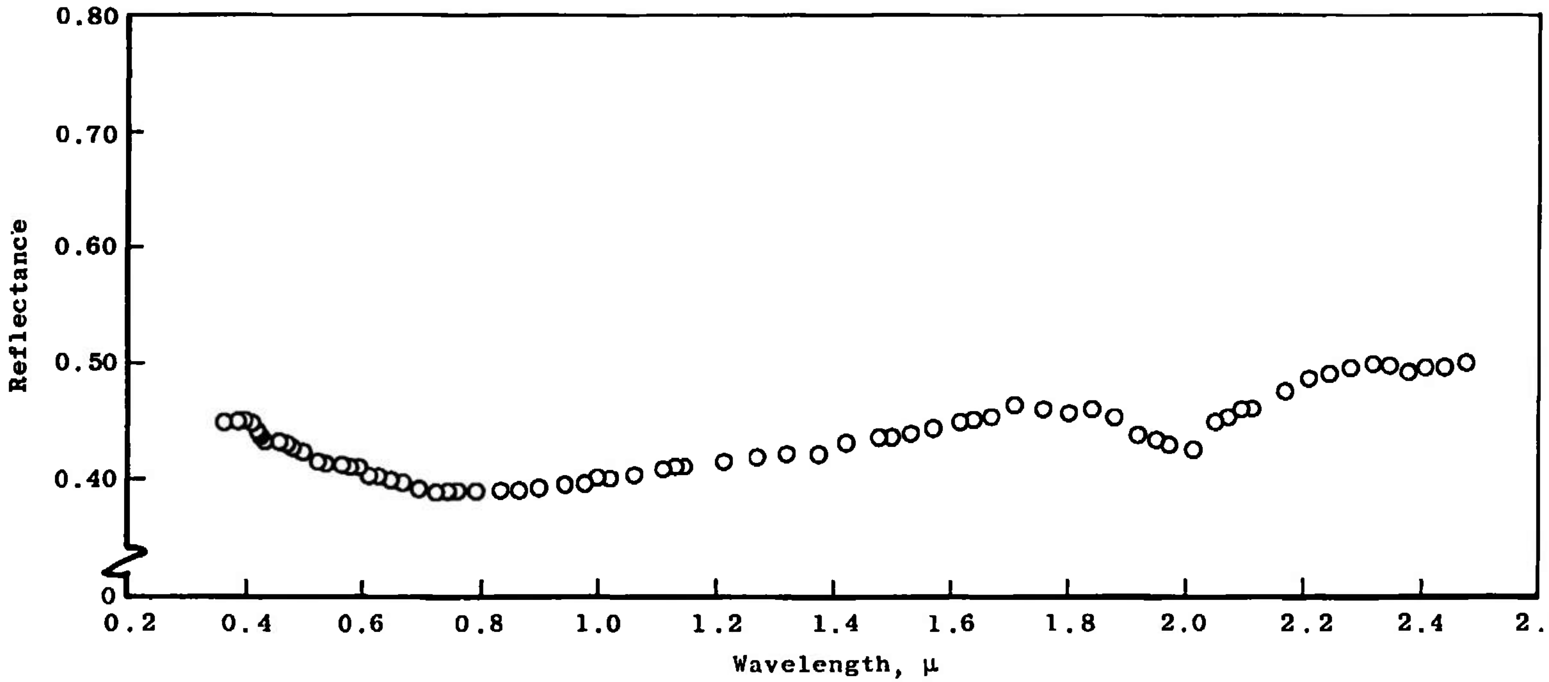

f. $\tau = 0.36$ mm
Fig. 9 Continued

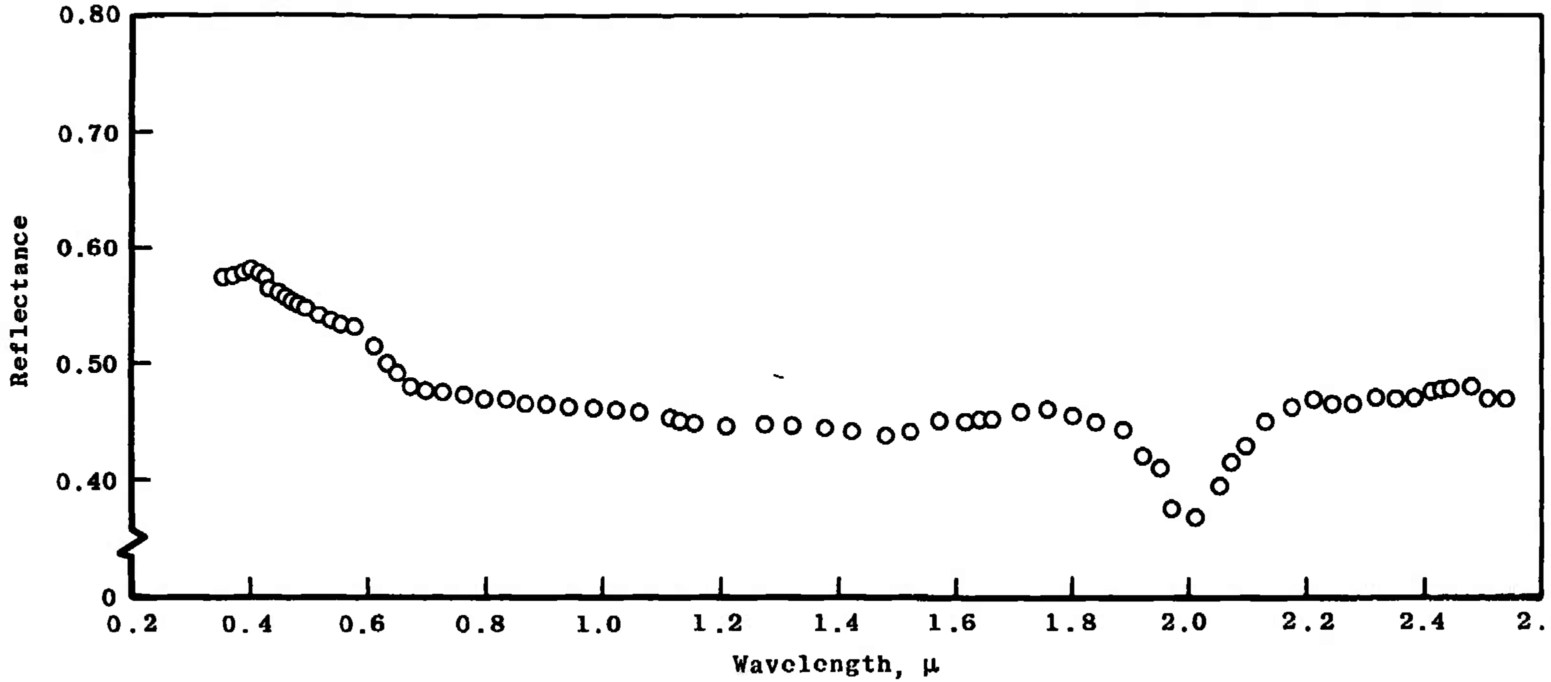

g. τ = 0.72 mm
Fig. 9 Continued

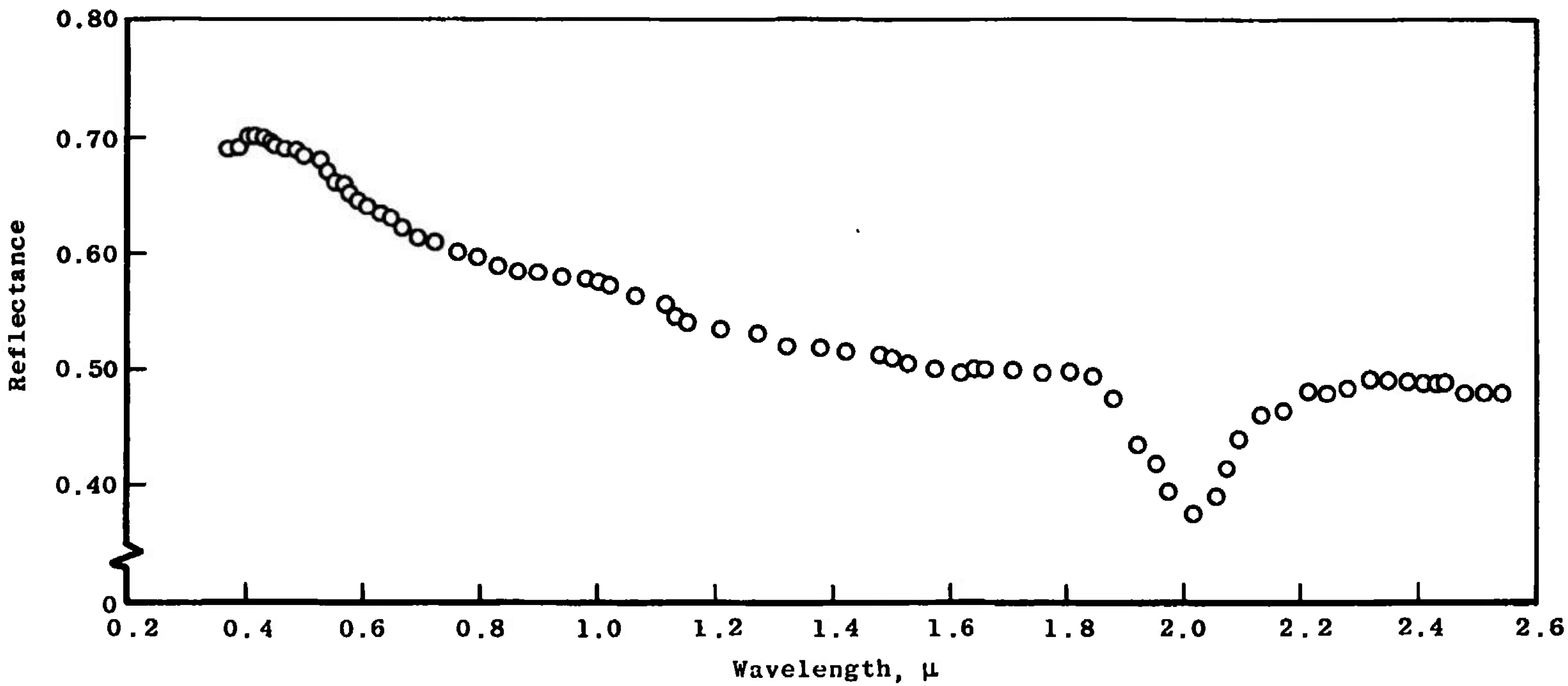

h. τ = 1.441 mm

Fig. 9 Continued

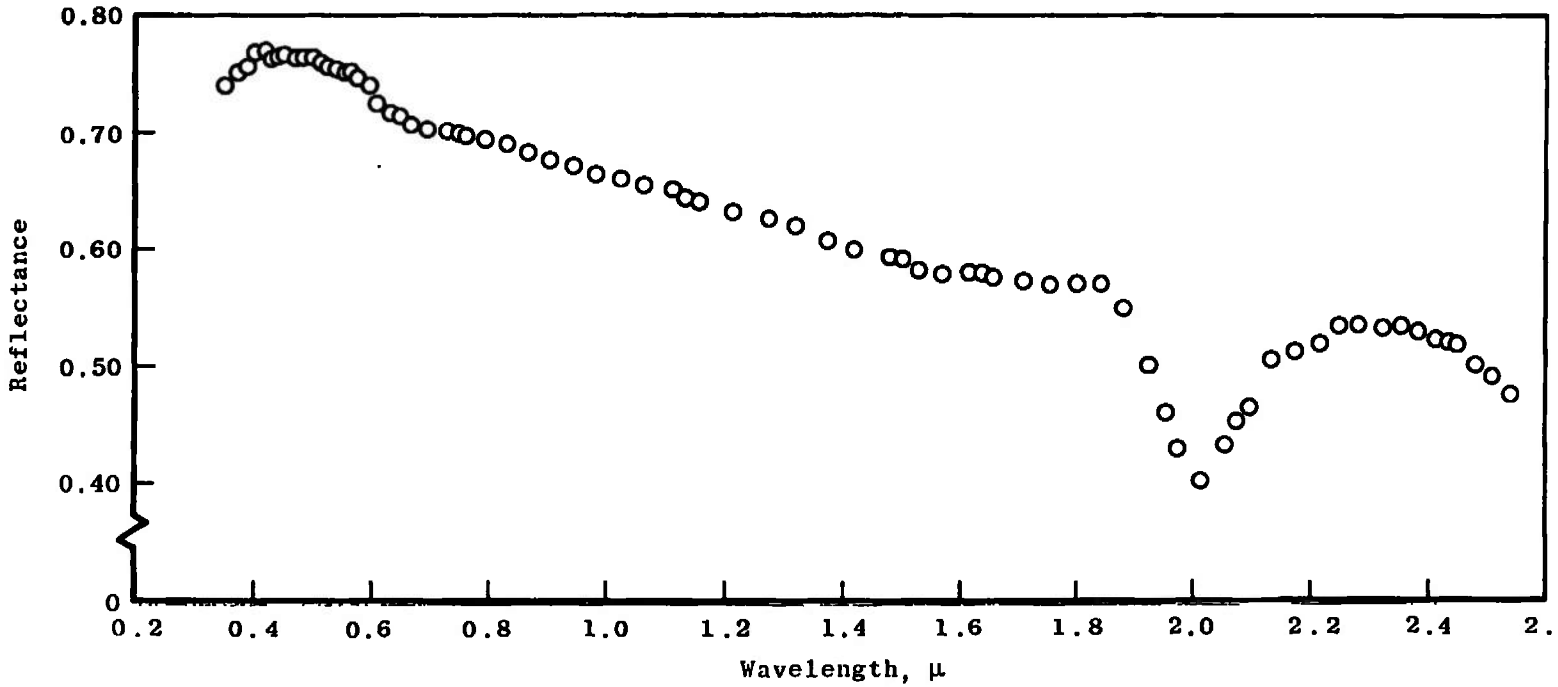

i. τ = 2.88 mm
Fig. 9 Concluded

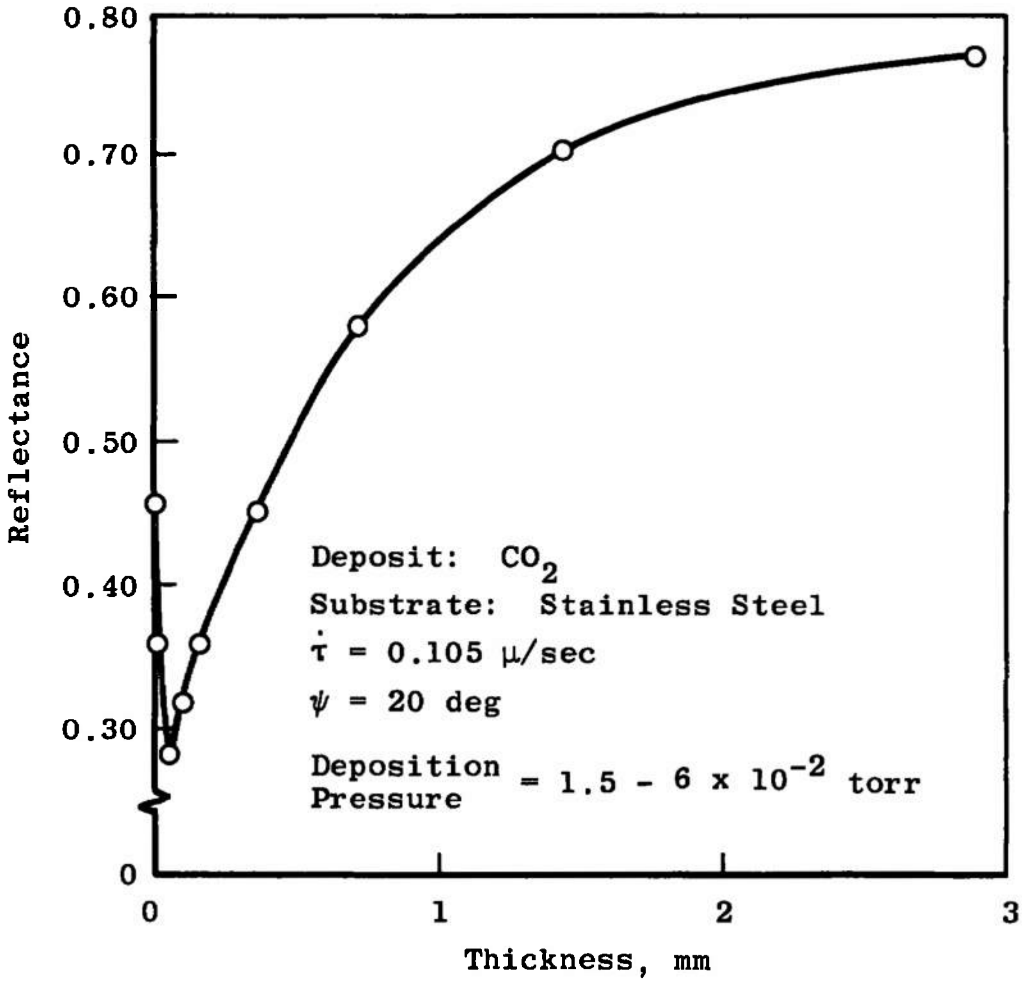

a. λ = 0.40 μ

Fig. 10 Reflectance Dependence on Thickness for CO_2 Deposits Formed on Polished Stainless Steel

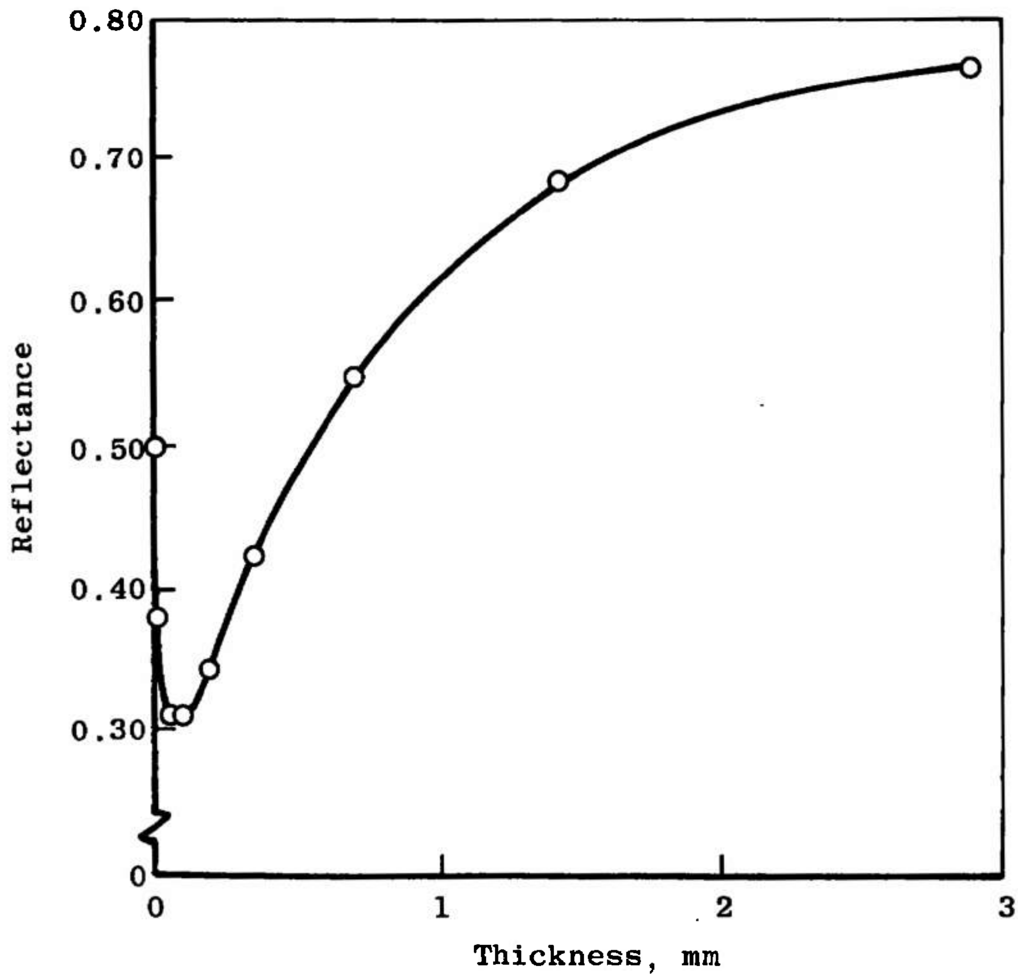

b. $\lambda = 0.50\ \mu$
Fig. 10 Continued

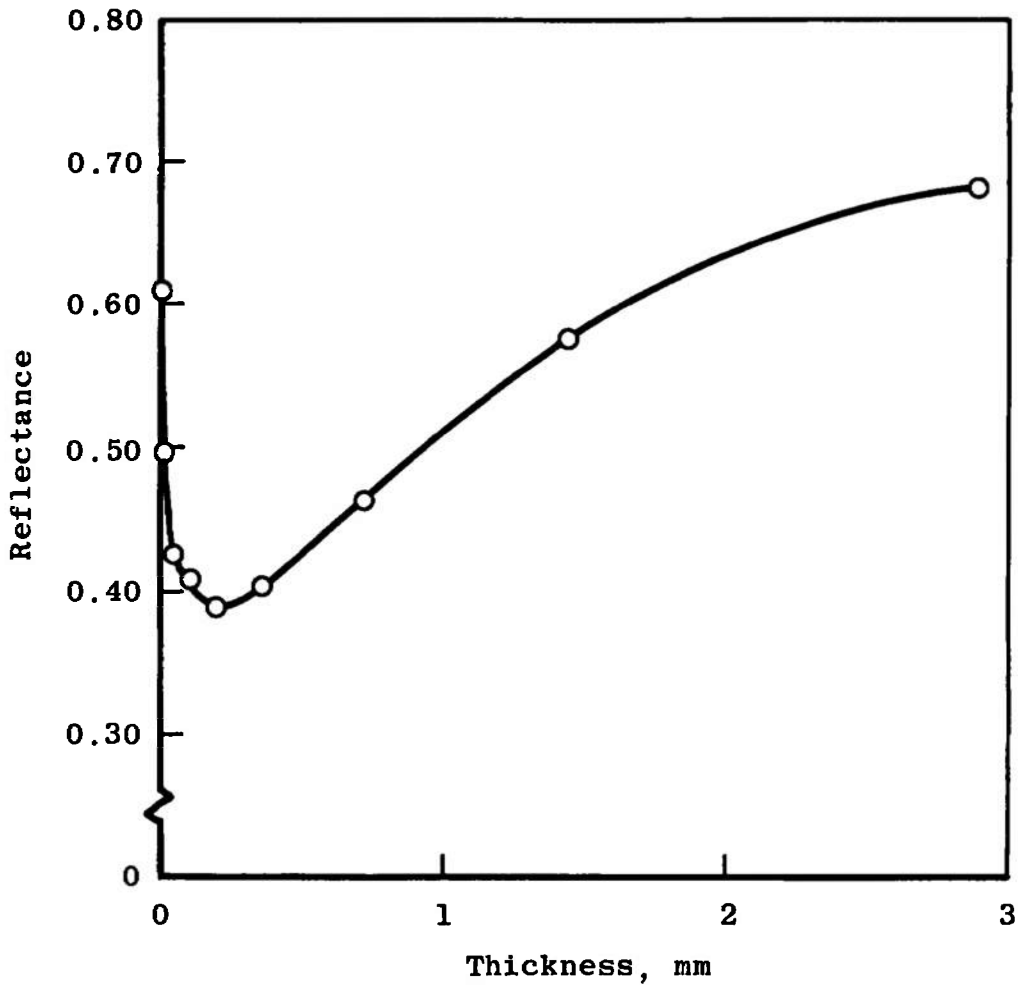

c. $\lambda = 1.00\ \mu$
Fig. 10 Continued

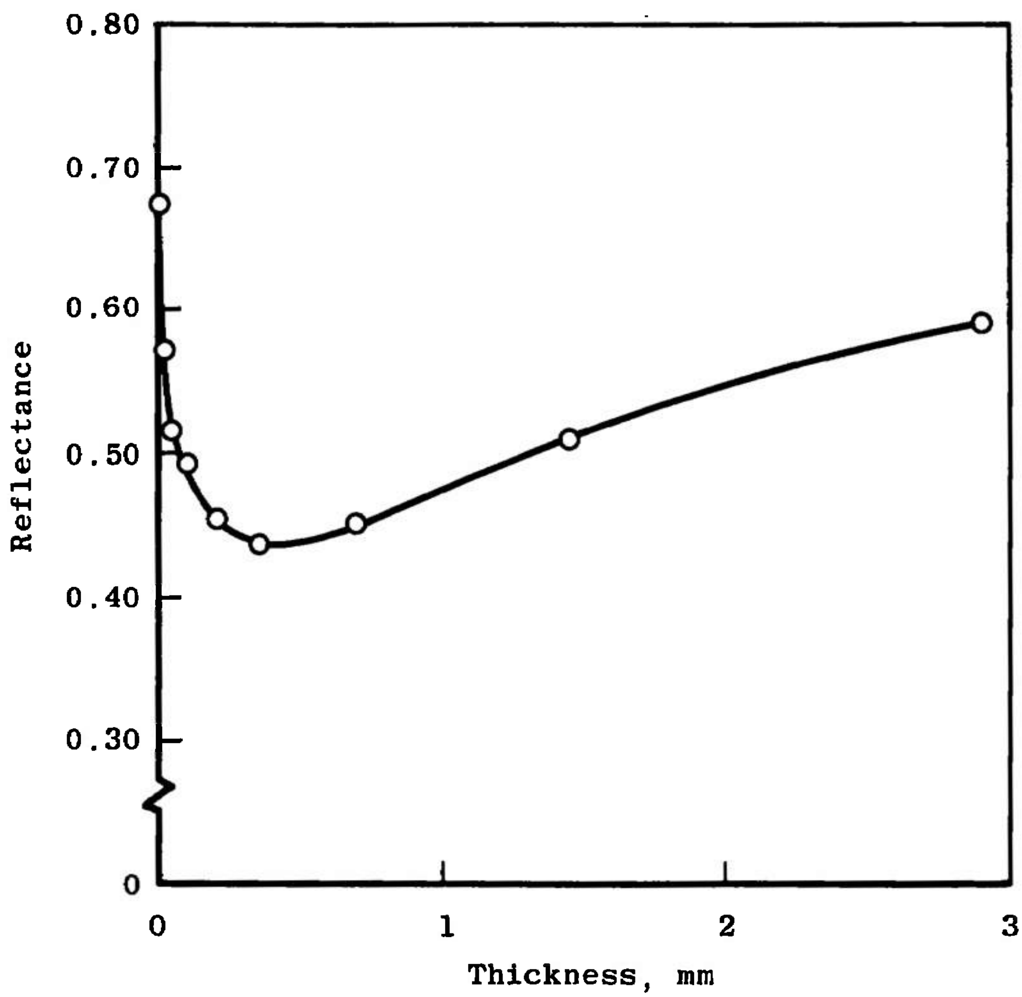

d. $\lambda = 1.50\ \mu$
Fig. 10 Continued

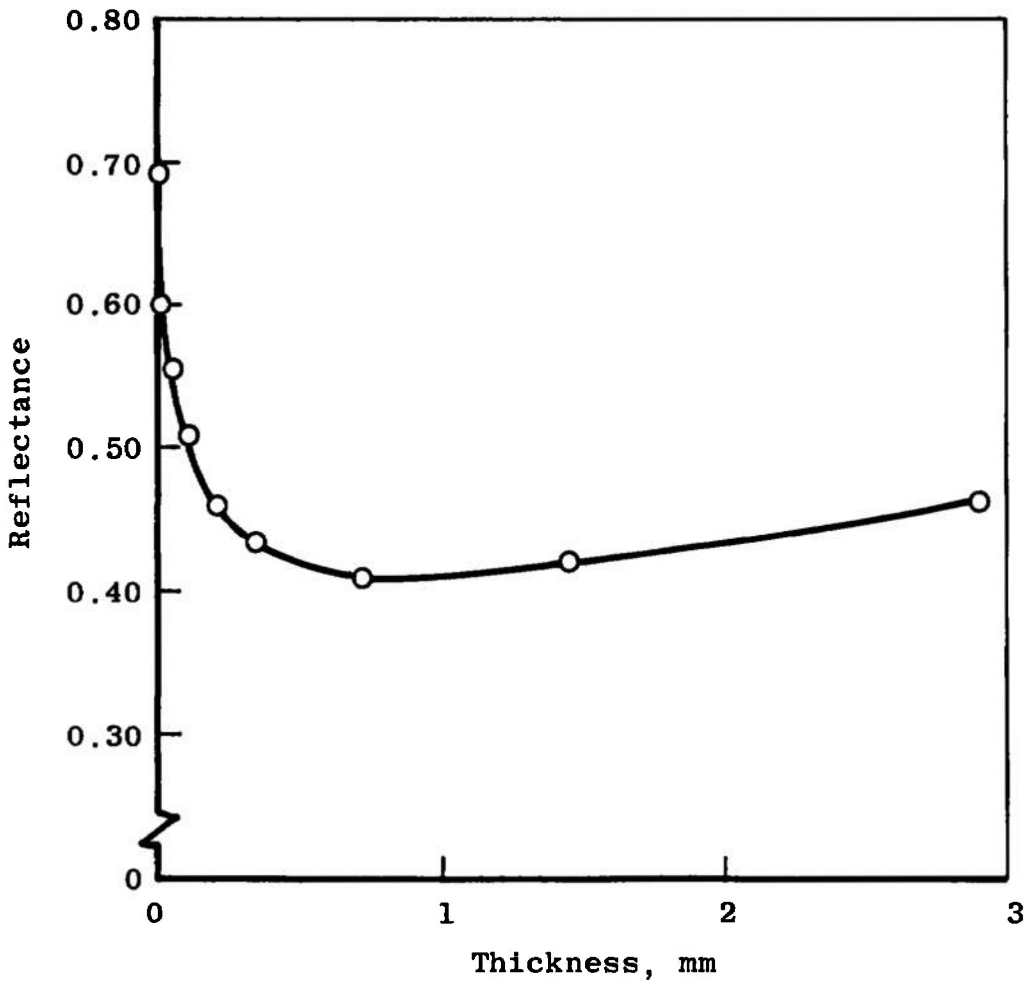

e. $\lambda = 1.95\ \mu$
Fig. 10 Concluded

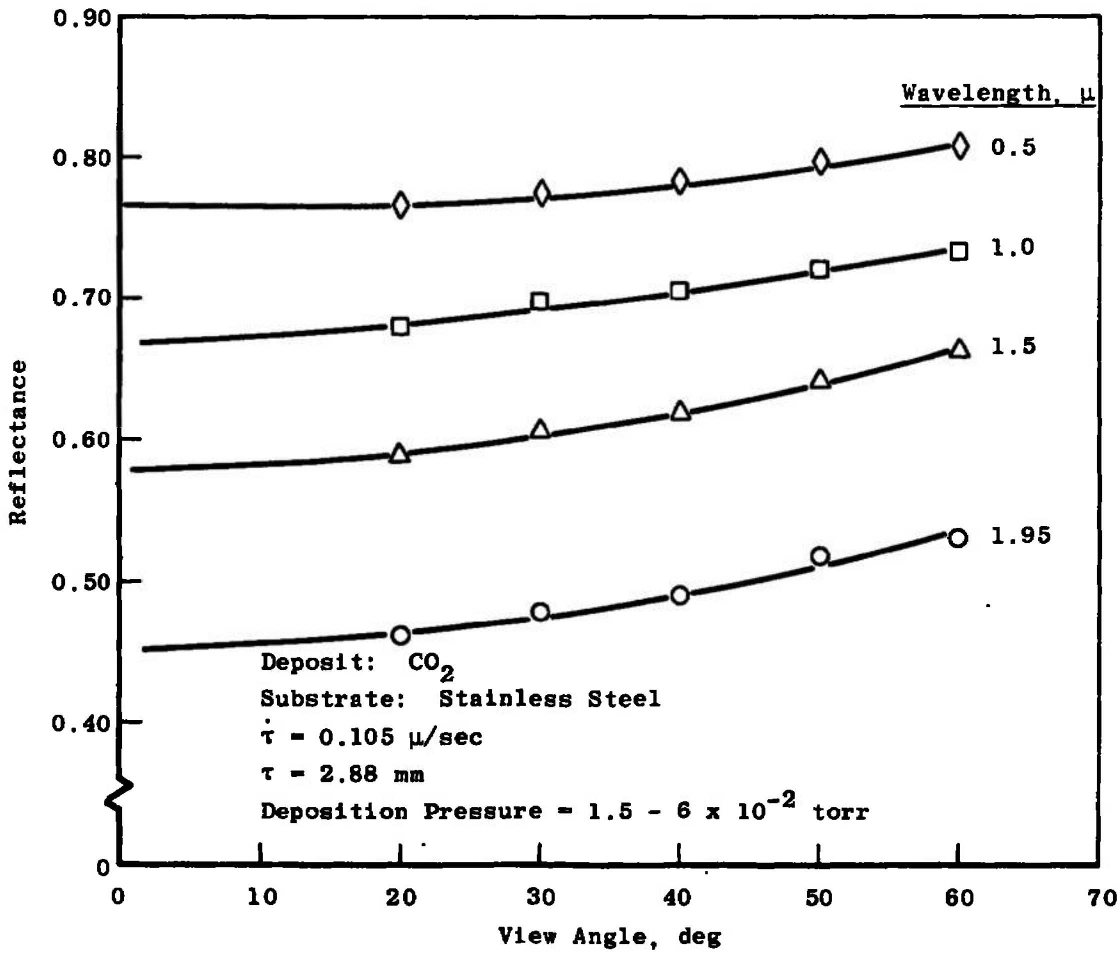

Fig. 11 Reflectance Dependence on View Angle for CO_2 Deposits Formed on Polished Stainless Steel

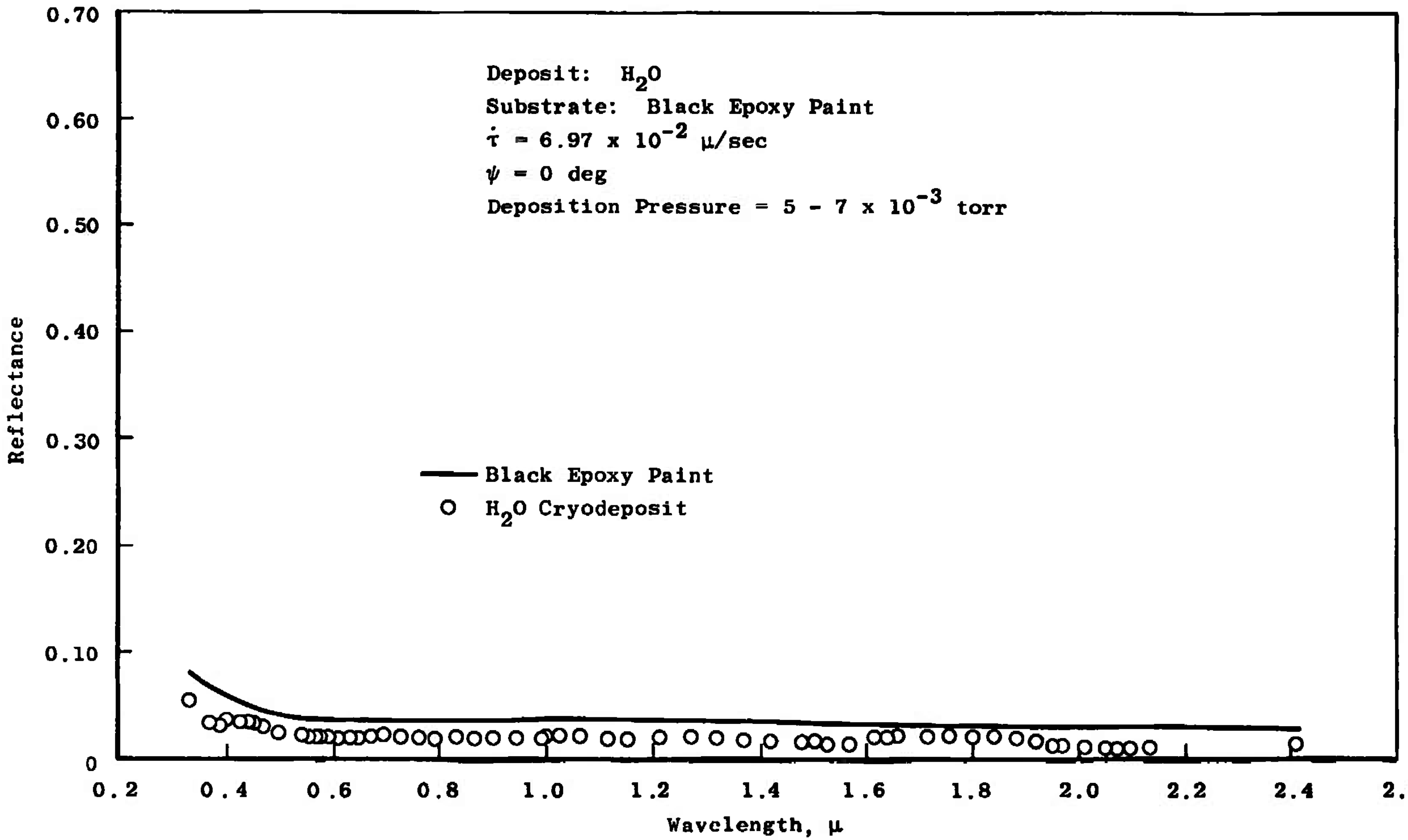

a. τ = 2.1 μ

Fig. 12 Spectral Reflectance of H_2O Deposits Formed on Black Epoxy Paint

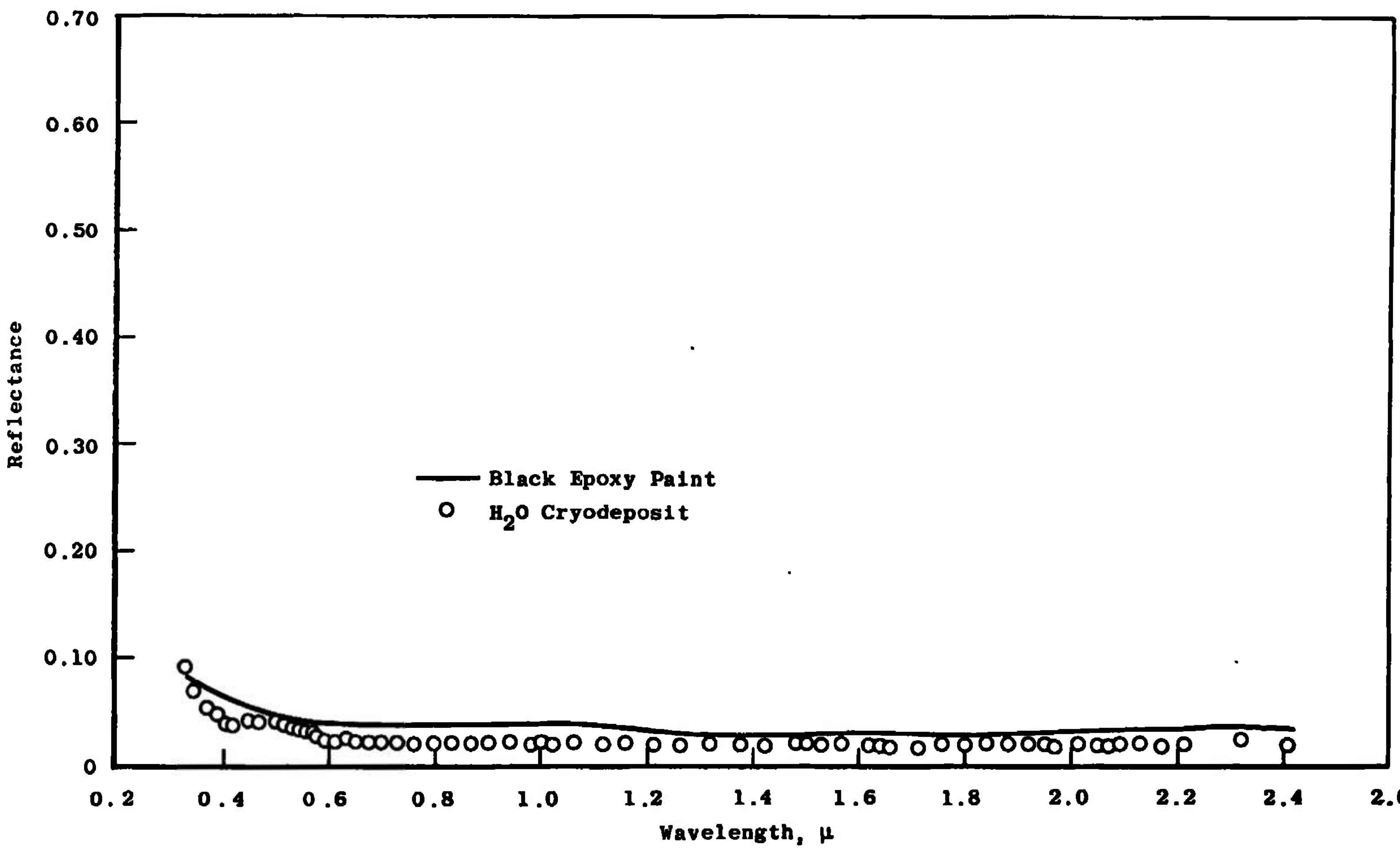

b. $\tau = 15.1\ \mu$

Fig. 12 Continued

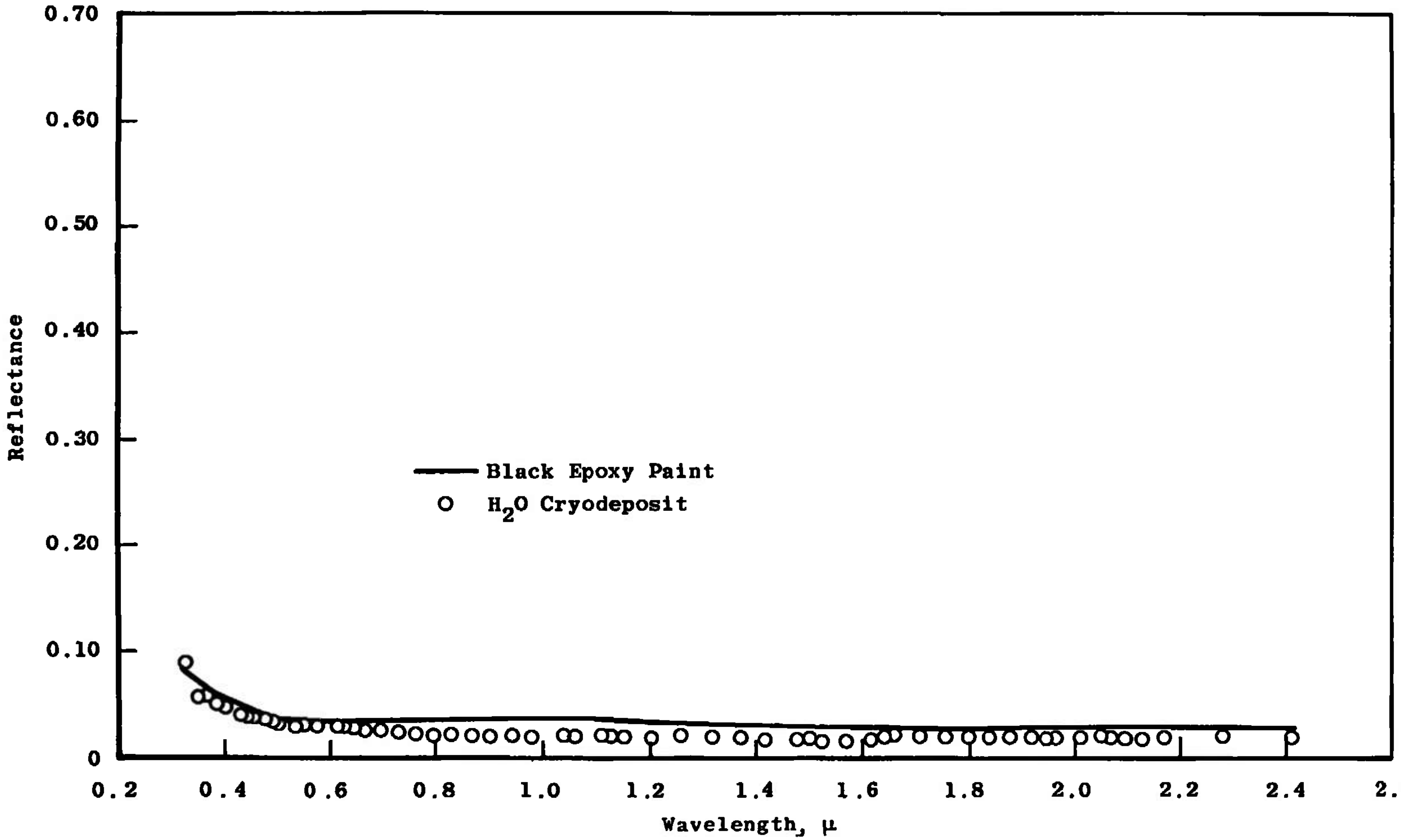

c. $\tau = 42.4\ \mu$

Fig. 12 Continued

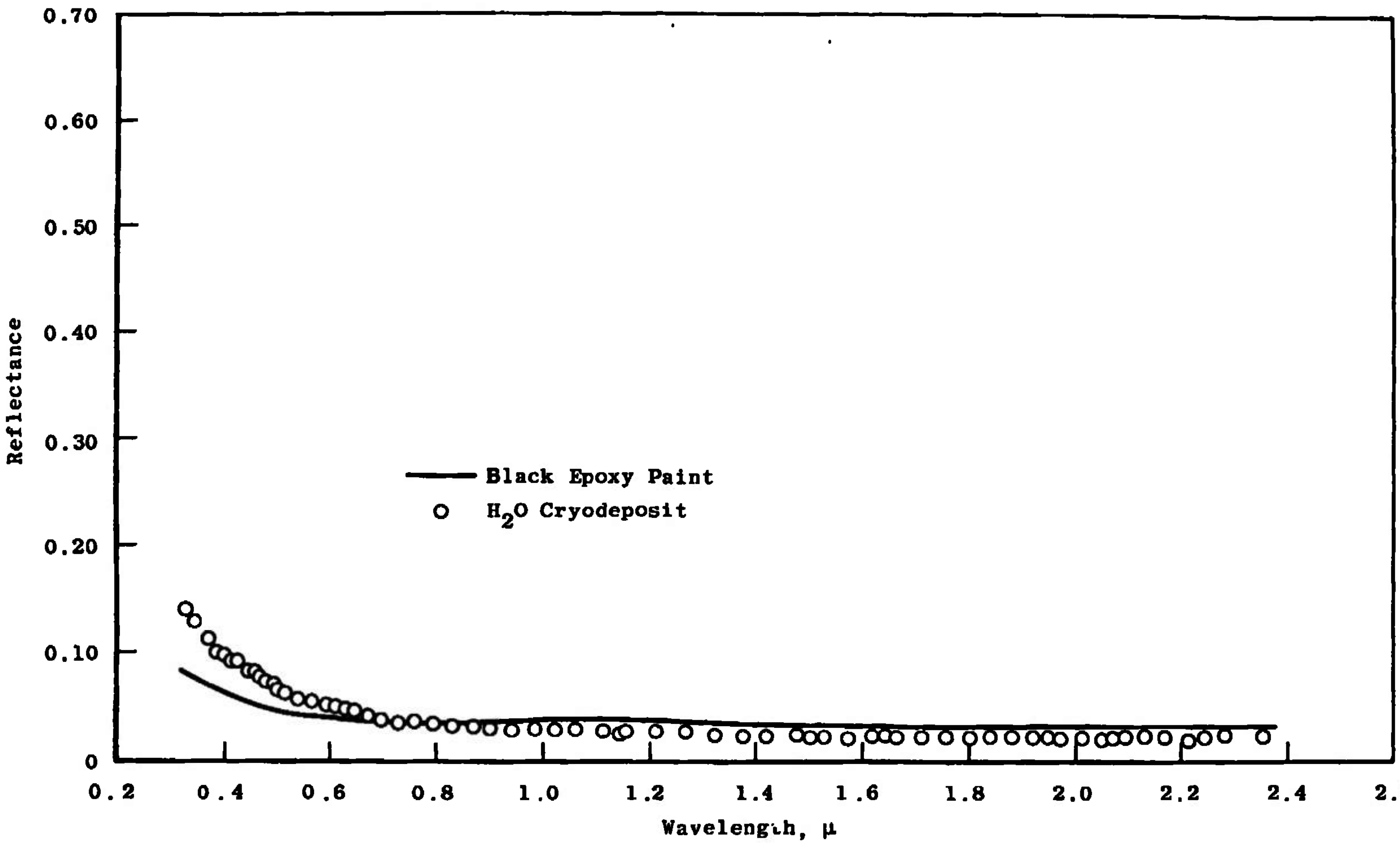

d. τ = 0.104 mm
Fig. 12 Continued

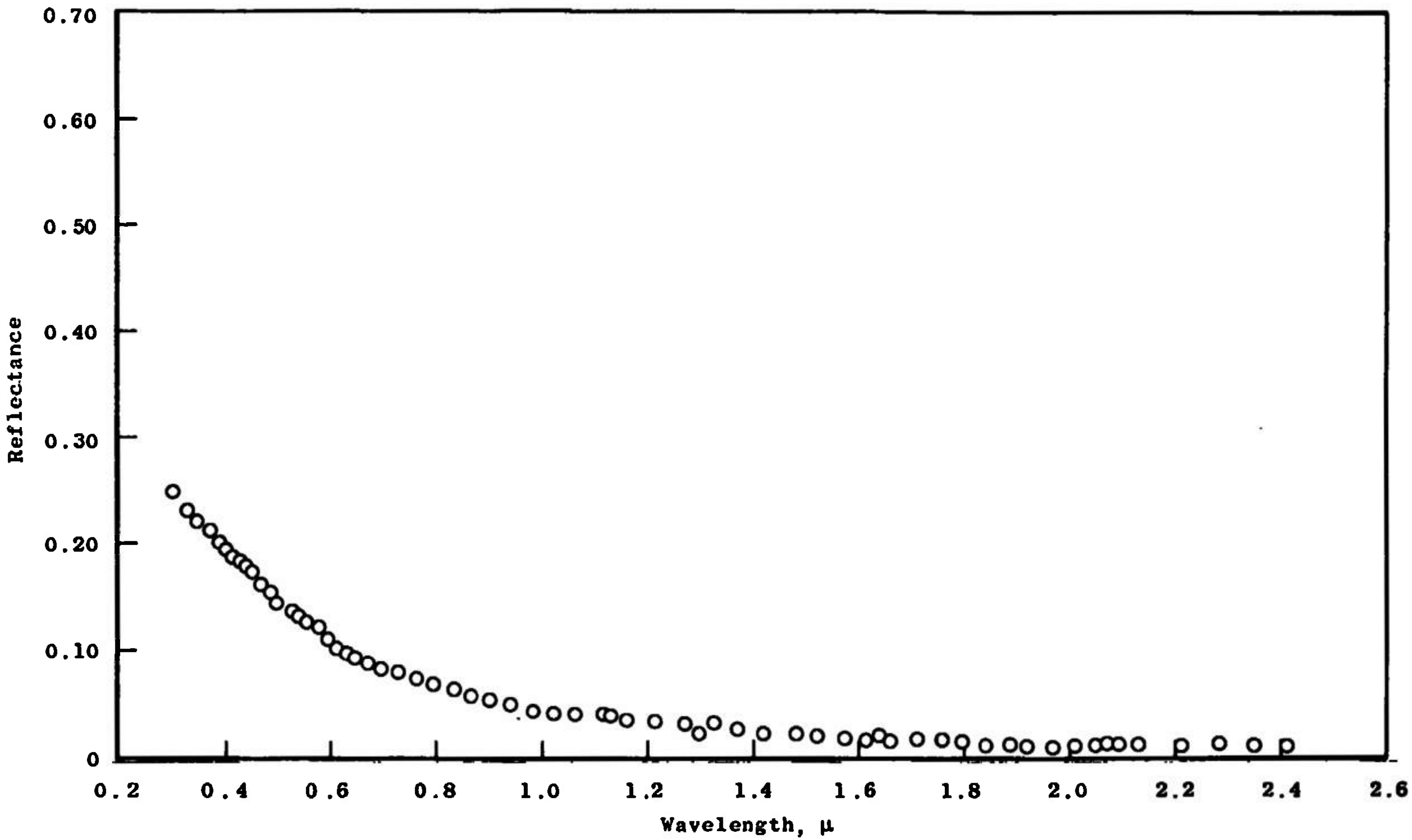

e. τ = 0.206 mm
Fig. 12 Continued

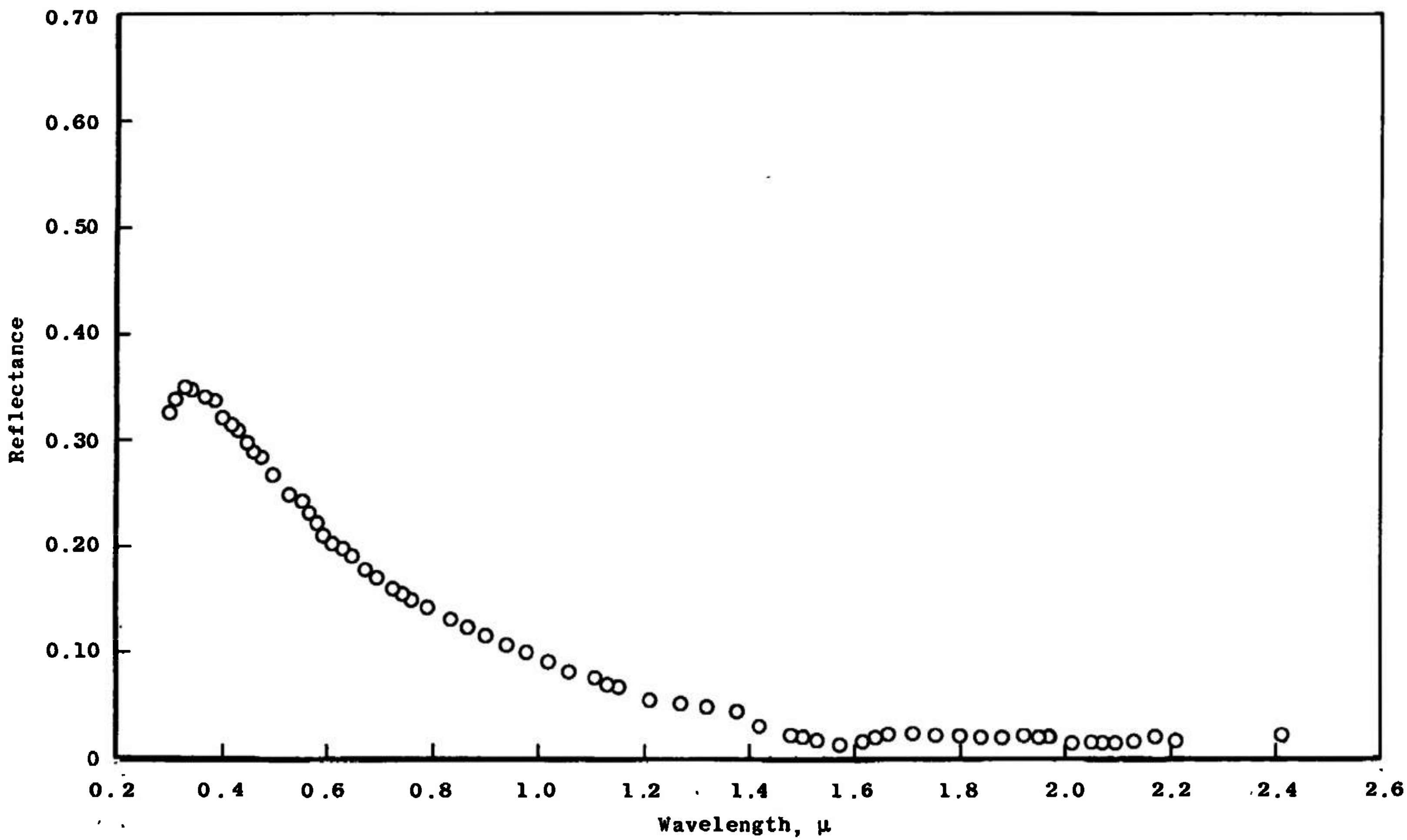

f. τ = 0.409 mm
Fig. 12 Continued

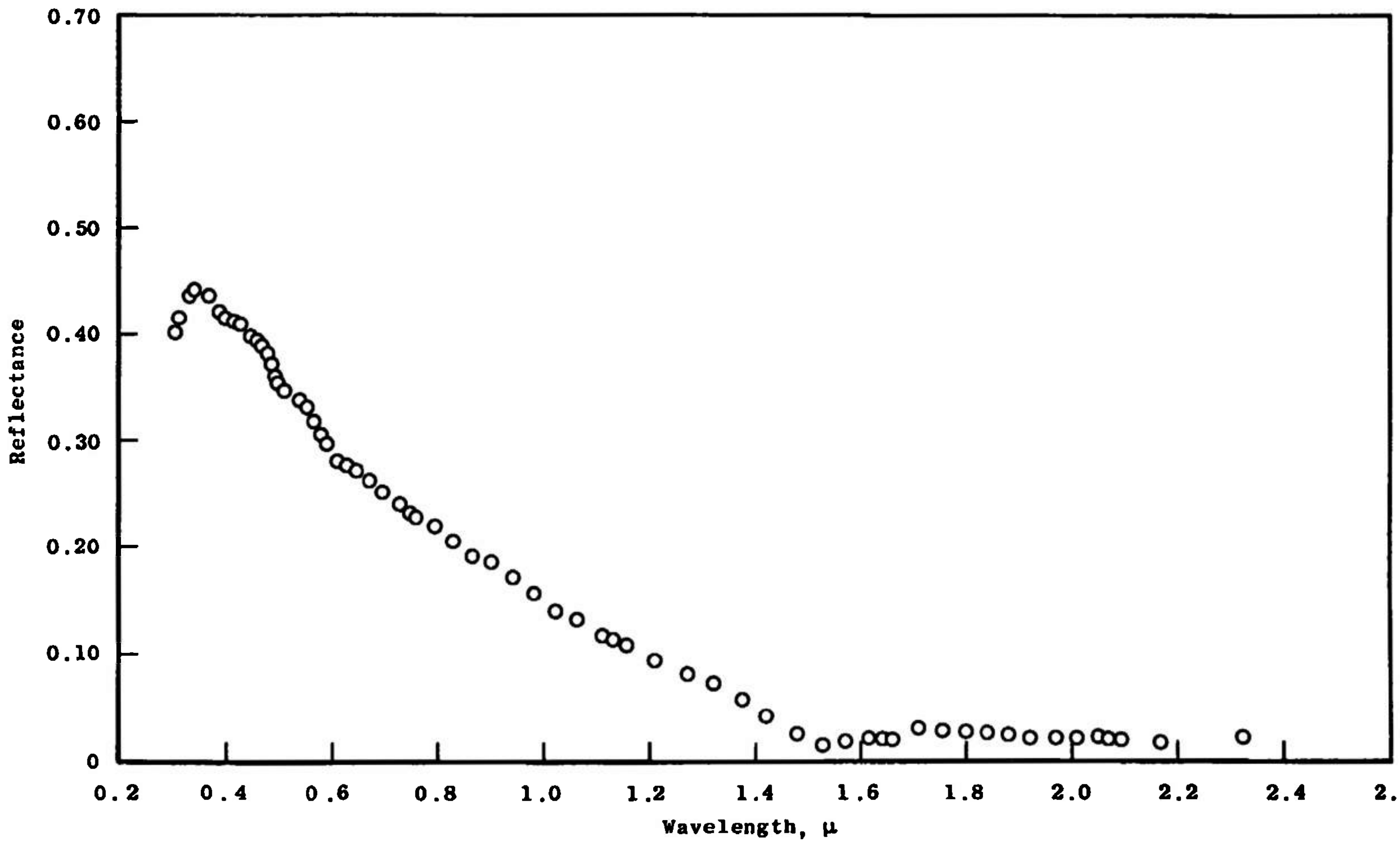

g. τ = 0.815 mm
Fig. 12 Continued

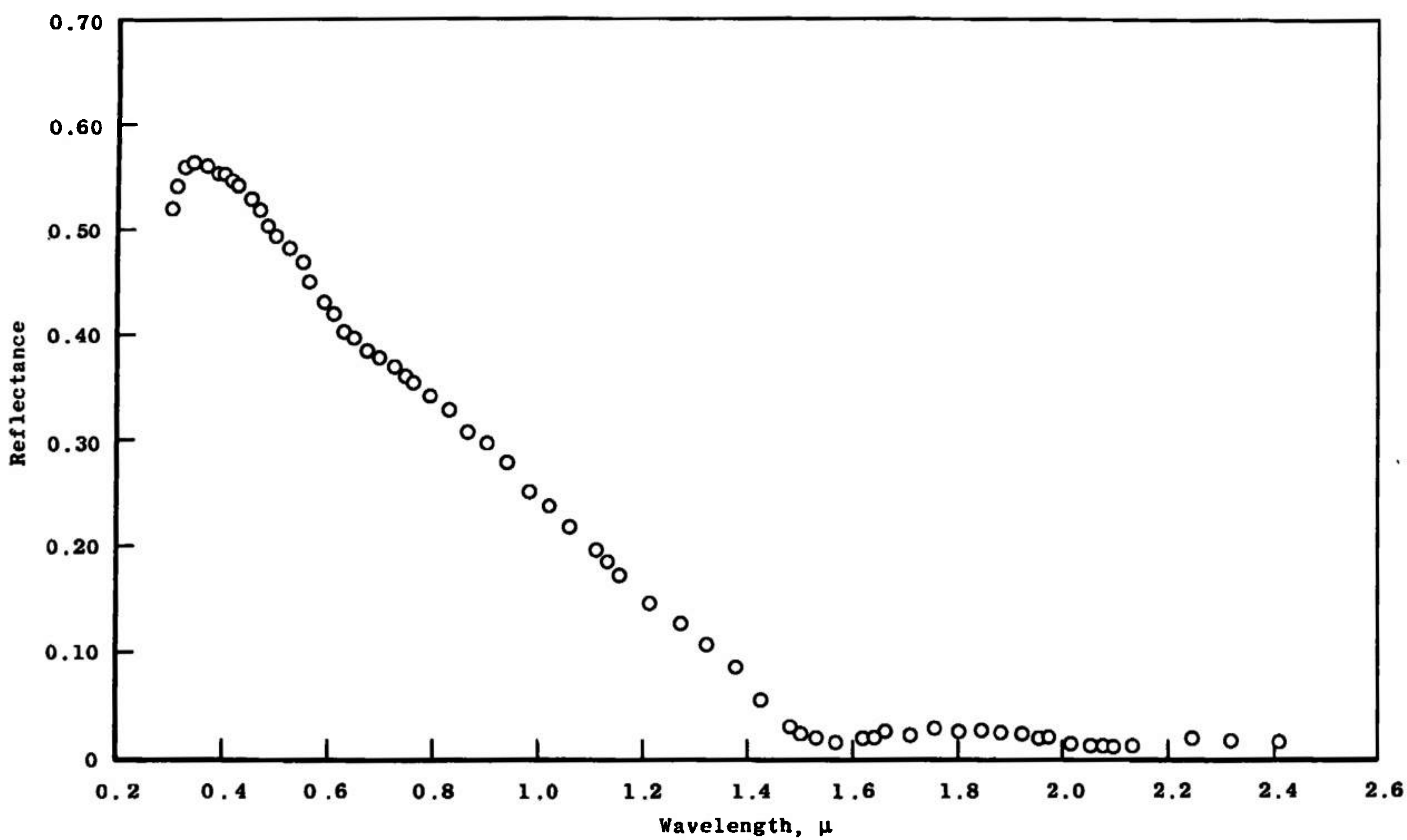

h. τ = 1.63 mm
Fig. 12 Continued

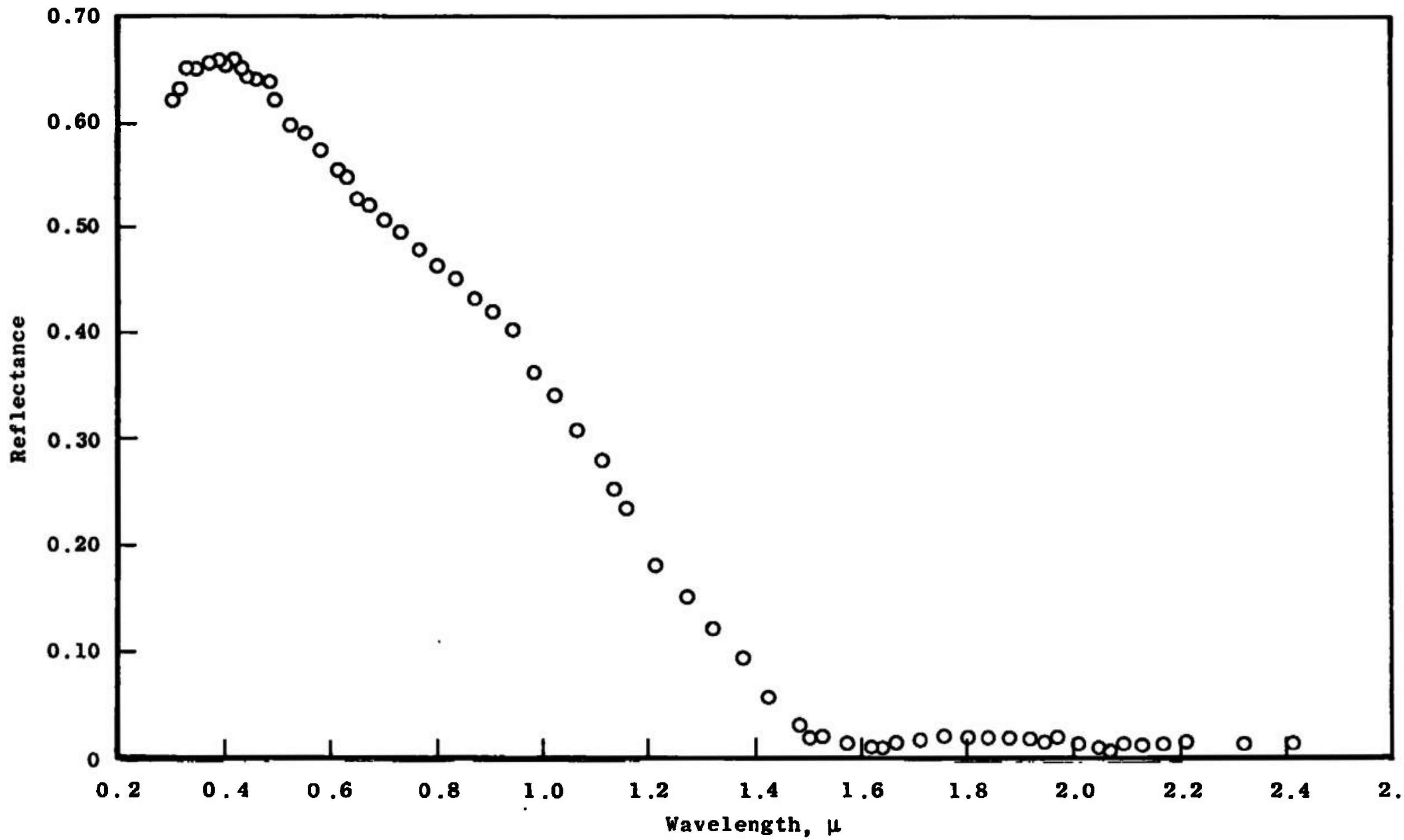

i. τ = 3.25 mm
Fig. 12 Concluded

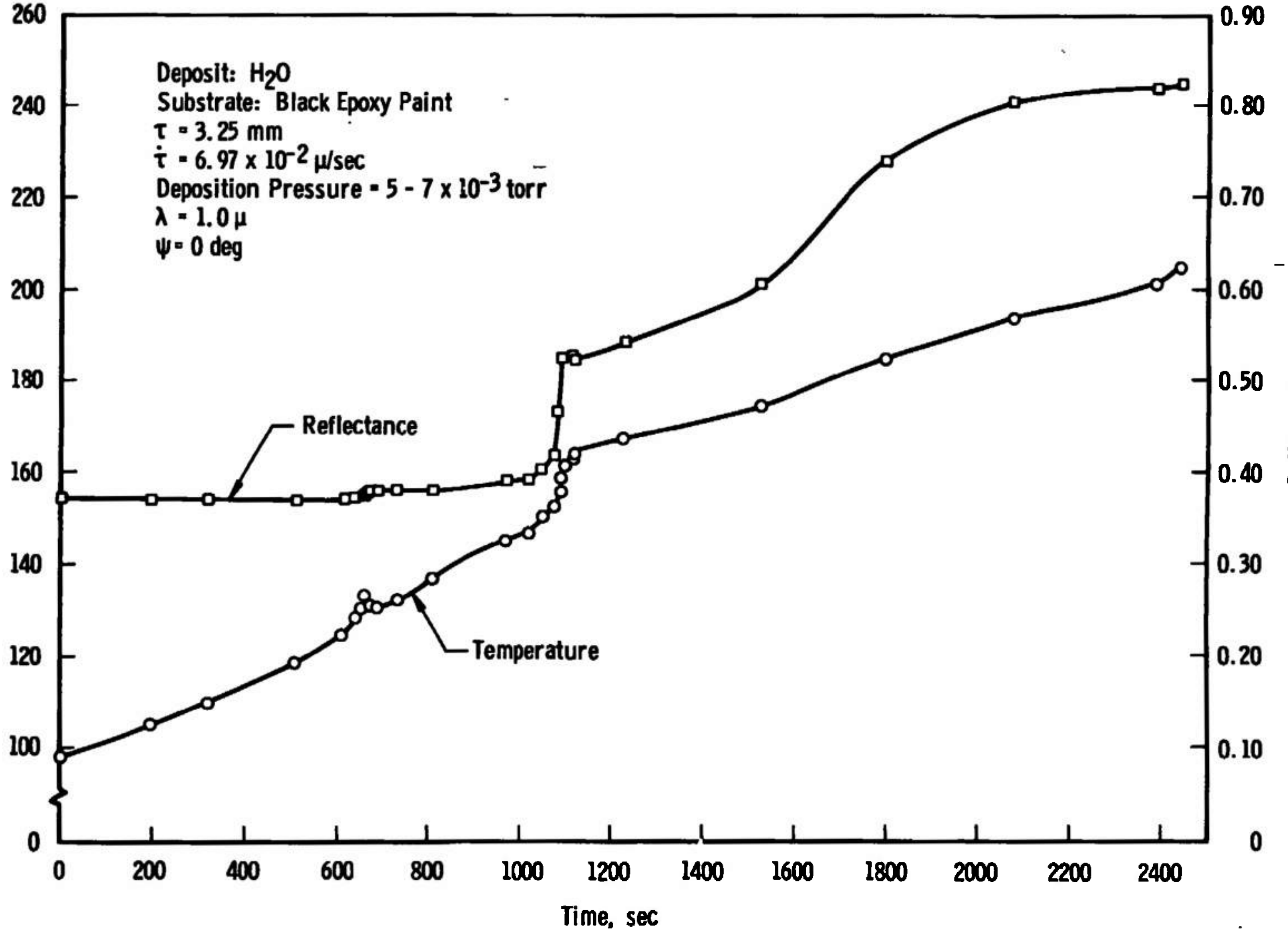

Fig. 13 Temperature and Reflectance Changes of H_2O Deposits during Warmup

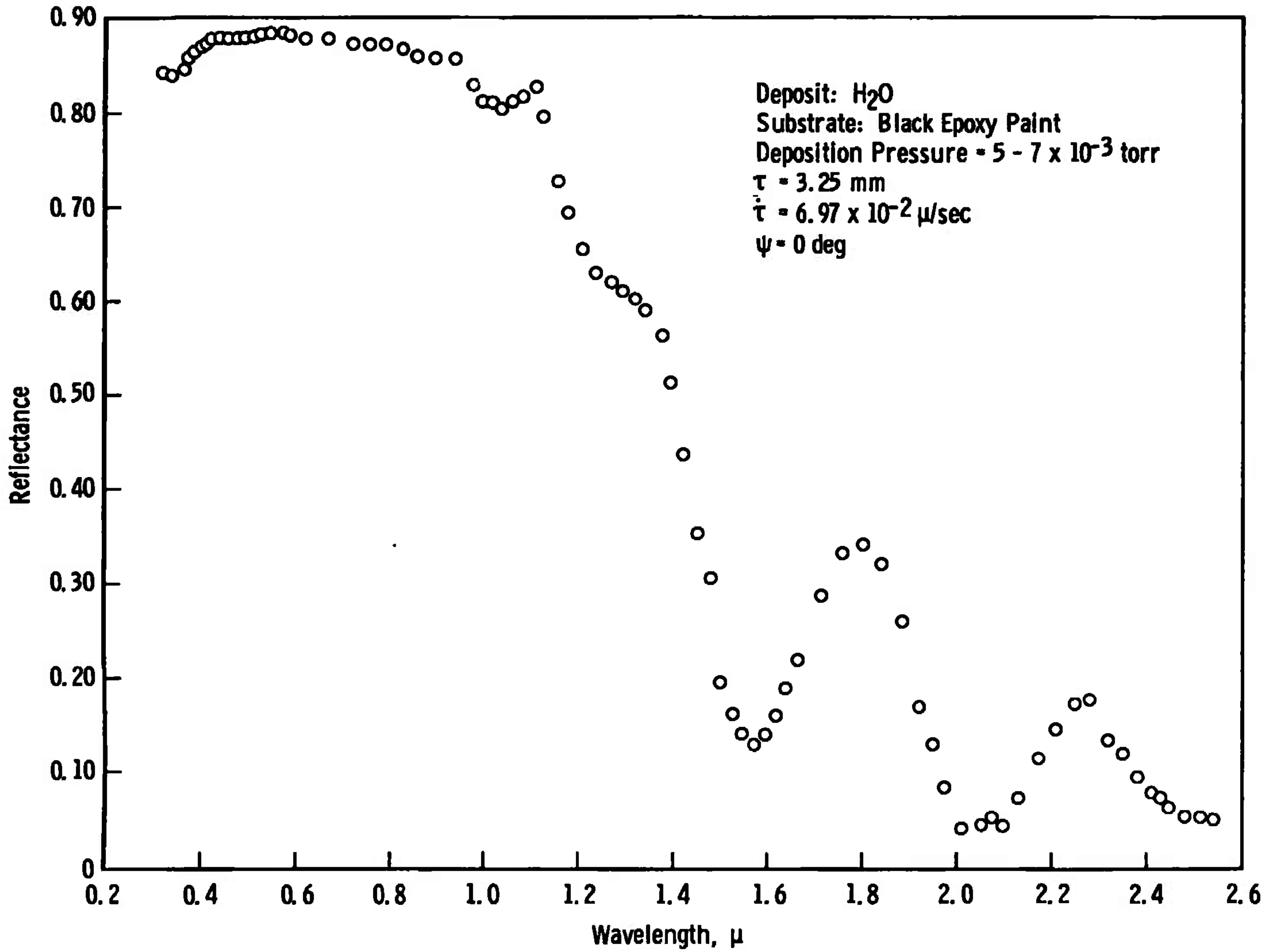

Fig. 14 Spectral Reflectance of H_2O Deposit after Warmup

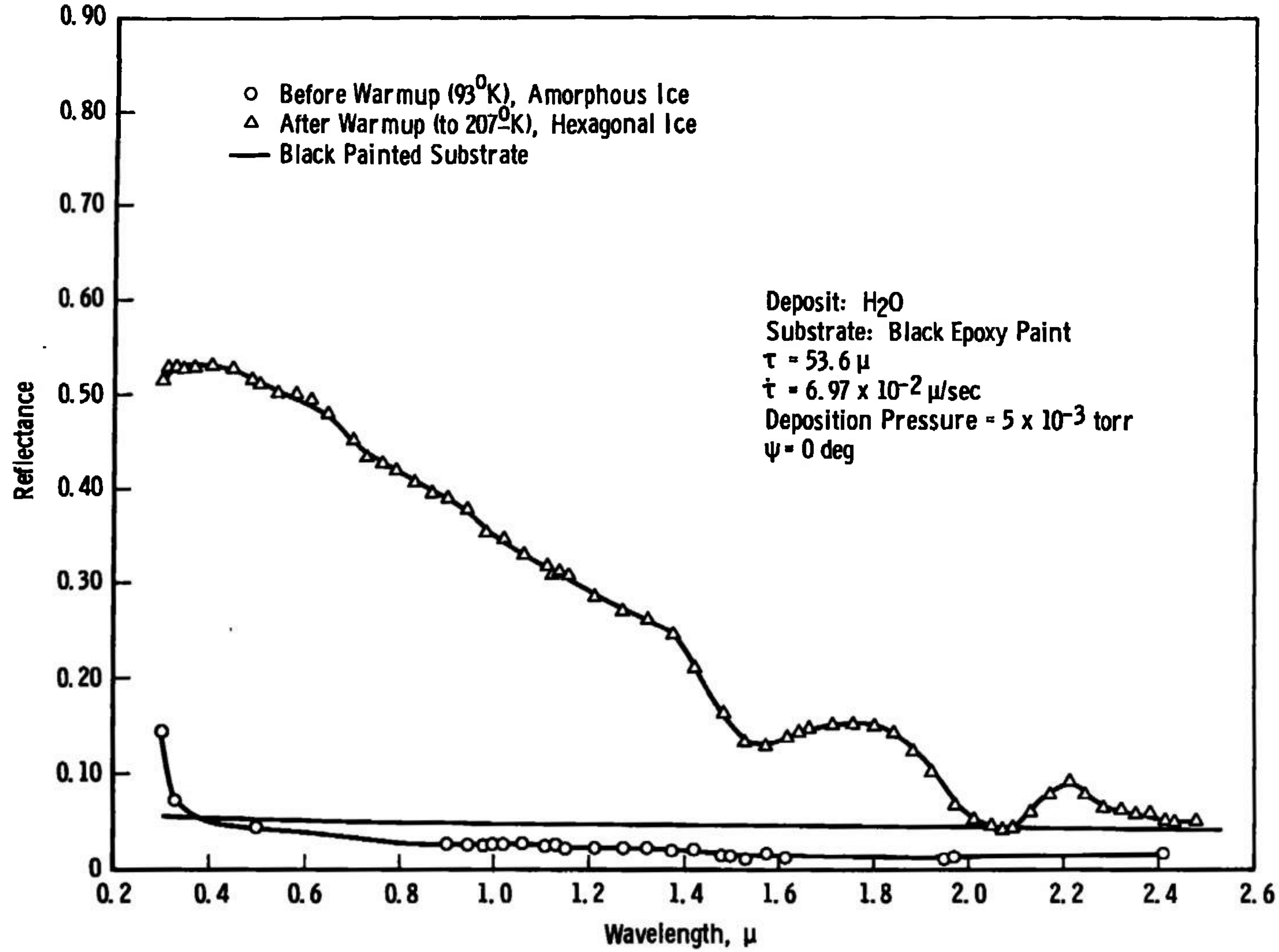

Fig. 15 Spectral Reflectance of a Thin H_2O Deposit on Black Epoxy Paint before and after Warmup

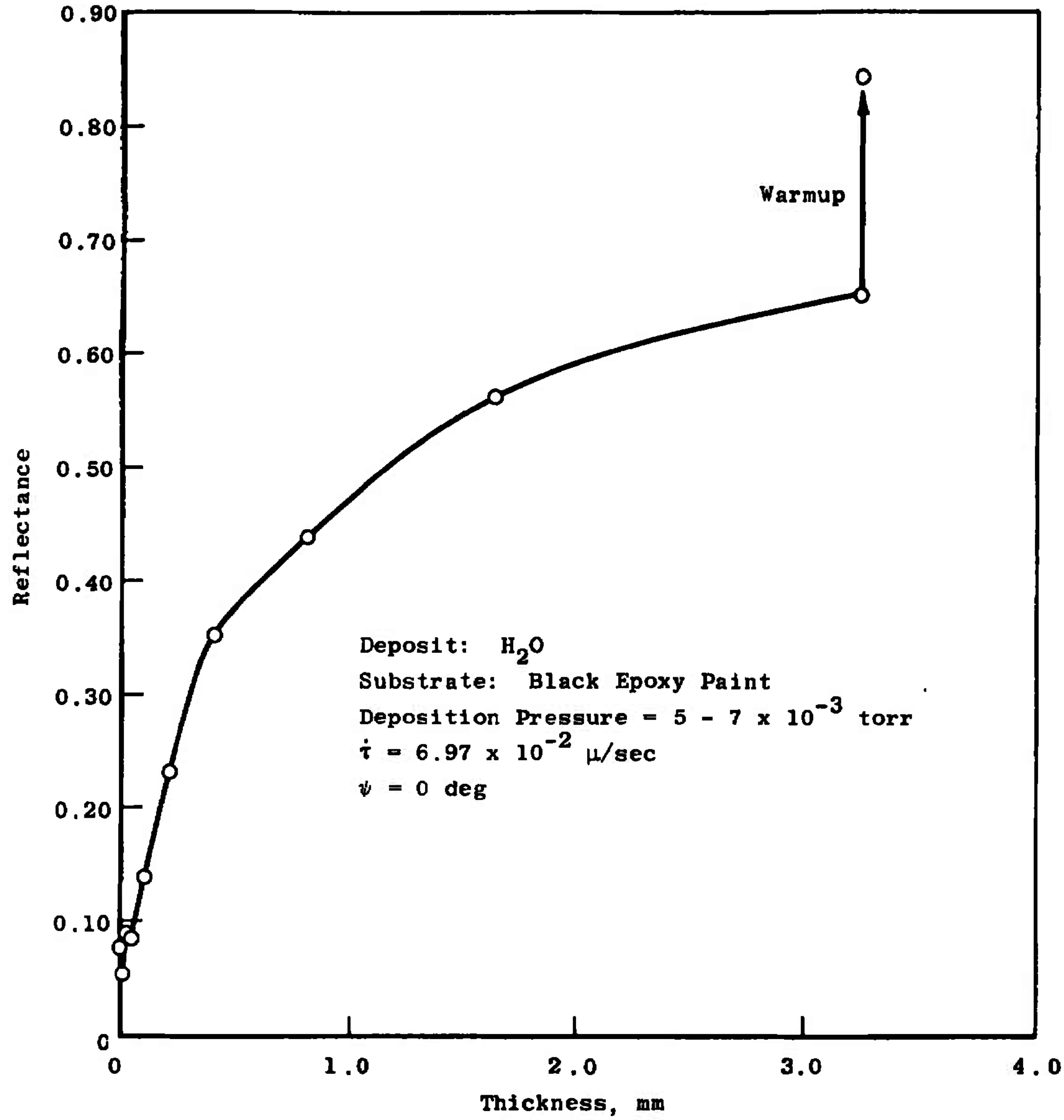

a. $\lambda = 0.325\ \mu$

Fig. 16 Reflectance Dependence on Thickness of H_2O Deposits Formed on Black Epoxy Paint

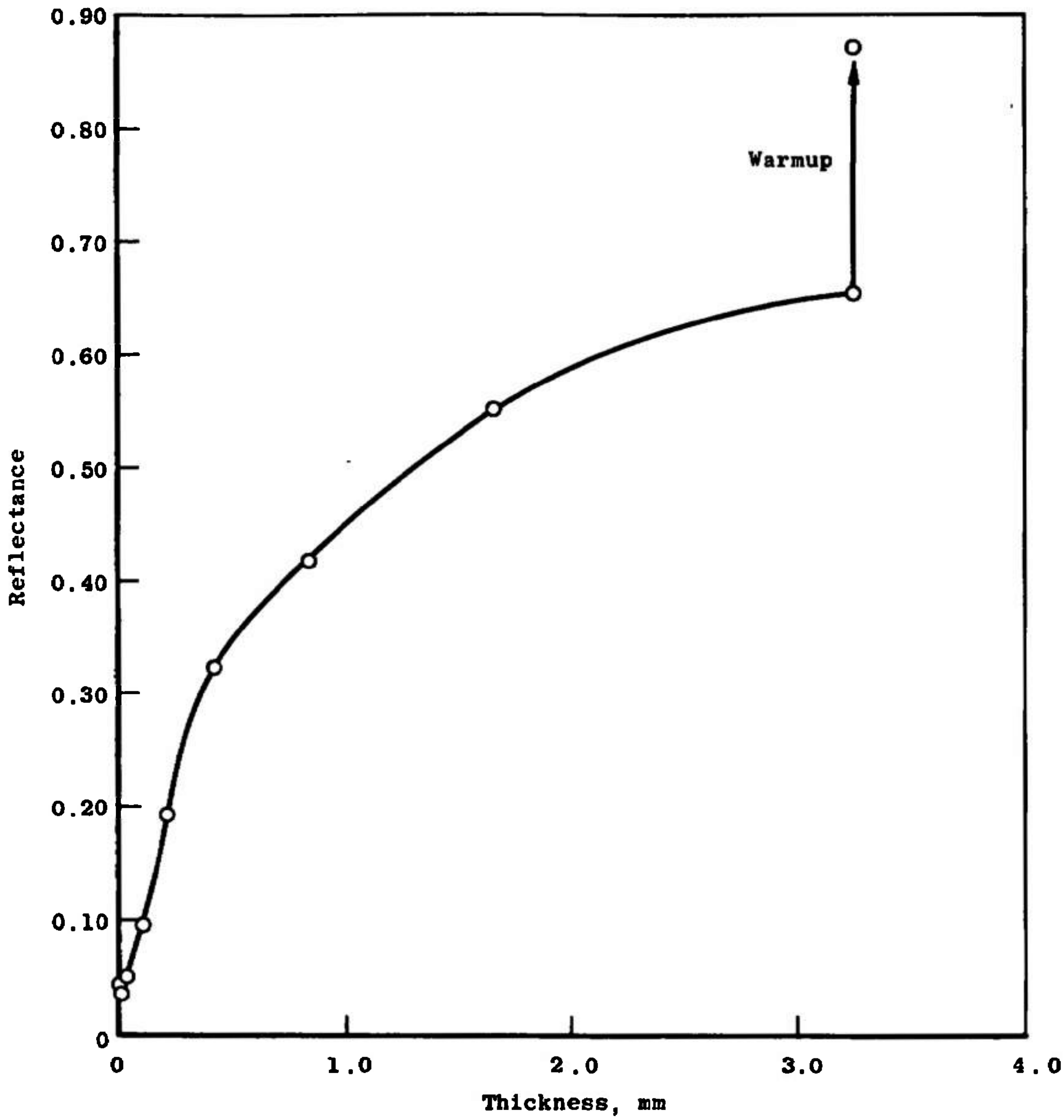

b. λ = 0.4 μ
Fig. 16 Continued

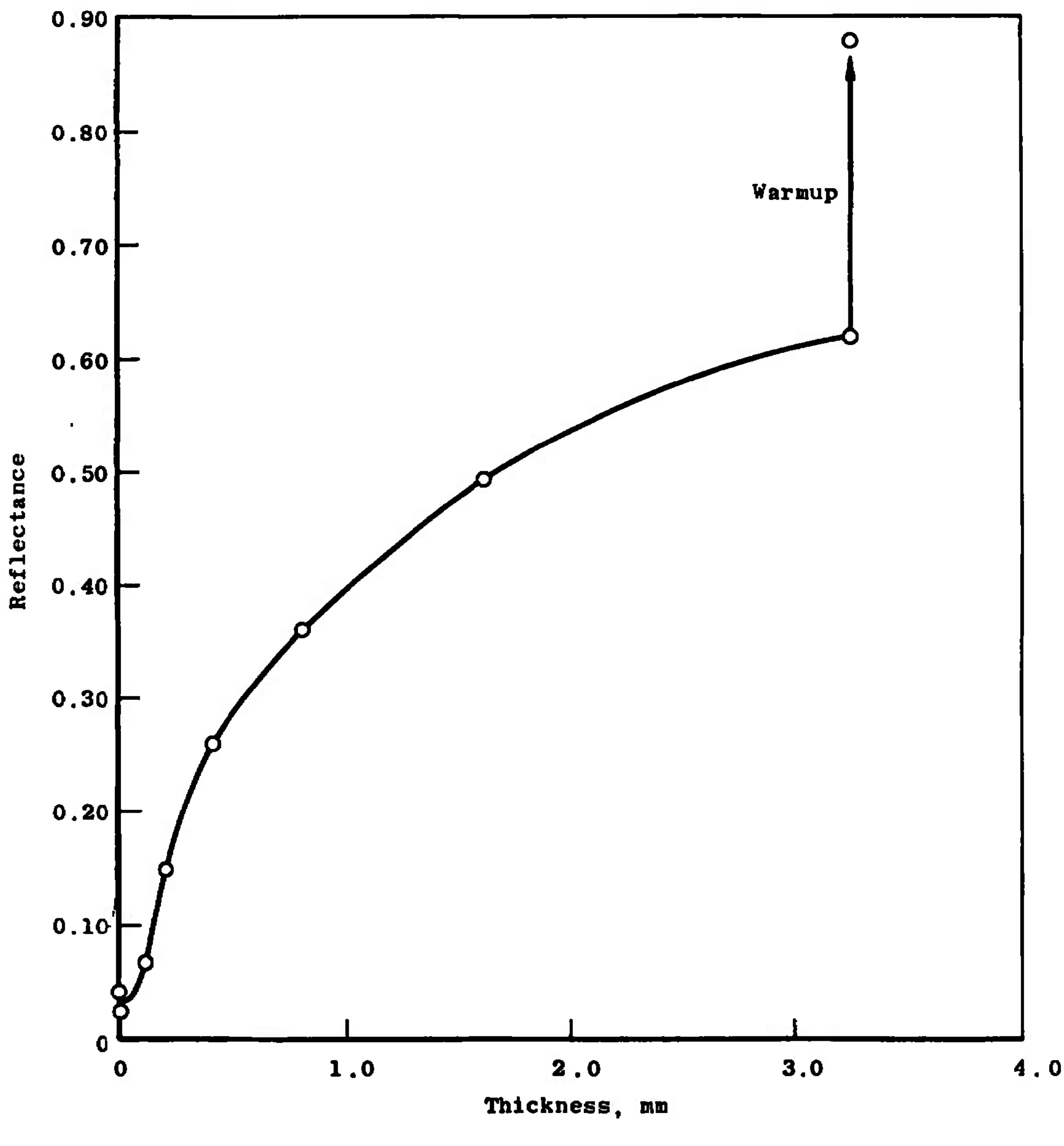

c. $\lambda = 0.5\ \mu$
Fig. 16 Continued

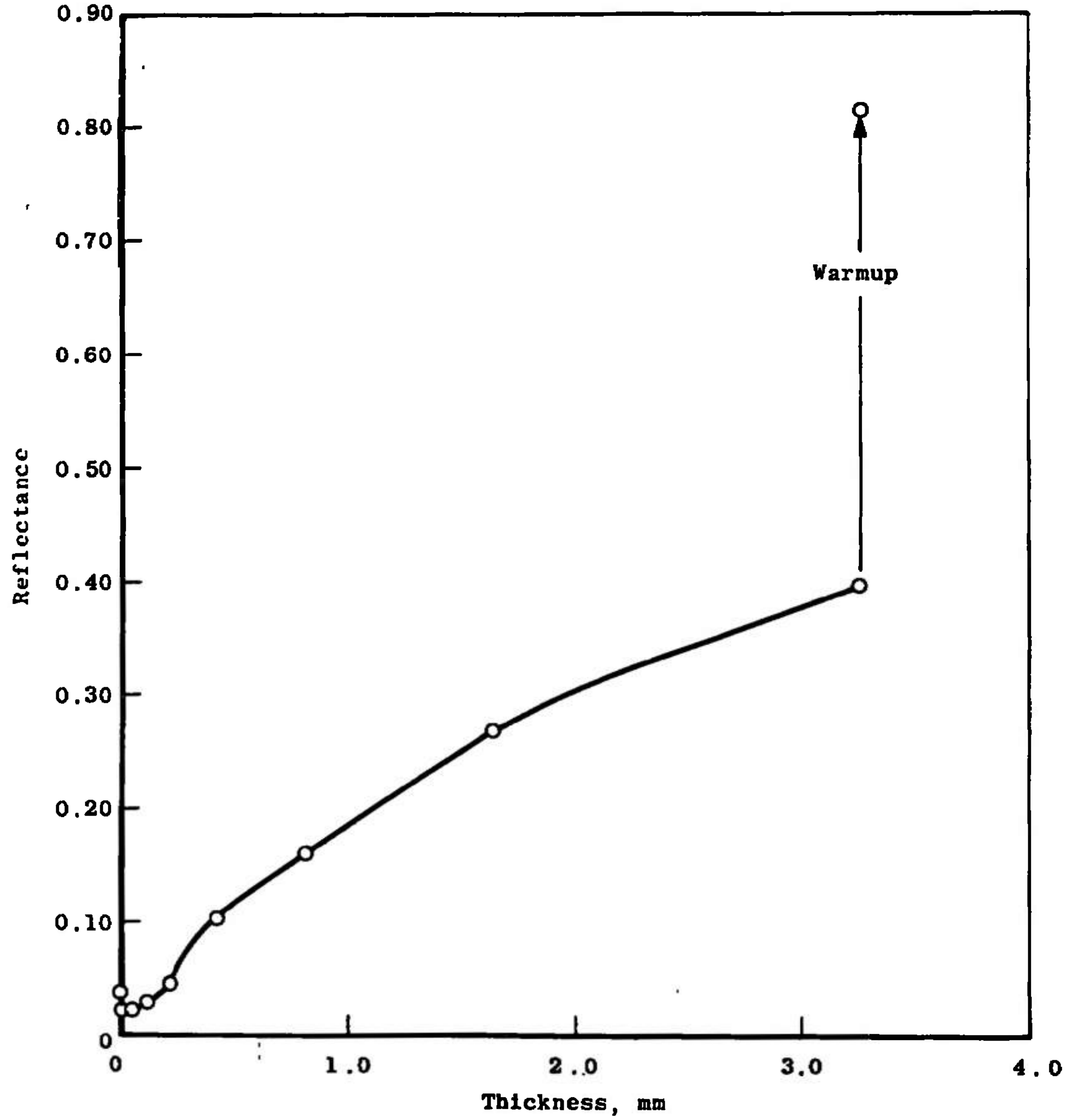

d. $\lambda = 1.0\ \mu$
Fig. 16 Continued

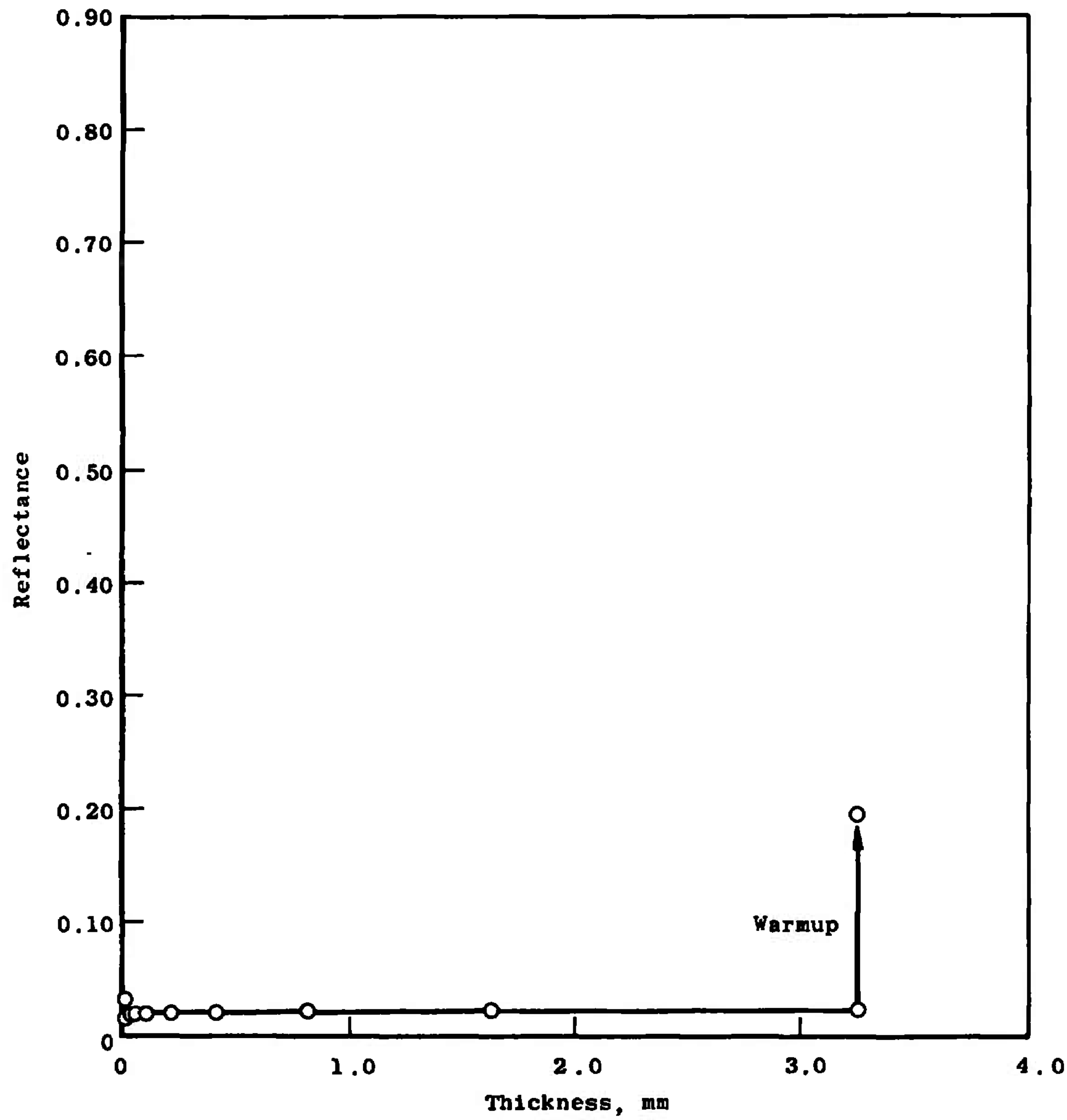

e. $\lambda = 1.5\ \mu$

Fig. 16 Continued

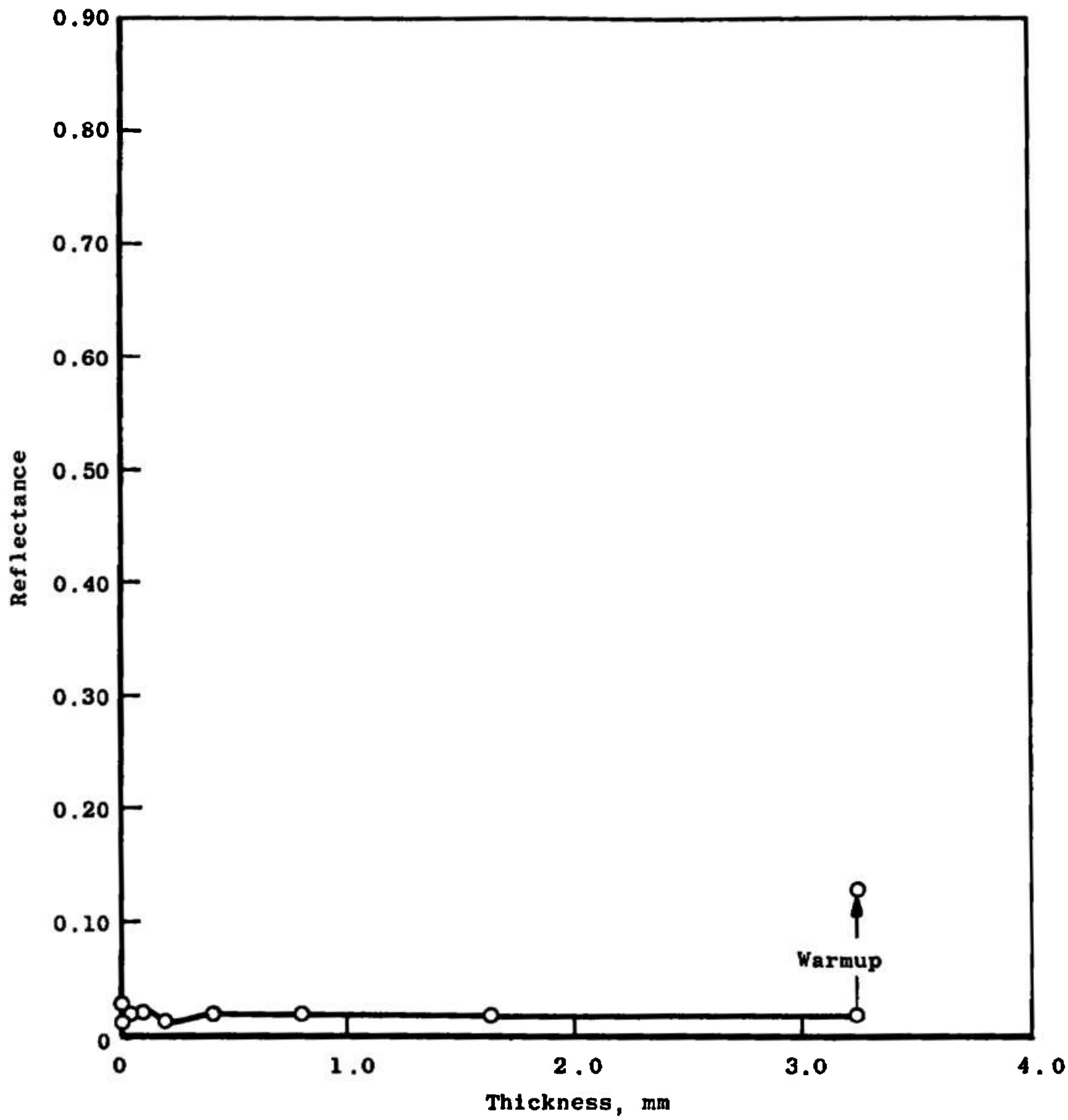

f. $\lambda = 1.95\ \mu$

Fig. 16 Concluded

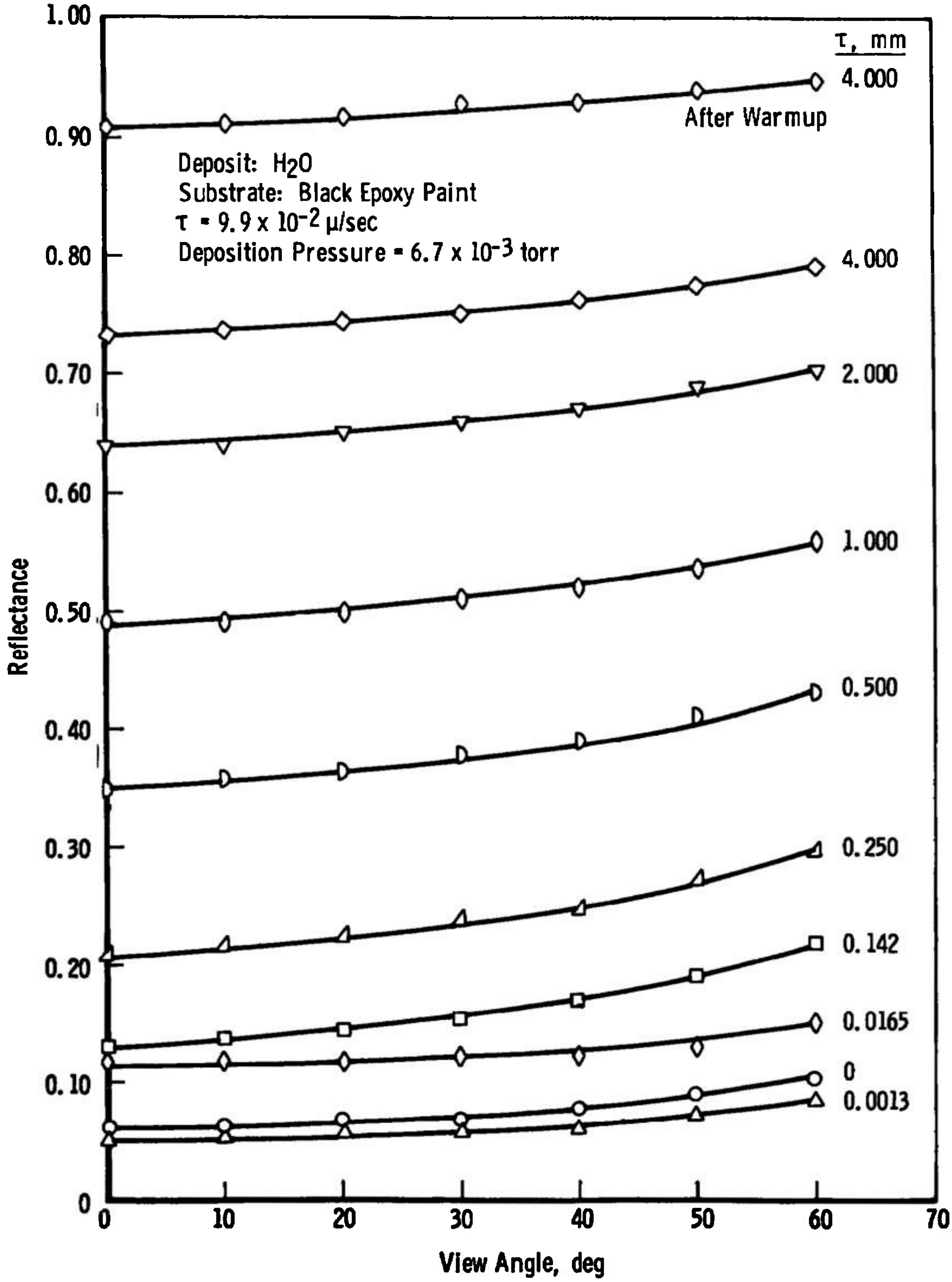

a. $\lambda = 0.4\ \mu$

Fig. 17 Reflectance Dependence on View Angle for H_2O Deposits on Black Epoxy Paint

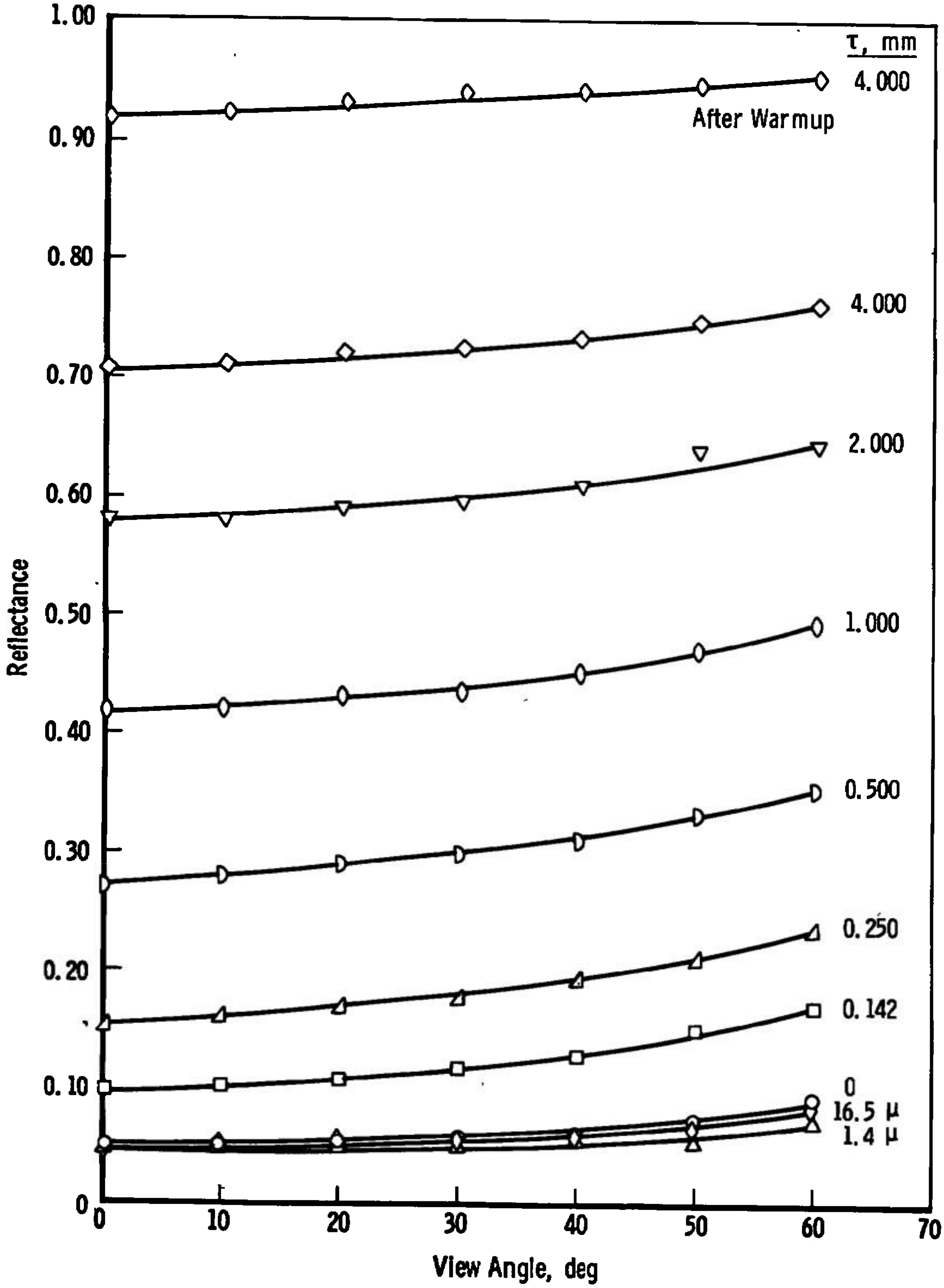

b. $\lambda = 0.5\ \mu$
Fig. 17 Continued

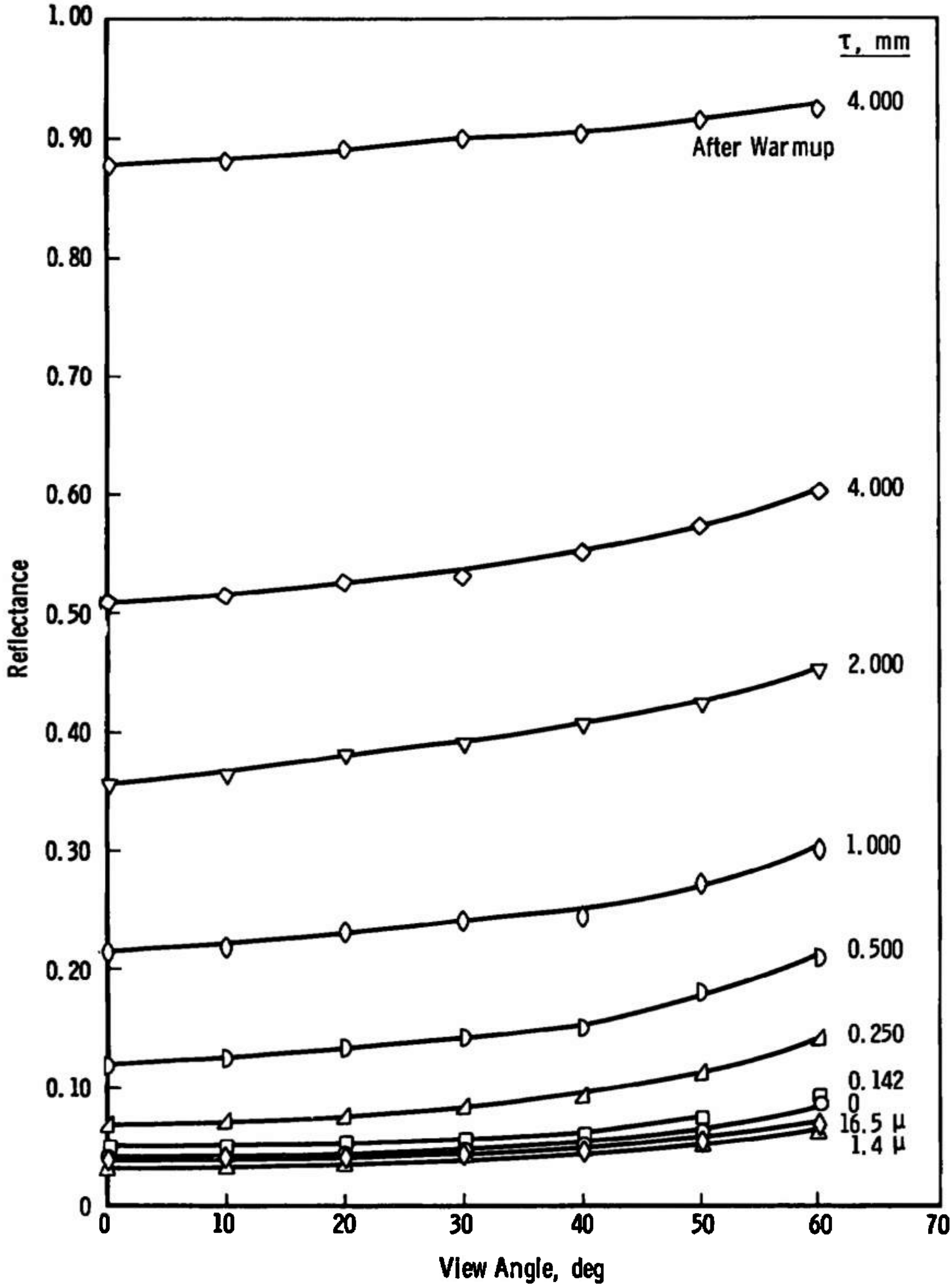

c. $\lambda = 1.0\ \mu$
Fig. 17 Continued

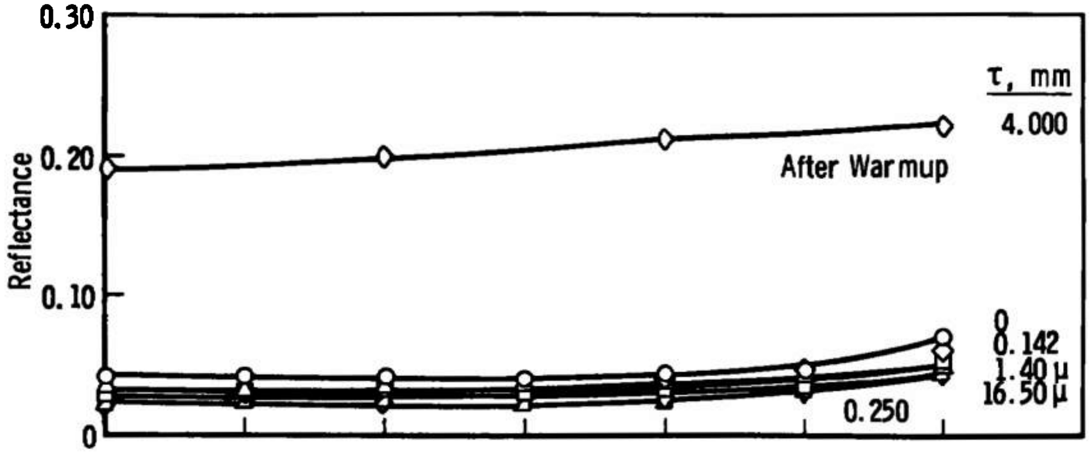

d. λ = 1.5μ

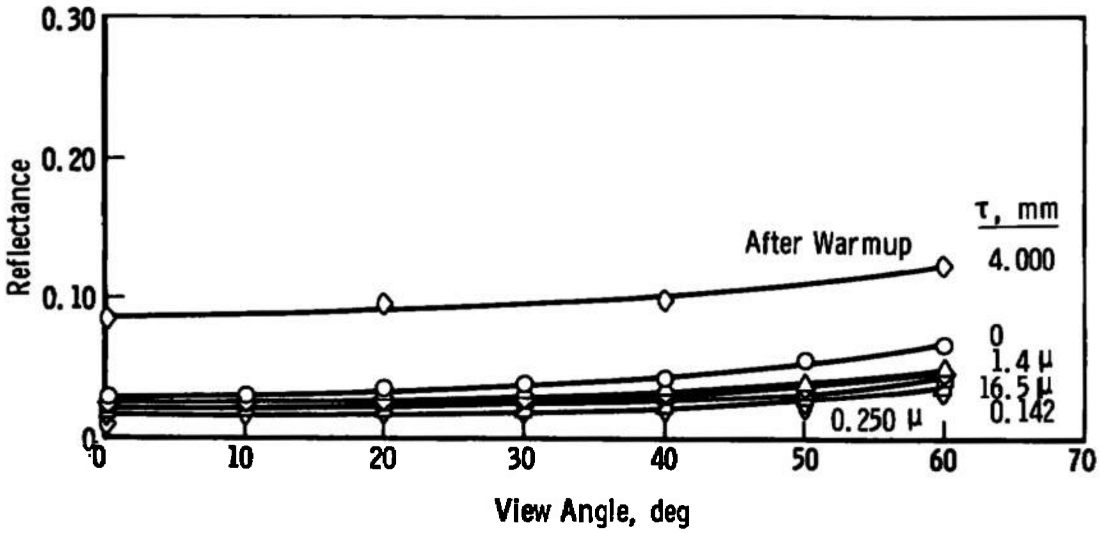

e. λ = 1.95 μ

Fig. 17 Concluded

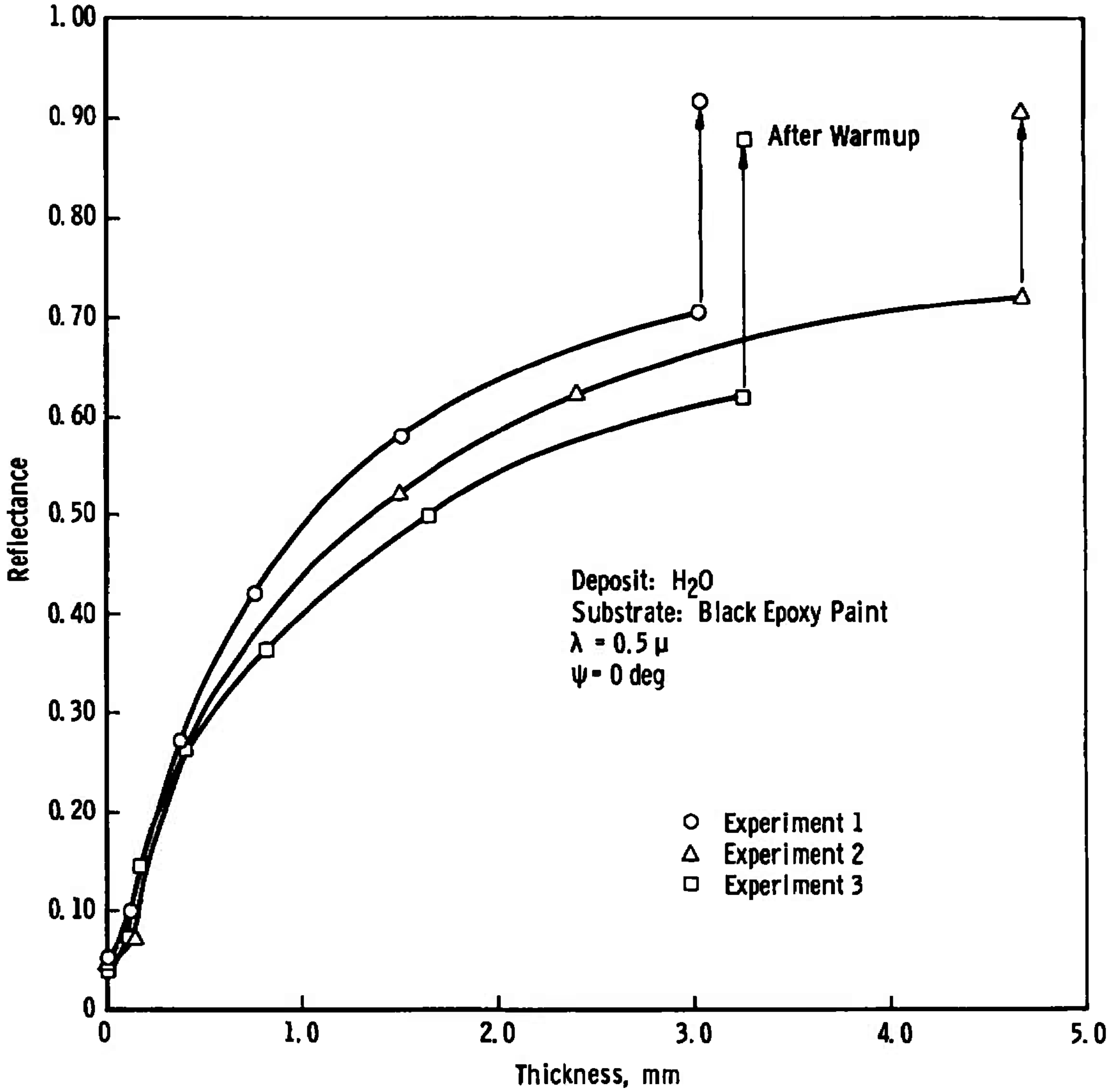

Fig. 18 Reflectance Dependence on H_2O Thickness-Comparison of Three Separate Experiments

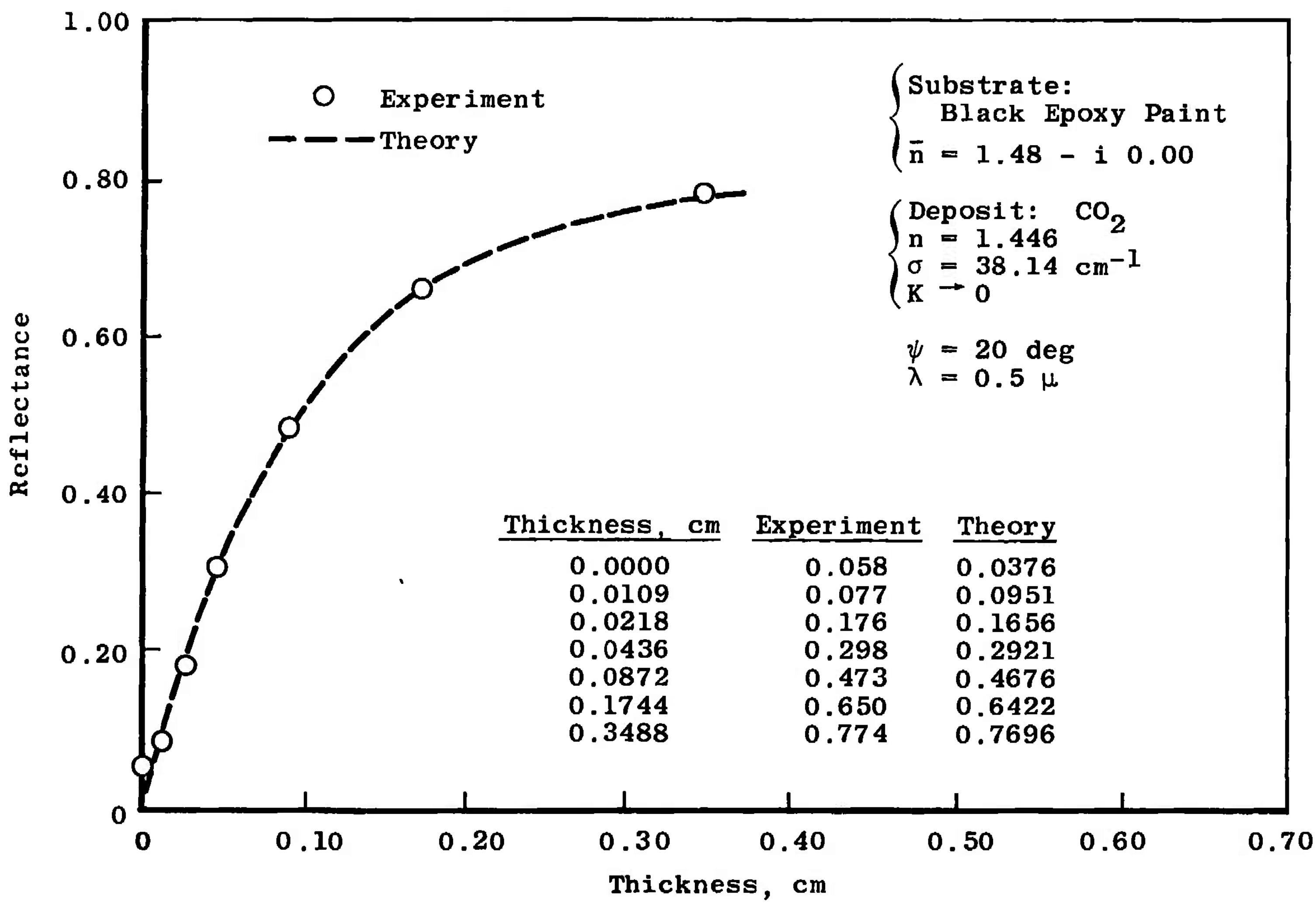

Thickness, cm	Experiment	Theory
0.0000	0.058	0.0376
0.0109	0.077	0.0951
0.0218	0.176	0.1656
0.0436	0.298	0.2921
0.0872	0.473	0.4676
0.1744	0.650	0.6422
0.3488	0.774	0.7696

a. $\lambda = 0.5\ \mu$

Fig. 19 Comparison of Theory and Experiment for a CO_2 Cryodeposit on a Black Epoxy Paint Substrate

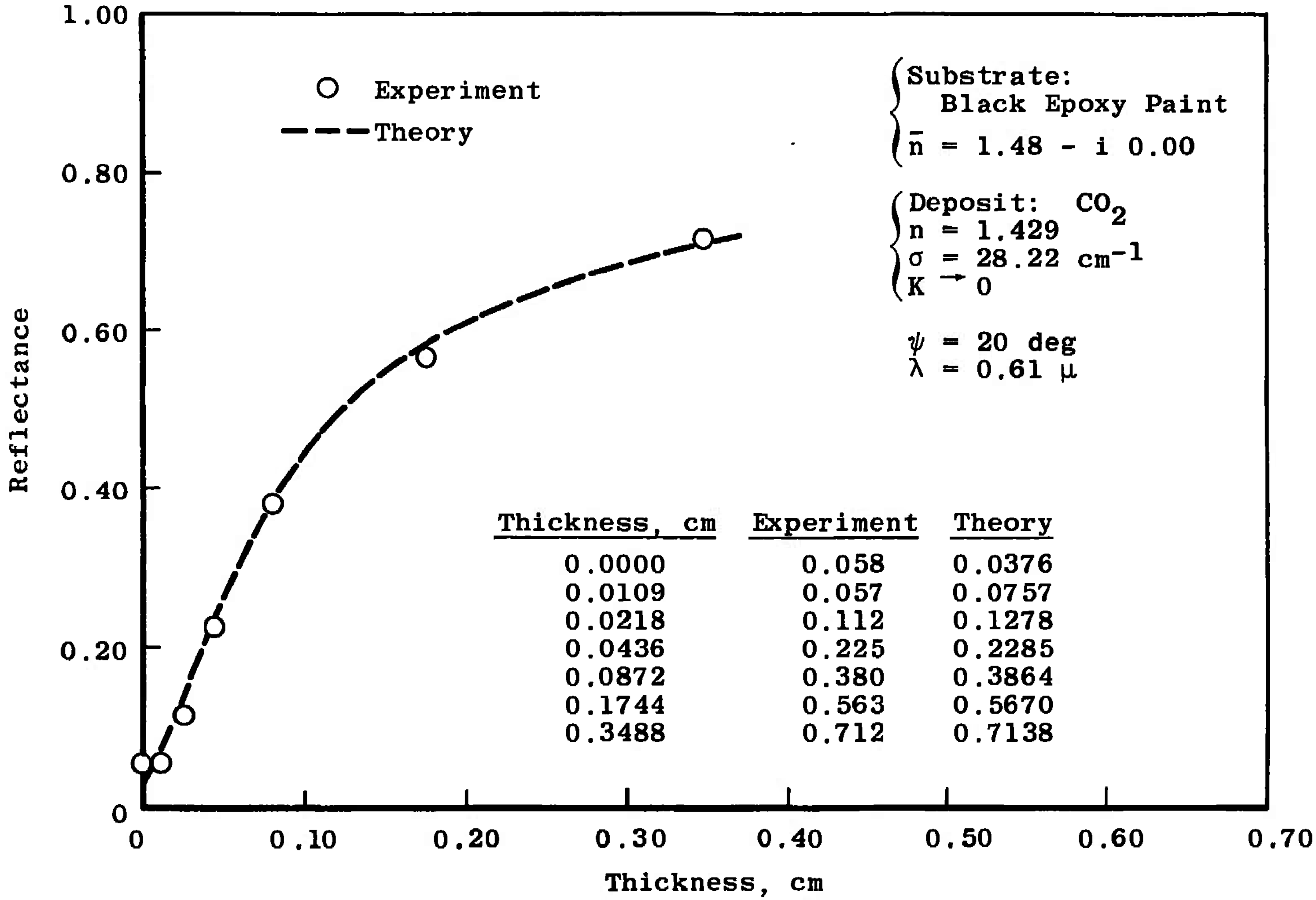

Thickness, cm	Experiment	Theory
0.0000	0.058	0.0376
0.0109	0.057	0.0757
0.0218	0.112	0.1278
0.0436	0.225	0.2285
0.0872	0.380	0.3864
0.1744	0.563	0.5670
0.3488	0.712	0.7138

b. λ = 0.61 μ

Fig. 19 Continued

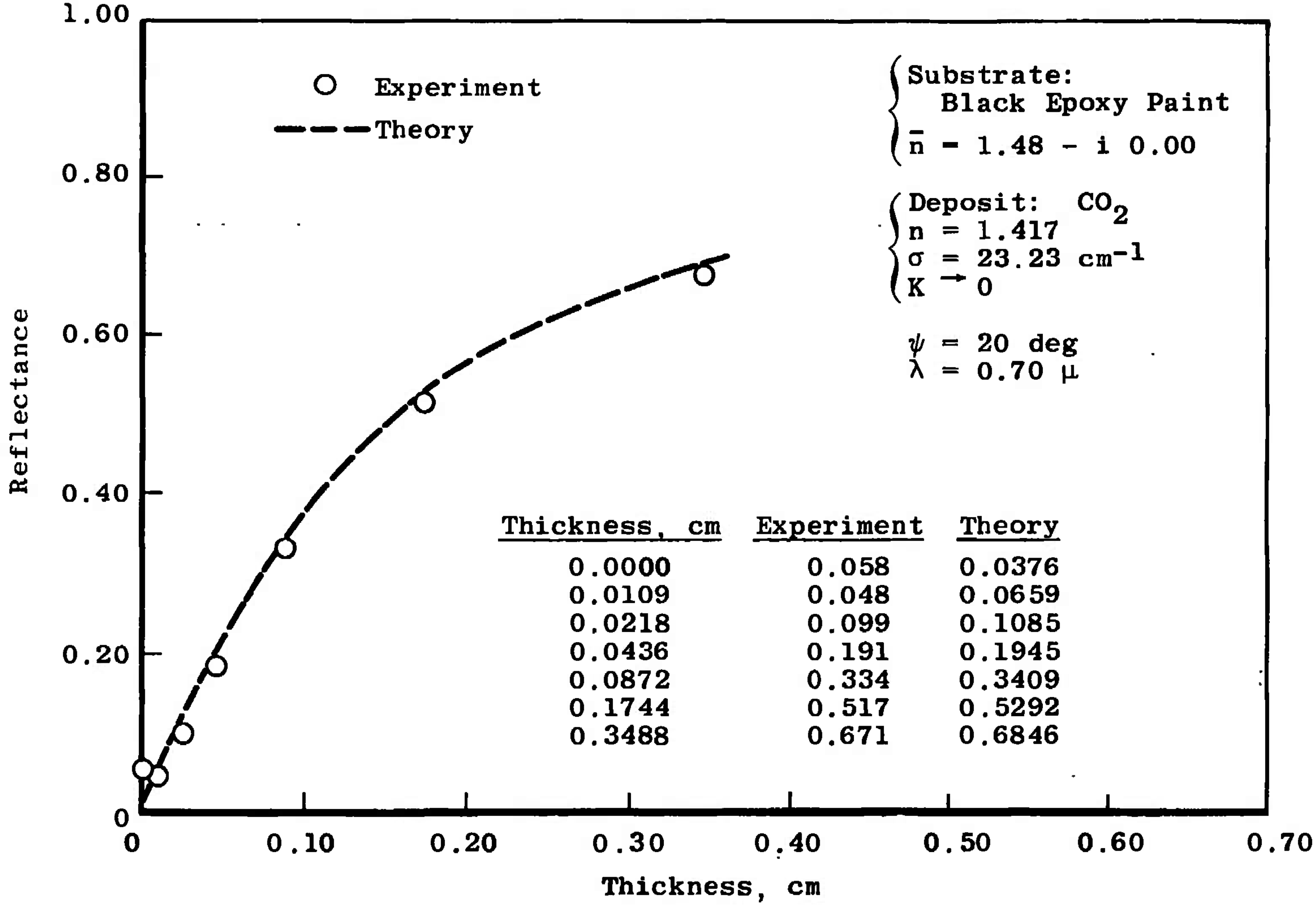

Thickness, cm	Experiment	Theory
0.0000	0.058	0.0376
0.0109	0.048	0.0659
0.0218	0.099	0.1085
0.0436	0.191	0.1945
0.0872	0.334	0.3409
0.1744	0.517	0.5292
0.3488	0.671	0.6846

c. $\lambda = 0.70\ \mu$

Fig. 19 Continued

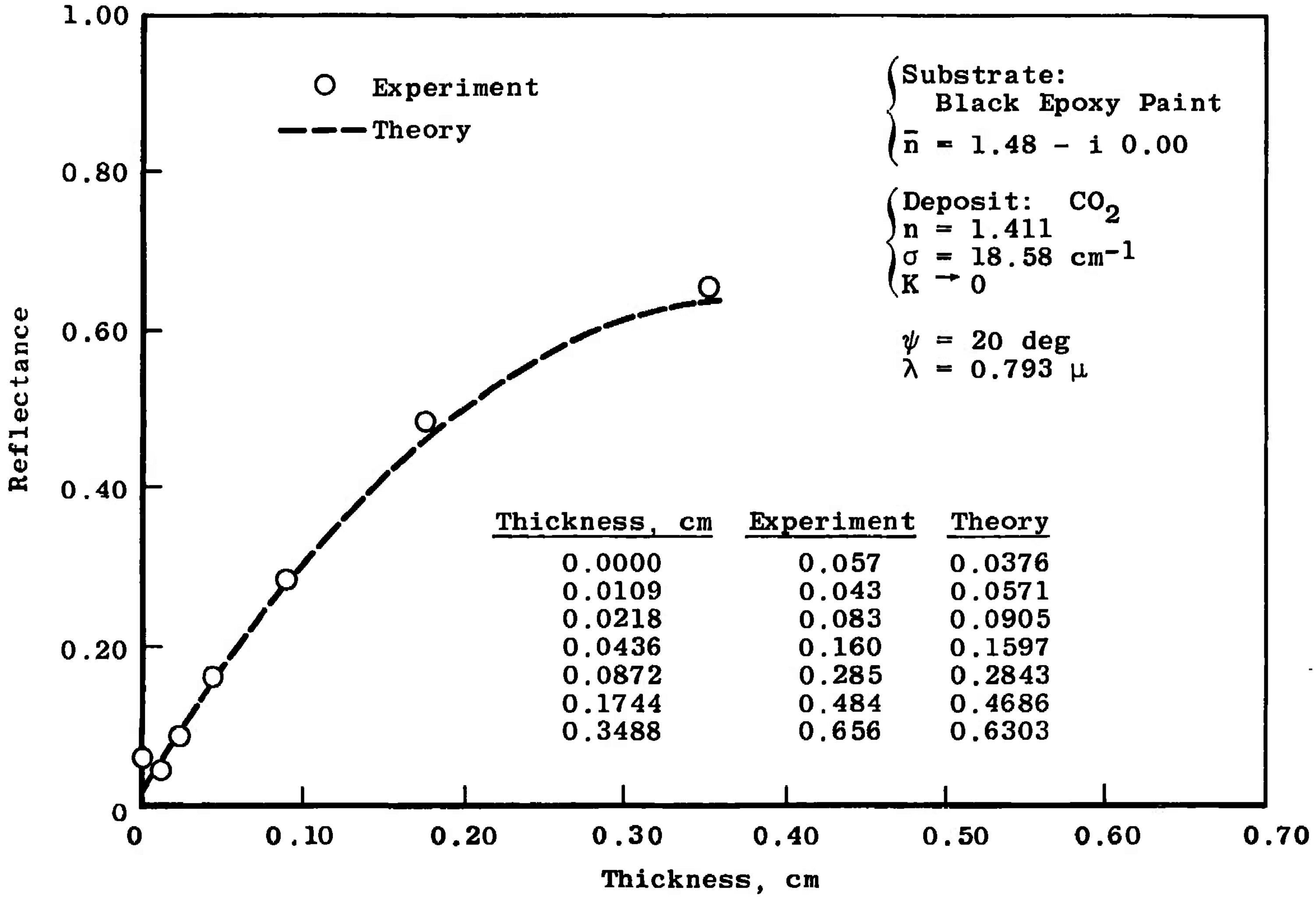

Thickness, cm	Experiment	Theory
0.0000	0.057	0.0376
0.0109	0.043	0.0571
0.0218	0.083	0.0905
0.0436	0.160	0.1597
0.0872	0.285	0.2843
0.1744	0.484	0.4686
0.3488	0.656	0.6303

d. $\lambda = 0.793\ \mu$

Fig. 19 Continued

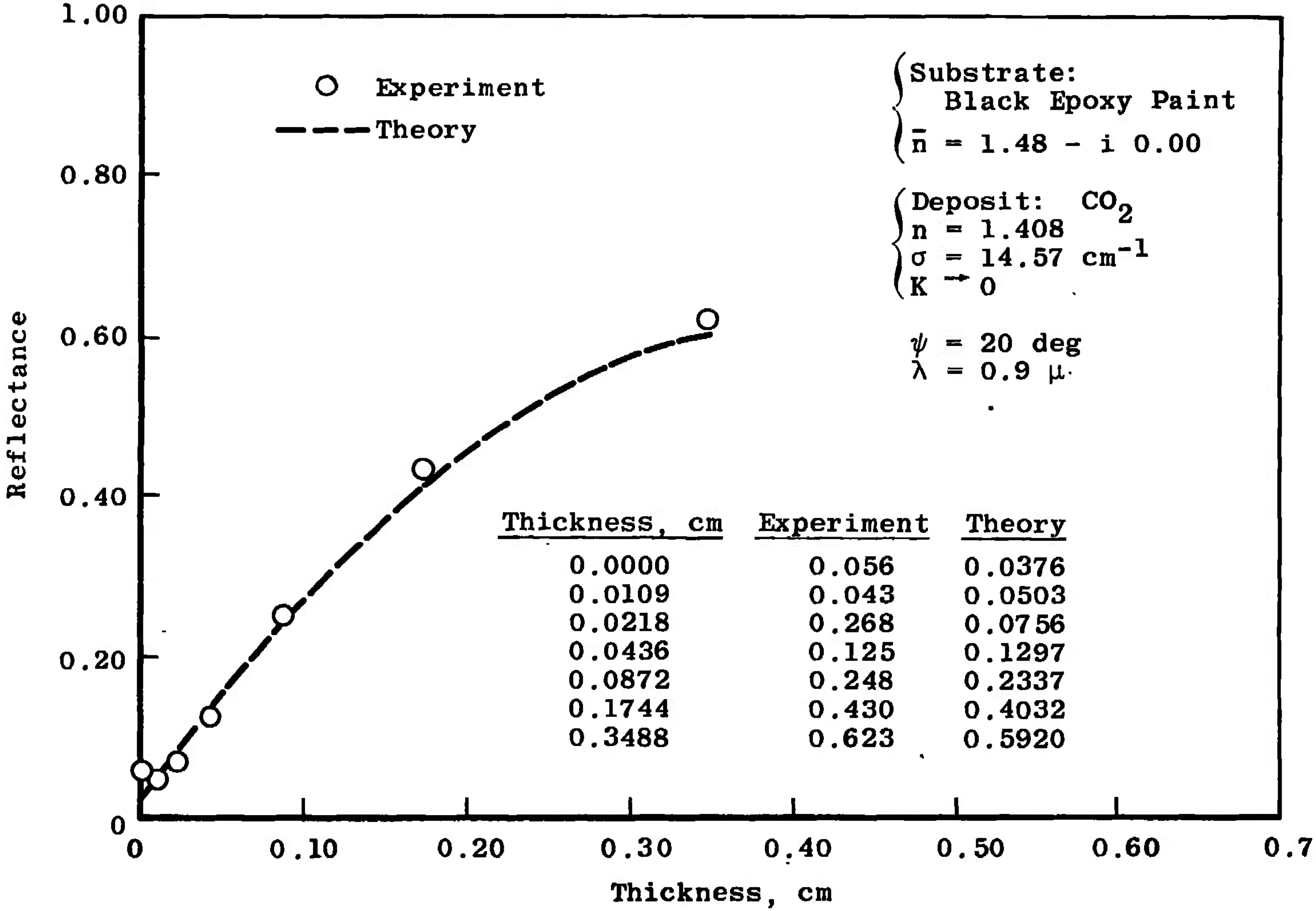

Thickness, cm	Experiment	Theory
0.0000	0.056	0.0376
0.0109	0.043	0.0503
0.0218	0.268	0.0756
0.0436	0.125	0.1297
0.0872	0.248	0.2337
0.1744	0.430	0.4032
0.3488	0.623	0.5920

e. $\lambda = 0.9\ \mu$

Fig. 19 Continued

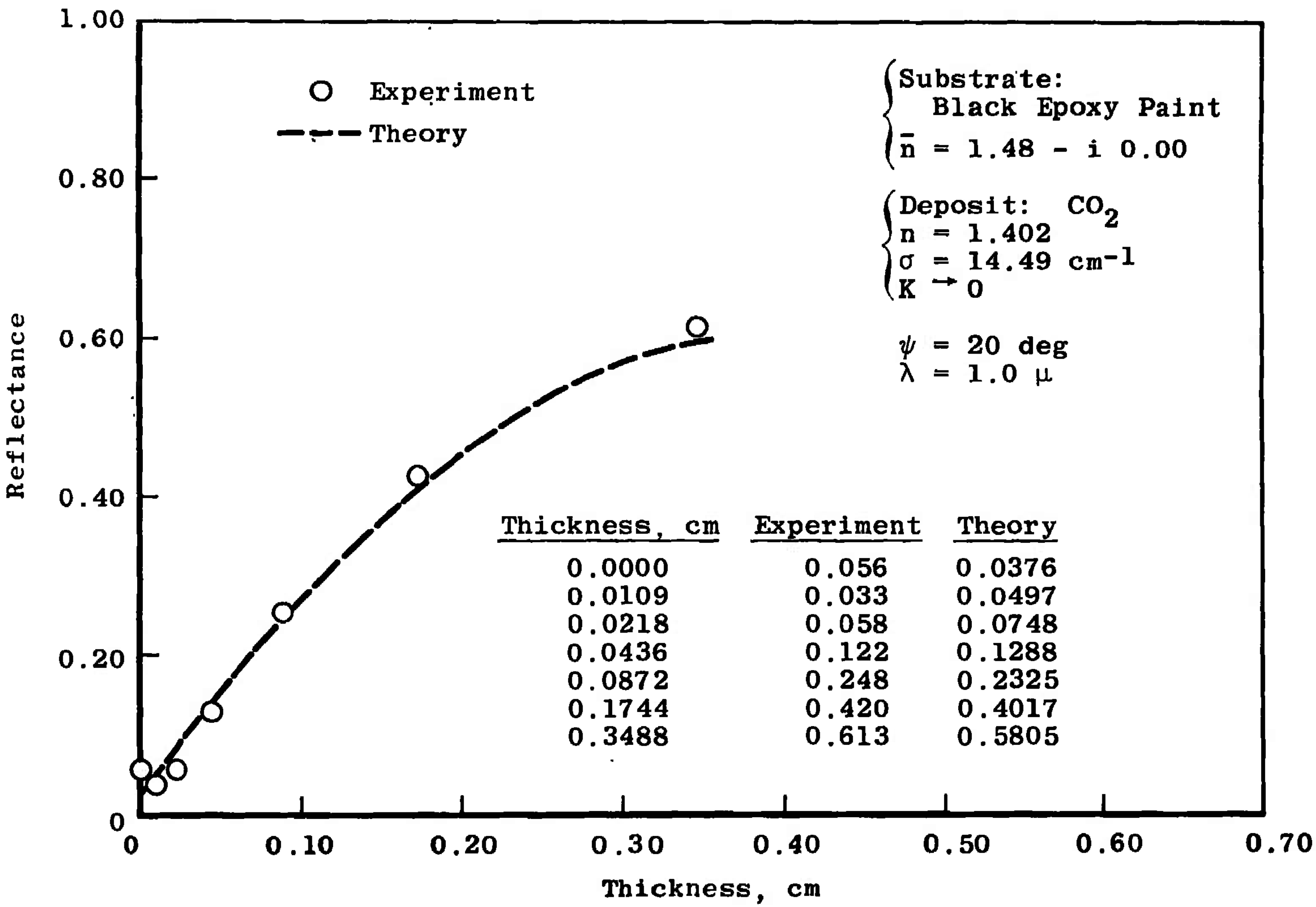

f. $\lambda = 1.0\ \mu$
Fig. 19 Concluded

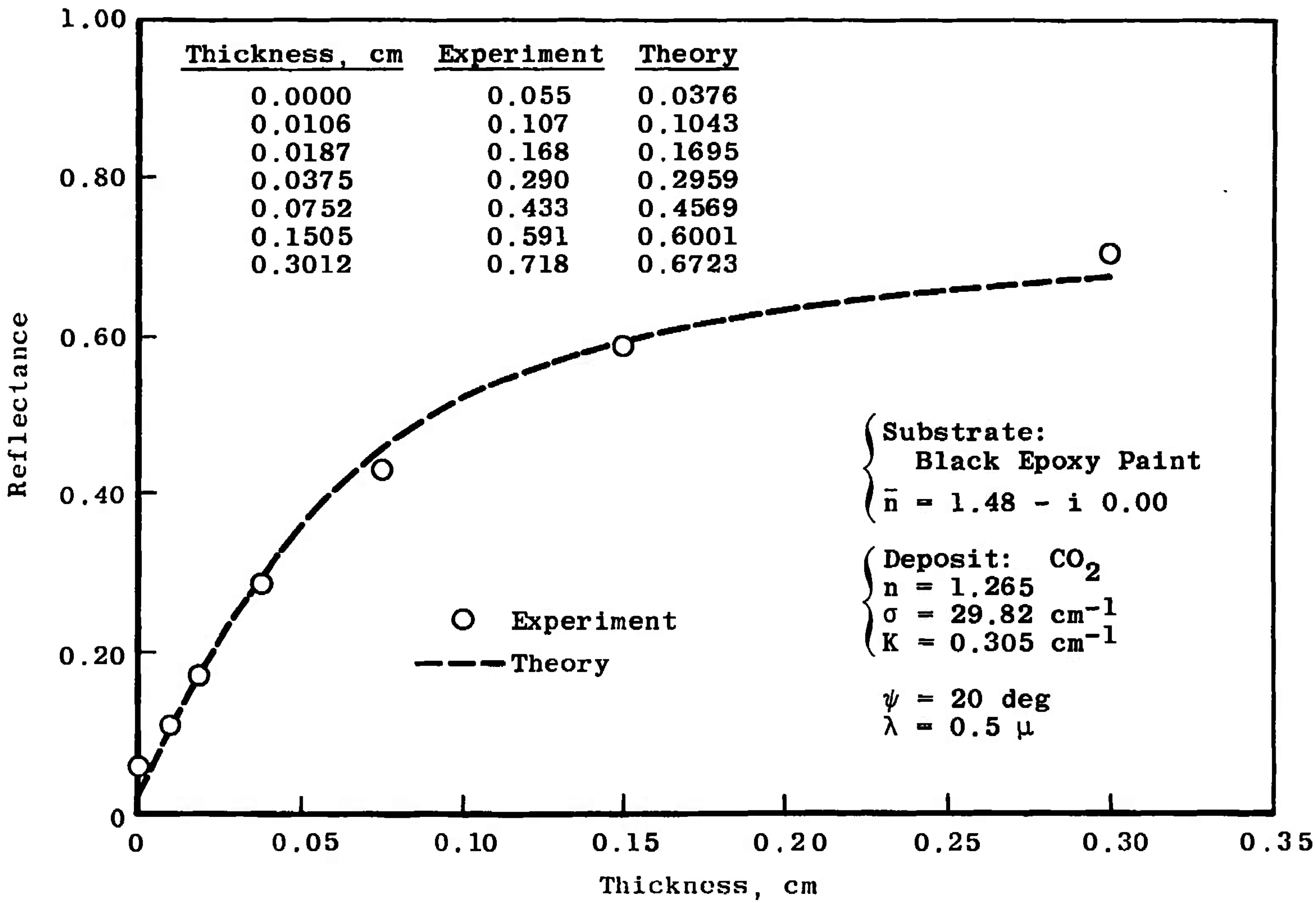

a. λ = 0.50 μ

Fig. 20 Comparison of Theory and Data for an H_2O Cryodeposit on a Black Epoxy Paint Substrate

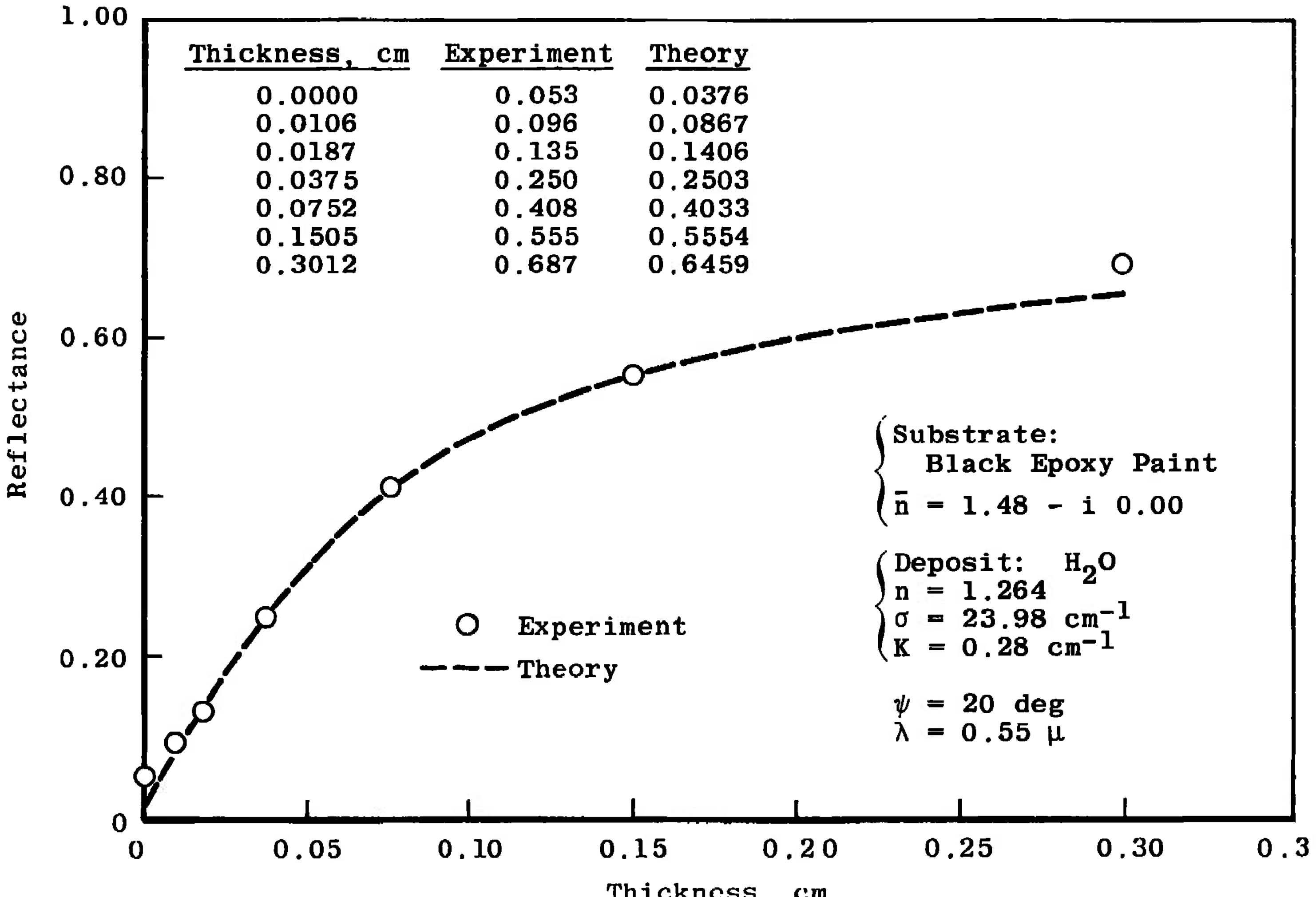

Thickness, cm	Experiment	Theory
0.0000	0.053	0.0376
0.0106	0.096	0.0867
0.0187	0.135	0.1406
0.0375	0.250	0.2503
0.0752	0.408	0.4033
0.1505	0.555	0.5554
0.3012	0.687	0.6459

b. $\lambda = 0.55\ \mu$
Fig. 20 Continued

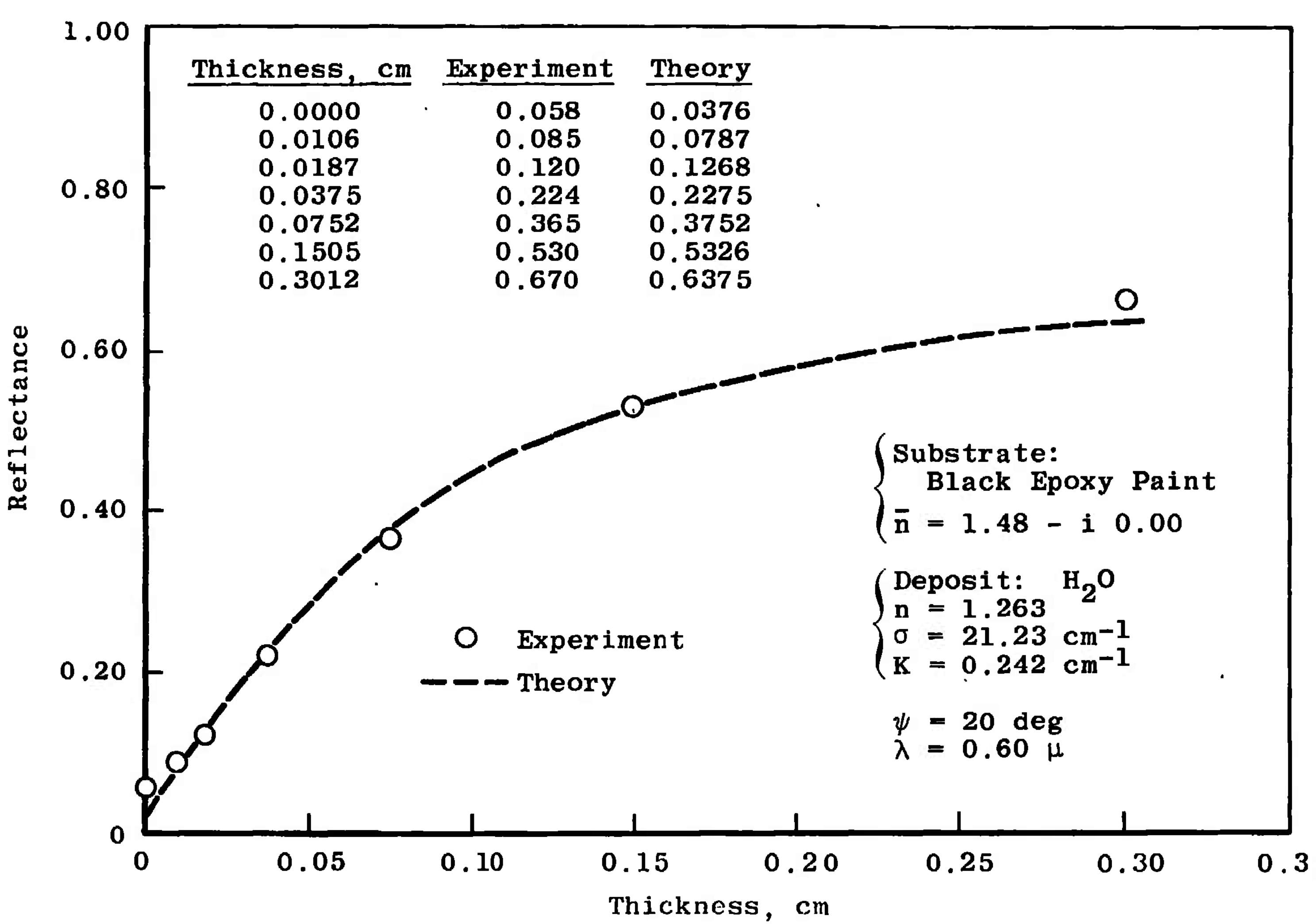

Thickness, cm	Experiment	Theory
0.0000	0.058	0.0376
0.0106	0.085	0.0787
0.0187	0.120	0.1268
0.0375	0.224	0.2275
0.0752	0.365	0.3752
0.1505	0.530	0.5326
0.3012	0.670	0.6375

c. λ = 0.60 μ
Fig. 20 Continued

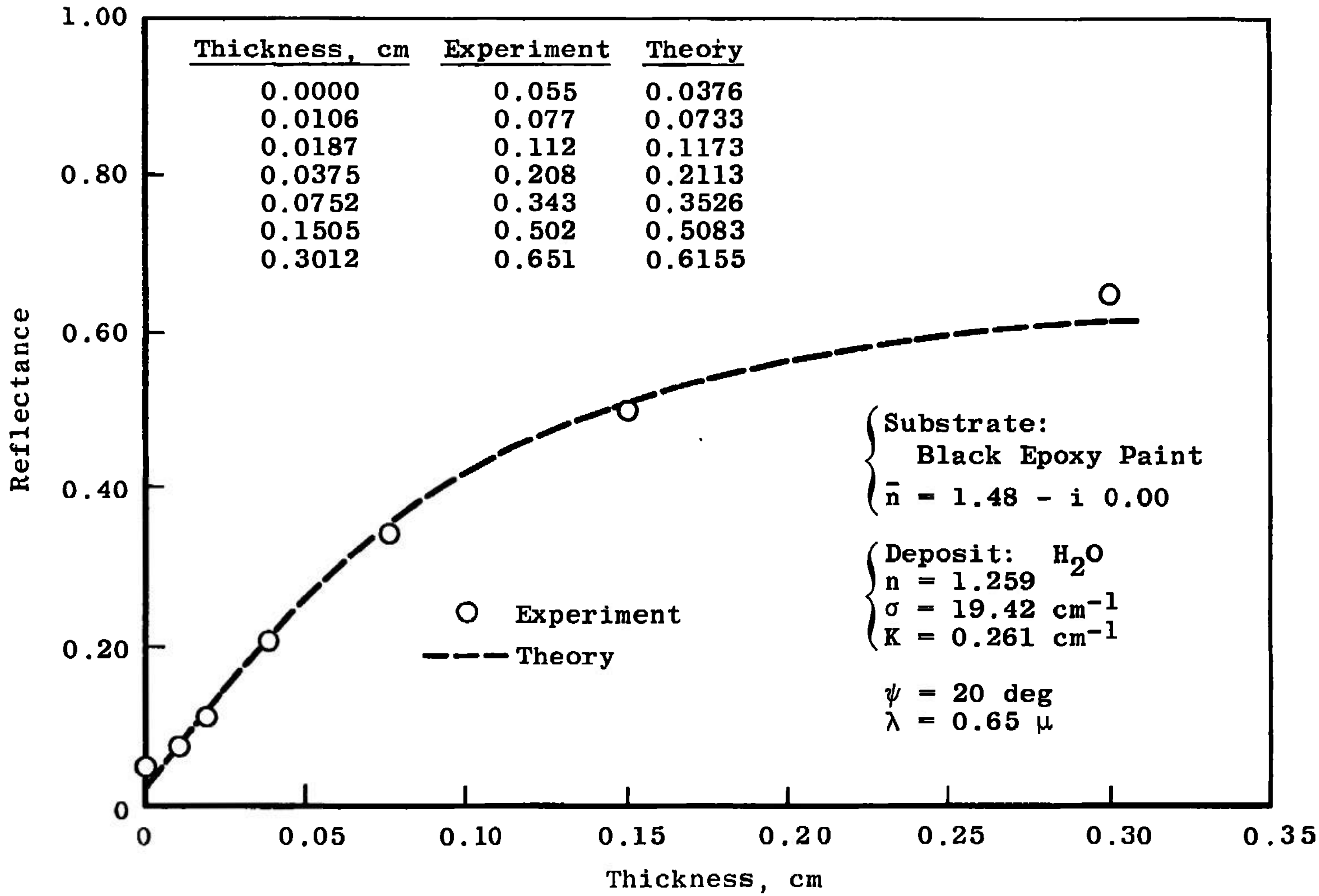

d. λ = 0.65 μ
Fig. 20 Continued

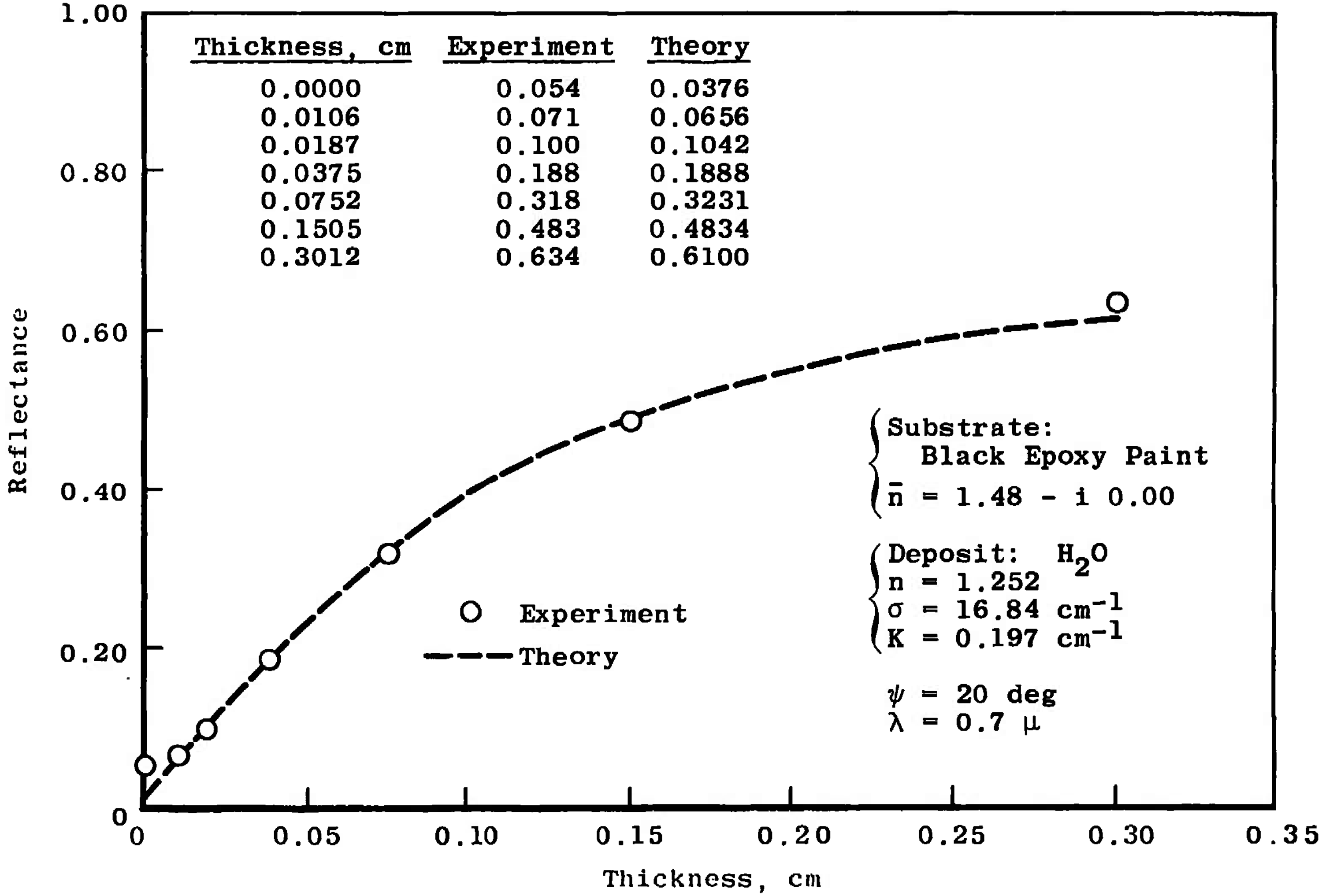

Thickness, cm	Experiment	Theory
0.0000	0.054	0.0376
0.0106	0.071	0.0656
0.0187	0.100	0.1042
0.0375	0.188	0.1888
0.0752	0.318	0.3231
0.1505	0.483	0.4834
0.3012	0.634	0.6100

e. $\lambda = 0.70\ \mu$
Fig. 20 Concluded

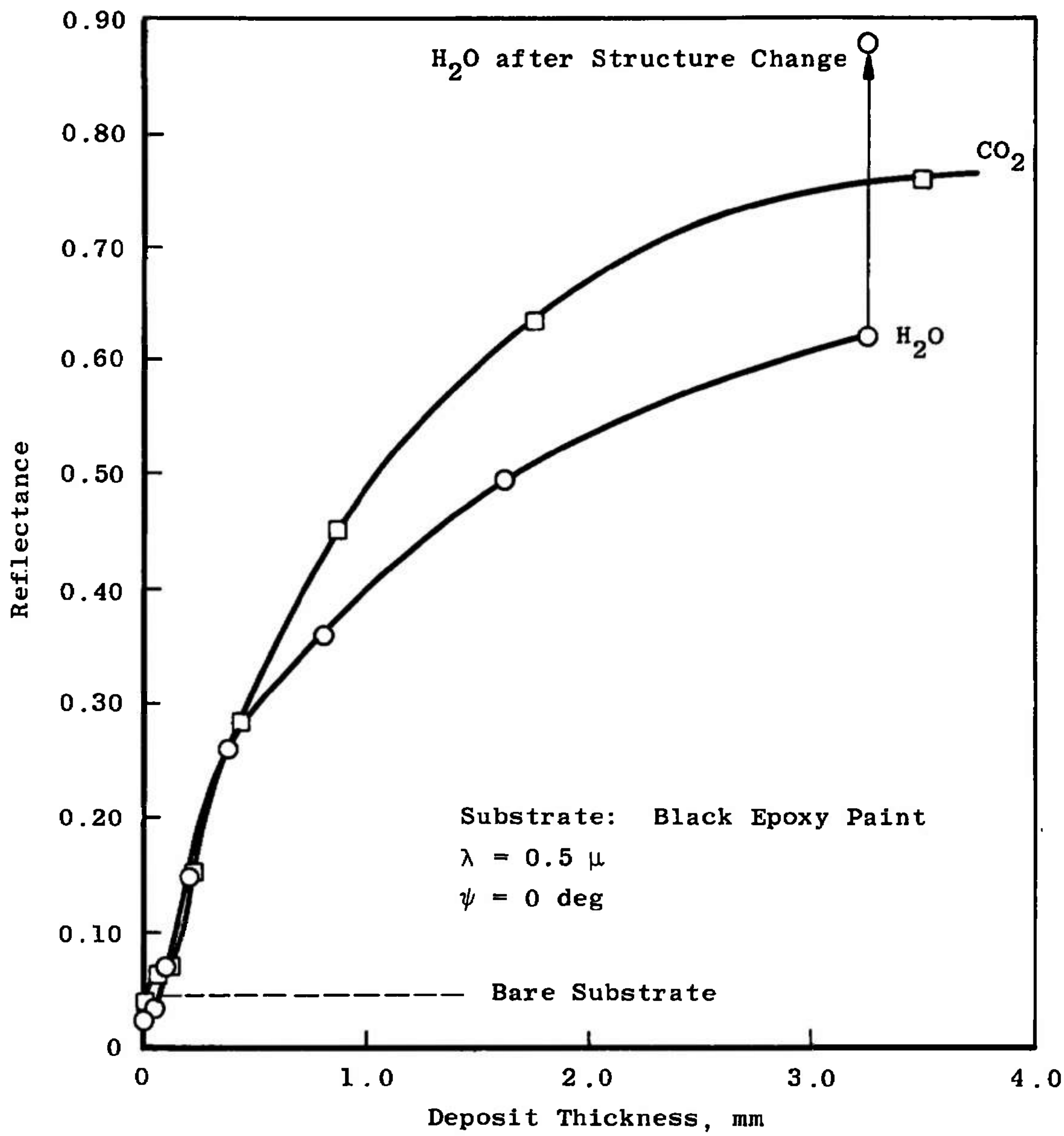

Fig. 21 Comparison of Experimentally Determined Reflectances of CO_2 and H_2O Deposits on Black Epoxy Paint

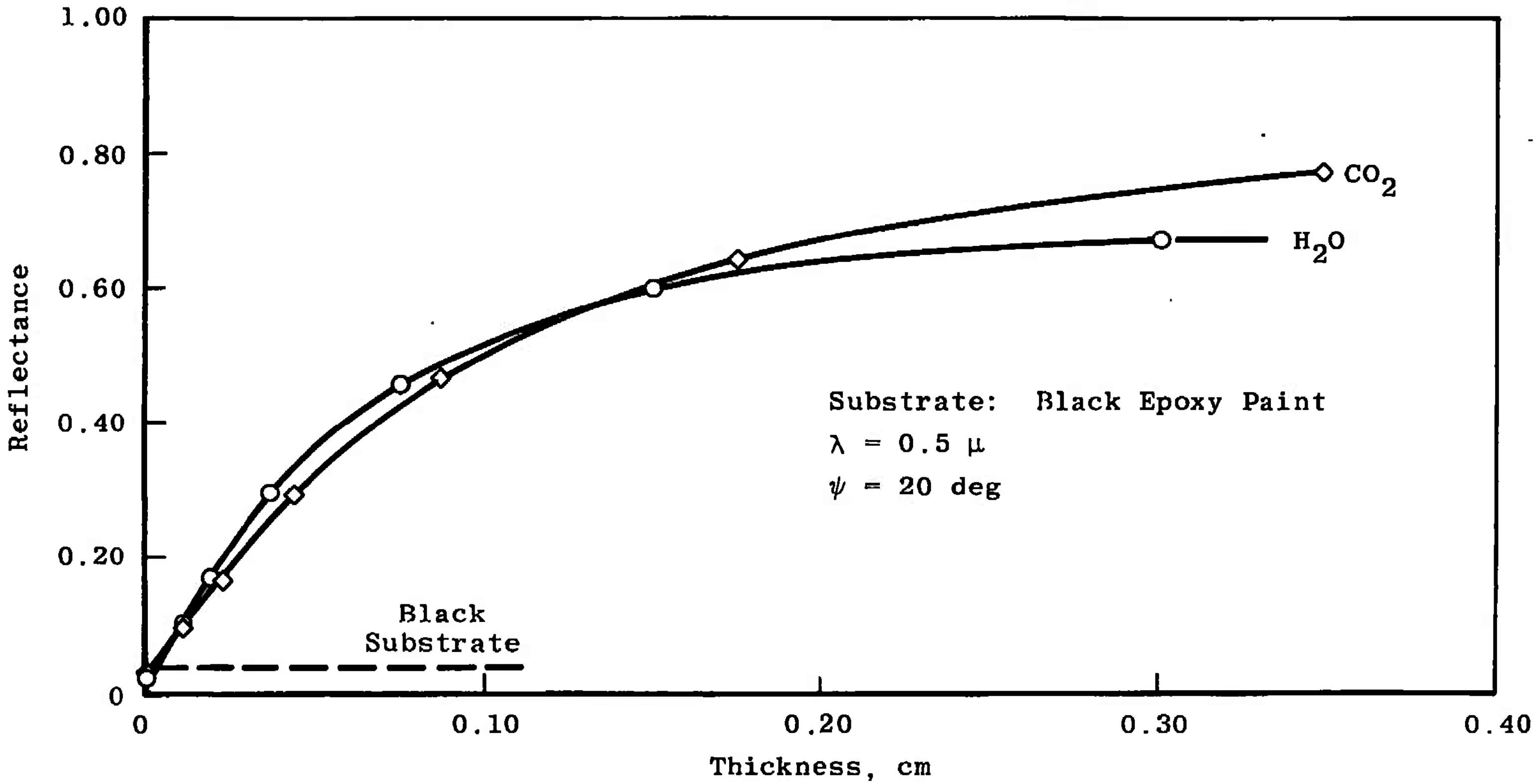

Fig. 22 Theoretical Comparison of CO_2 and H_2O Cryodeposits on Black Epoxy Paint

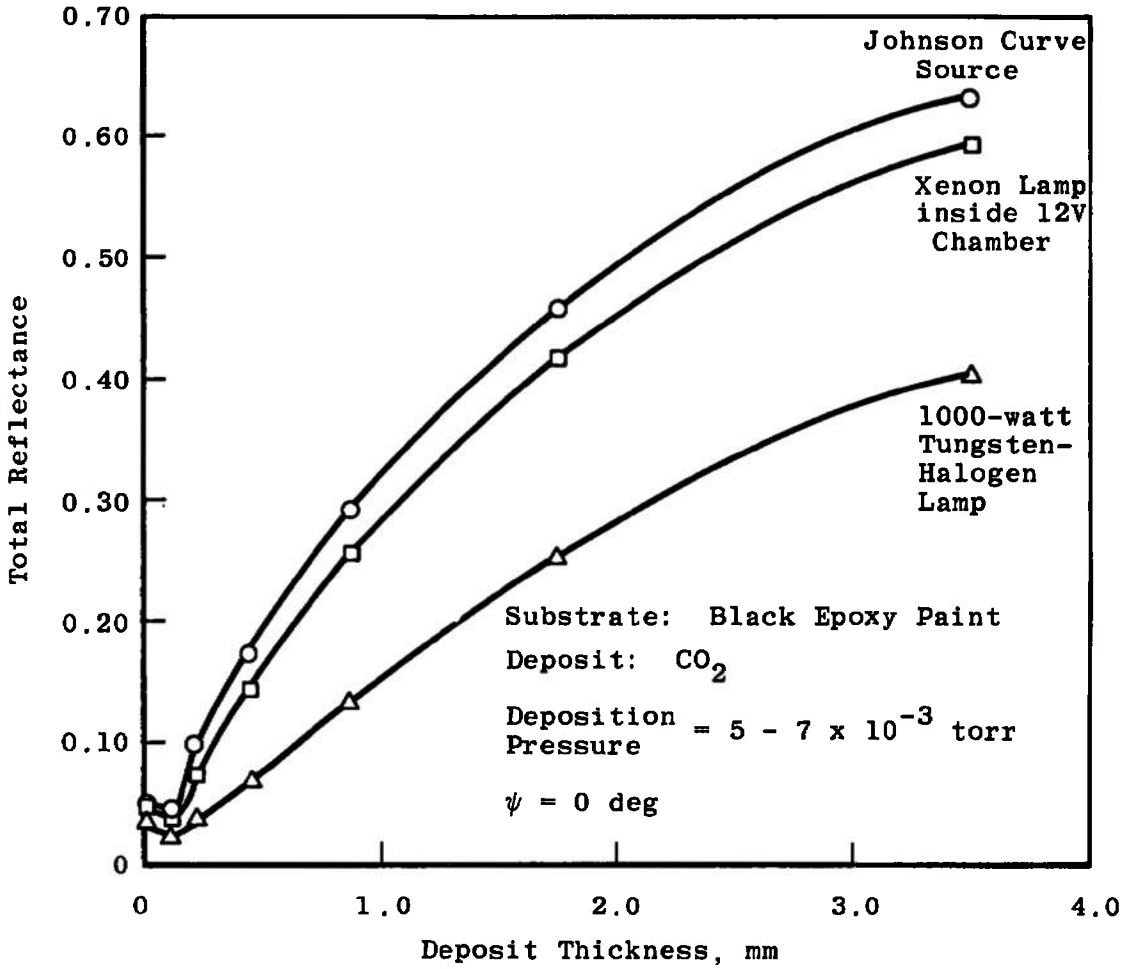

Fig. 23 Total Reflectance of CO_2 on Black Epoxy Paint for Solar Radiation (Johnson-Curve) and for Solar Simulator Radiation (Xenon Lamp and Tungsten-Halogen Lamp)

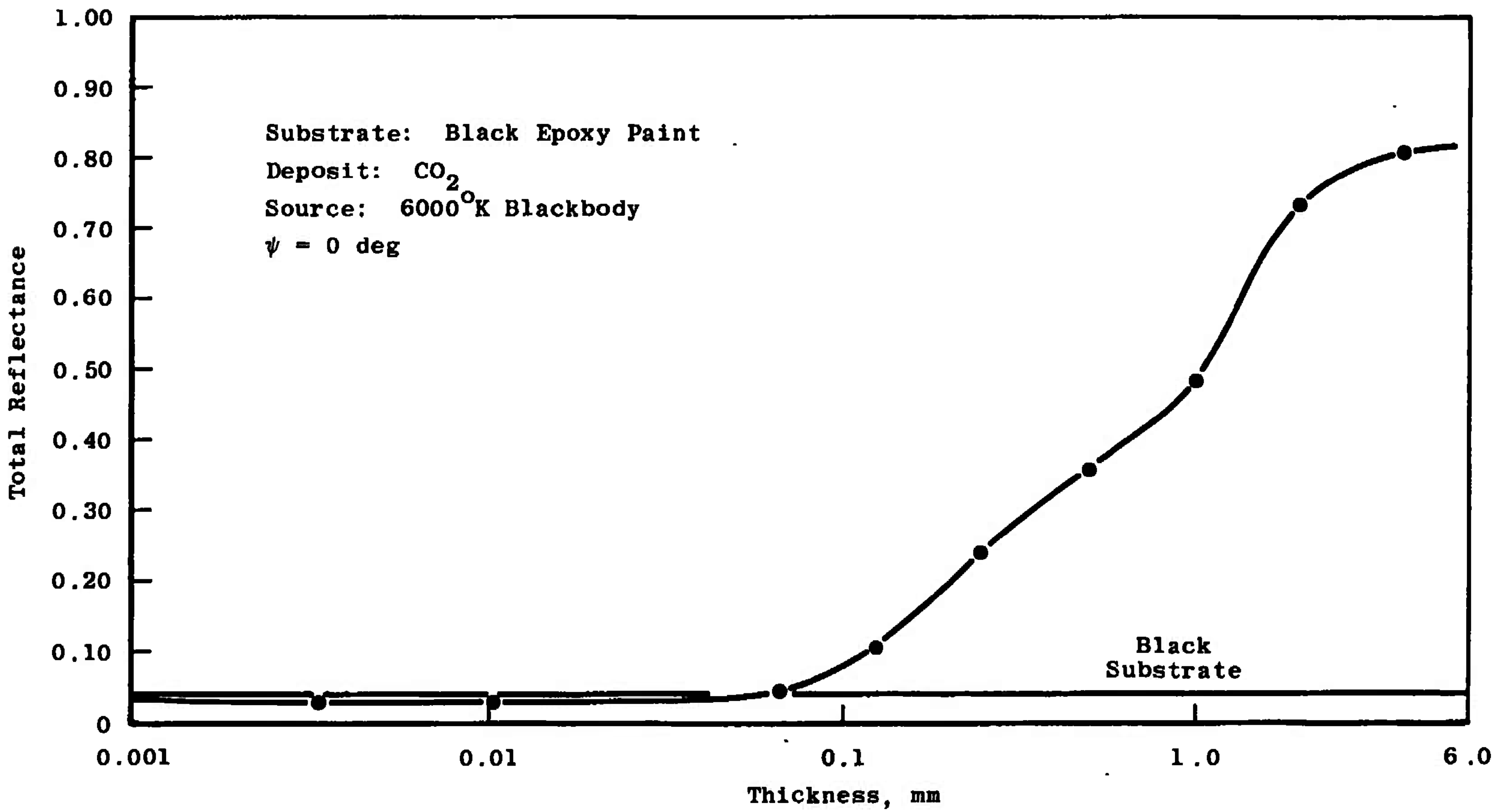

Fig. 24 Total Reflectance of CO_2 on Black Epoxy Paint for a 6000°K Blackbody Source

UNCLASSIFIED

Security Classification

DOCUMENT CONTROL DATA - R & D		
(Security classification of title, body of abstract and indexing annotation must be entered when the overall report is classified)		
1. ORIGINATING ACTIVITY (Corporate author) Arnold Engineering Development Center, Arnold Air Force Station, Tennessee 37389	2a. REPORT SECURITY CLASSIFICATION UNCLASSIFIED	2b. GROUP N/A
3. REPORT TITLE REFLECTANCES OF CO_2 AND H_2O CRYODEPOSITS AT SOLAR WAVELENGTHS		
4. DESCRIPTIVE NOTES (Type of report and inclusive dates) January 1970 through June 1971--Final Report		
5. AUTHOR(S) (First name, middle initial, last name) B. A. Seiber, A. M. Smith, and B. E. Wood, ARO, Inc.		
6. REPORT DATE November 1971	7a. TOTAL NO. OF PAGES 94	7b. NO. OF REFS 9
8a. CONTRACT OR GRANT NO.	9a. ORIGINATOR'S REPORT NUMBER(S) AEDC-TR-71-241	
b. PROJECT NO. Program Element 64719F		
c.	9b. OTHER REPORT NO(S) (Any other numbers that may be assigned this report) ARO-VKF-TR-71-172	
d.		
10. DISTRIBUTION STATEMENT Approved for public release; distriubtion unlimited.		
11. SUPPLEMENTARY NOTES Available in DDC	12. SPONSORING MILITARY ACTIVITY Arnold Engineering Development Center (XON), Air Force Systems Command, Arnold AF Stn., Tenn.37389	

13. ABSTRACT

A careful study of the reflectances of carbon dioxide and water cryodeposits was made in a vacuum integrating sphere in the solar wavelength range (0.30 to 2.55 μ). These deposits were formed on liquid-nitrogen-cooled black epoxy paint and polished stainless steel substrates. The reflectances of these deposits were studied while varying the deposit thickness, view angle, and wavelength. The reflectance dependence on thickness was also predicted theoretically and the values obtained were in excellent agreement with the experimentally determined values. Most of the water deposits studied were of amorphous structure, but upon warming, the deposits crystallized resulting in a significant change in the reflectance. No structural changes were observed when the carbon dioxide frosts were warmed. From the results of this study, conclusions are drawn with regard to the application of these findings to several current problems.

DD FORM 1 NOV 65 1473

UNCLASSIFIED

Security Classification

UNCLASSIFIED
Security Classification

14. KEY WORDS	LINK A		LINK B		LINK C	
	ROLE	WT	ROLE	WT	ROLE	WT
space environment simulation						
cryogenics						
cryopumping						
ice formation						
crystallization						
solidified gases						
reflectance						
carbon dioxide						
water						
deposits						
wavelengths						
vacuum chambers						

AFSC
Arnold AFS Tenn

UNCLASSIFIED
Security Classification